MARCH 1960 VOLUME 6 (1960) No. 4

GREGG M. SINCLAIR LIBRARY
UNIVERSITY OF HAWAII
8-7-63

NUCLEAR INSTRUMENTS & METHODS

A JOURNAL ON ACCELERATORS, INSTRUMENTATION AND TECHNIQUES IN NUCLEAR PHYSICS

EDITOR: K. SIEGBAHN – UPPSALA

LAST NUMBER OF THIS VOLUME

CONTENTS

EKBAL BASHANDY, Energy dependent instrumental time delays in millimicrosecond delayed coincidence experiments . . . 289
W. LOTZ, A. SITTKUS und W. HASSLER, Untersuchungen an einer Anordnung zur Messung der Nukleonenkomponente der kosmischen Strahlung . . . 296
R. D. CONNOR, The action of fast spherical ionization chambers . . . 301
O. J. ORIENT, On the mechanism of multiple discharges in self-quenching Geiger counters. . 309
W. M. GOOD, Millimicrosecond pulsing – Its application and technique . . . 323
R. BALLINI and S. M. SHAFROTH, Detection of low energy neutrons with a NaI(Tl) crystal and time of flight . . . 331
R. D. CONNOR and M. K. HUSAIN, Some factors affecting the gain and resolution of photomultiplier tubes . . . 337
J. E. MONAHAN and F. P. MOORING, An investigation of properties of thin lithium films by use of the $Li^7(p,n)Be^7$ reaction . . . 343
A. BOUCHERIE, Système de soustraction à tube cathodique mémoire . . . 354
V. J. KOWALEWSKI and R. A. HOFFMAN, A nuclear magnetic resonance spectrometer . . . 357
Letter to the Editor: W. S. C. WILLIAMS, A proposal to decrease the deadtime of the Hutchinson-Scarrot type pulse height analyser . . . 361
Author Index . . . 362
Subject Index . . . 364

NORTH-HOLLAND PUBLISHING COMPANY – AMSTERDAM

NUCLEAR INSTRUMENTS AND METHODS

A journal on accelerators, instrumentation and techniques in nuclear physics

EDITOR: K. SIEGBAHN, UPPSALA

EDITORIAL BOARD:

J. B. ADAMS (CERN)
F. A. ALSINA (Buenos Aires)
E. AMALDI (Rome)
H. L. ANDERSON (Chicago)
K. T. BAINBRIDGE (Cambridge, Mass.)
C. J. BAKKER (CERN)
P. R. BELL (Oak Ridge)
R. E. BELL (Montreal)
A. BERTHELOT (Saclay)
H. BRINKMAN (Groningen)
E. H. COOKE–YARBOROUGH (Harwell)
S. DE BENEDETTI (Pittsburgh)
M. DE HEMPTINNE (Louvain)
A. DE-SHALIT (Rehovoth)
M. DEUTSCH (Cambridge, Mass.)
S. DU TOIT (Pretoria)
B. S. DŽELEPOV (Leningrad)
W. GENTNER (Heidelberg)
P. C. GUGELOT (Amsterdam)
H. HALBAN (Paris)
O. HAXEL (Heidelberg)
P. HUBER (Basel)
D. J. HUGHES (Brookhaven)
S. KIKUCHI (Tokyo)
J. KOCH (Copenhagen)
M. S. KOZODAEV (Moscow)
S. LIVINGSTON (Cambridge, Mass.)
E. M. MCMILLAN (Berkeley)
M. G. MEŠČERJAKOV (Moscow)
P. B. MOON (Birmingham)
M. L. OLIPHANT (Canberra)
W. PAUL (Bonn)
A. S. RAO (Bombay)
G. SALVANI (Rome)
P. SAVIĆ (Belgrade)
P. SCHERRER (Zürich)
CH. SCHMELZER (CERN)
H. W. B. SKINNER (Liverpool)
R. TANGEN (Oslo)
D. TAYLOR (Northampton)
V. I. VEKSLER (Moscow)
G. VON DARDEL (CERN)
O. WERNHOLM (Stockholm)
R. R. WILSON (Cornell)
S. D. WINTER (Saclay)

INSTRUCTIONS FOR CONTRIBUTORS

Contributions may be sent to the Editor, Professor K. Siegbahn, Institute of Physics, University of Uppsala, Sweden, either directly or through the intermediation of one of the members of the Editorial Board. Contributions may be written in English, French or German but should always, except for very short papers, be supplied with a brief abstract in English. Figures should be in inked original drawings or glossy prints and they should be sufficiently large. Contributors should make sure that important details in drawings and photographs will show up clearly in the diminished copy used by the publisher.

Books for review should be sent to Professor Siegbahn.

Objective and descriptive material on endeavours and product developments from the industry for the section "Spotlight on Industry" should be sent directly to the publishers, North-Holland Publishing Company, P.O. Box 103, Amsterdam.

Nuclear Instruments and Methods is published monthly. The subscription price of a volume of 360 pages is $ 17.00 (130 s), postage free.

Subscriptions should be sent to the publishers, North-Holland Publishing Company, P.O. Box 103, Amsterdam or to any subscription-agent.

No part of this issue may be reproduced in any form, by print, photoprint, microfilm or any other means without written permission from the publisher. Reprints, photoprints or microfilms are obtainable at cost from the publisher.

Portable transistorized contamination monitor type PW 4012.

PHILIPS

equipment for Nuclear Physics and Atomic Energy

PW 4012 with probe extension.

This rugged, watertight and tropicallized battery-operated instrument incorporating the Philips G.M. counter tube type 18503 has been designed for the detection and measurement of radio-activity in such applications as:

- General radiation intensity checks in isotope laboratories, around isotope containers etc.
- Contamination checks of benches and apparatus.
- Radiation exposure measurements of personnel working with isotopes or X-rays.

It incorporates the following features:

- Three measuring ranges resp. 0-1, 0-10 and 0-100 mr/h (Ra γ).
- Compensation for voltage drop during battery life ensures maintenance of accuracy.
- Provision to insert probe extension.
- Beta sensitive G.M. tubes 18504 (2-3 mgr/cm^2) and 18505 (1.5-2 mgr/cm^2) can be used as well.
- Large, easy readable and shock-proof measuring instrument.

- Synchro-cyclotrons for various final energies.
- Cockcroft-Walton accelerators.
- Generators for very high d.c. voltages.
- Linear electron accelerators.
- Reactor control instrumentation
- Radiation measuring and detection equipment.
- Civil defence instruments.
- Area monitoring instrumentation.
- Geiger counter tubes.
- Photomultipliers.
- Radio-active isotopes.
- Air & gas liquefiers.

PHILIPS

Nuclear Equipment

For further information please apply to:

N.V. PHILIPS' GLOEILAMPENFABRIEKEN,
Scientific Equipment Department, Eindhoven-Holland
RESEARCH & CONTROL INSTRUMENTS LTD.,
Instrument House, 207/215, King's Cross Road, London WC 1

PHILIPS

NDO

NEW!

E-H MILLIMICROSECOND PULSE GENERATOR

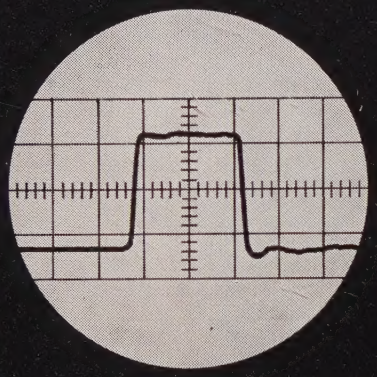

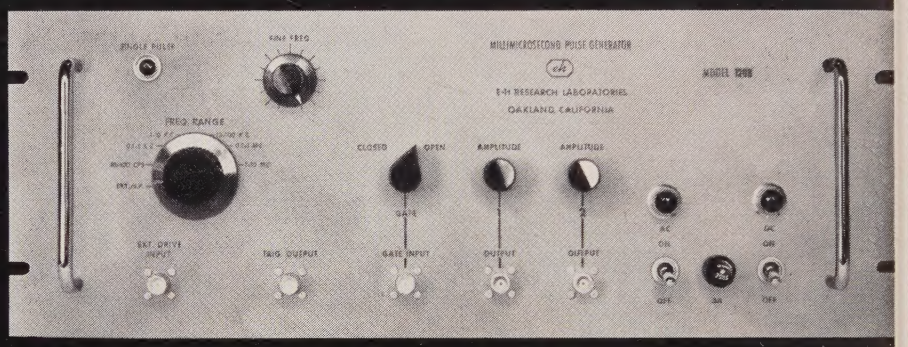

Model 120B f.o.b. Oakland, Calif. $1275

RISE TIME OF LESS THAN 2.5 MILLIMICROSECONDS

REPETITION RATE OF 10 cps to 10 Mc

plus these other features

- **PRECISION PULSE WIDTHS** 2.5 to 25 millimicroseconds
- **INDEPENDENT OUTPUTS** Two fully controlled 0-8 volt outputs
- **FLEXIBLE** Internal or external drive, provision for external gating and single pulse operation

Here is a new all-electronic instrument with the performance features—and quality engineering—you need for advanced applications.

The 120B's fast rise time and high repetition rate make it unexcelled for general laboratory use in development, production and testing of diodes, fast transistors, cables, pulse transformers, delay lines and video amplifiers . . . for development and check-out work in the computer field, for rf applications, and in nuclear test work. *For more information on the 120B or other E-H pulse generators, write or wire E-H.*

SPECIFICATIONS

RISE TIME (10% to 90%)
Less than 2.5 millimicroseconds

PULSE WIDTH
2.5 to 25 millimicroseconds

REPETITION RATE (External or Internal)
10 cps to 10 Mc

OUTPUTS
(Two Independent Output Channels)
Amplitude, 0 to minus 8 volts (use E-H model ZT pulse transformer for polarity inversion and impedance matching)
Impedance, 93 ohms

TRIGGER OUTPUT
Positive 15 volt pulse

CONNECTORS
All BNC type

TRIGGER ADVANCE
120 millimicroseconds

EXTERNAL DRIVE
Delay, 50 millimicroseconds
Amplitude required, 3 volts rms

ELECTRONIC GATE
Gating time, less than 100 millimicroseconds
Amplitude required, positive 20 volts

E-H RESEARCH LABORATORIES, INC.
1922 PARK BLVD. • GLENCOURT 2-1314 • OAKLAND 6, CALIFORNIA

on behavior... The operator of one of the first production models of our 110 systems returned to his lab one Monday morning to find that the analyzer had printed readout on paper tape continuously for three days. "Faulty, bug-filled instrument", was his accusation. "Human error", our engineers replied. The operator in his haste had called for a preset count *and* non-destructive readout. The obedient instrument just printed and printed readout without destroying it. This is why we hasten to point out that our instruments are instructed not to reason why... not to second-guess... to just do what they're told. When you use a "110" you can be sure it will do exactly as you tell it.

"cramming" parts... We discovered just in time that it is possible to go too far with this "compactness" business — to the point of defeating the purpose of the design. Some circuit boards have so many components on them they begin to look like popcorn balls. They're miserable to repair and cost a small fortune to replace. In our 110 Analyzer, we fought the initial urge to cram all parts on two or three boards. By using a few more, with fewer parts on each, we've made repairs easy, total replacement costs much lower — and the little extra space required isn't worth mentioning.

NON-TECHNICAL THOUGHTS...

about the TMC Portable 256-channel Pulse Analyzer

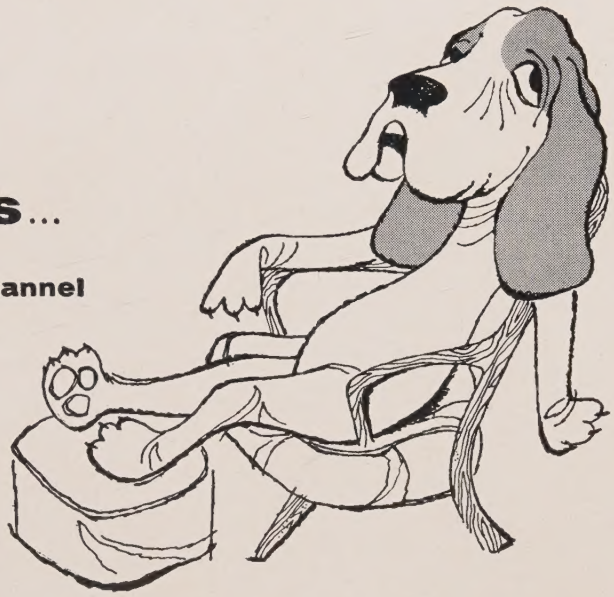

pricing... We have set prices on our instruments that we think are reasonable — not so that we can cut them just for underselling purposes. Price wars and bargains are for department stores. We'll stick to our guns because we're confident about our products.

These are 3 of the "110's" characteristics that have pleased the people who are now using the system. For complete summary of all the virtues of the analyzer, its plug-in logic units and data handling unit, see our new 6-page folder. Besides the usual advantages of transistor circuits (low heat, bench-top size, etc.) the 110 has several unique characteristics which are also prominently mentioned. A copy is yours on request.

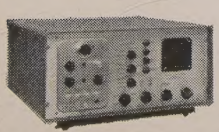

If you're a Transistor Design Engineer and you're restless, we'd like to talk with you. The "110" is typical of the transistor instruments we are now working on.

TMC

TECHNICAL MEASUREMENT CORPORATION
441 Washington Ave., North Haven, Connecticut

Pulse Height Analysis

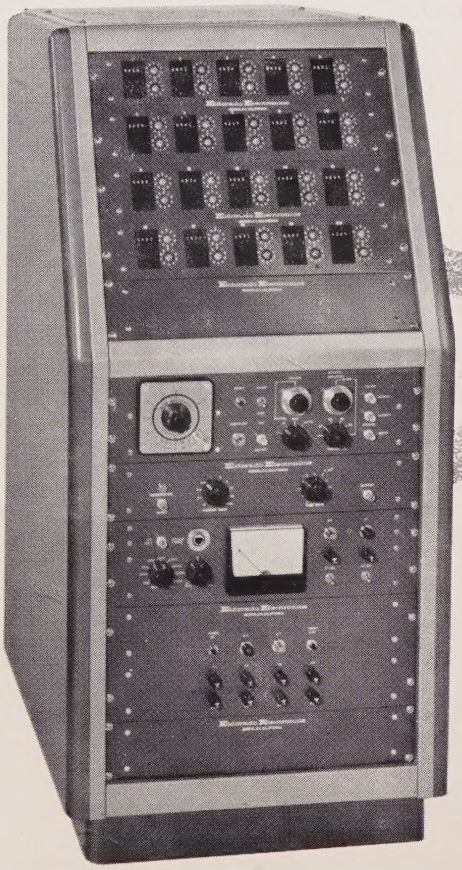

Hours faster with the

Eldorado 4100

The Eldorado 4100 is the fastest multi-channel pulse height analyzer commercially available to the nuclear physicist. Its high resolution and exceptional stability dramatically shorten many experiments. For example, an experiment requiring from 7 to 42 hours with a time conversion type analyzer can be done in 8 to 25 minutes with the 4100. Such performance considerably reduces research costs.

APPLICATIONS *The 4100 is particularly well-suited for experiments requiring accurate analysis of (1) isomeric states, (2) isotopes with extremely short half-lives, (3) isotope mixtures having complex photo-peak structures.*

SPECIAL ADVANTAGES

Stability. The 4100's double pulse resolution—better than 1.0 microsecond—is achieved without sacrifice of stability. The system's stability figures (see specifications) compare favorably to the best for slower computer-type analyzers. Since lower ordered channels are free from non-linearity, each data point in the spectrum is equally useful and valid.

Low Dead Time. Users of the 4100 can often neglect count-loss correction factors because dead time is less than 0.2 microsecond. At an input counting rate of 300,000 counts per minute, dead time is less than 2% of the total experiment time.

KEY SPECIFICATIONS **Number of Channels,** 20. **Channel Width,** 1 volt, nominal. **Channel Width Stability,** Typically, better than 1% of a channel per week. **Zero Level Stability,** Better than 0.1% per week. **Window Width,** 20 volts, nominal. **Window Position Range,** 5 to 105 volts in 5 preset steps or continuous. **Channel Count Capacity,** 1,000,000. **Double Pulse Resolution Complete Analyzer,** 1.0 microsecond at window amplifier input. **Channel Scalers,** 10.0 microseconds.

For more details, write for Eldorado Bulletin D-4100.
Please address Dept . 3

Eldorado Electronics

2821 TENTH STREET • BERKELEY 10, CALIFORNIA

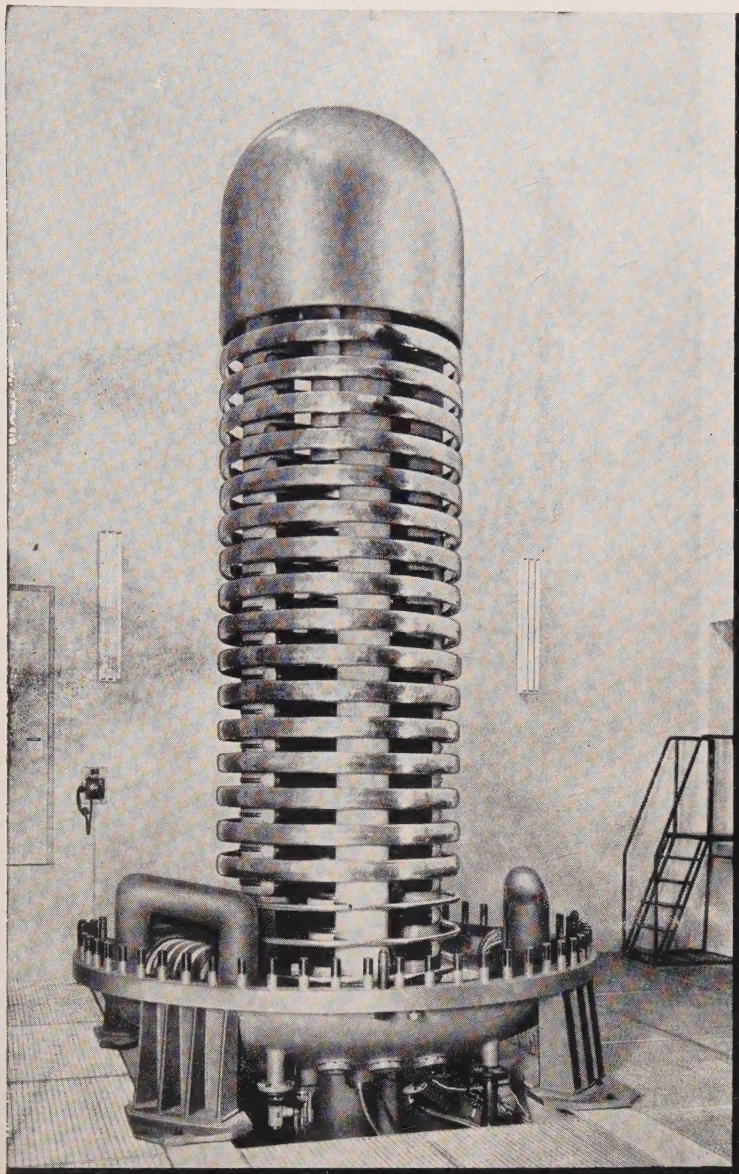

4 MV Particle Accelerator in the Physical Institute of the University of Basel (Switzerland)

HAEFELY

Particle Accelerators up to 4 MV with high beam intensity

for basic nuclear research

for industrial radiation processing

Continuous irradiation of plastics

Sterilisation of drugs and preservation of foods

X-ray equipment for non-destructive product inspection

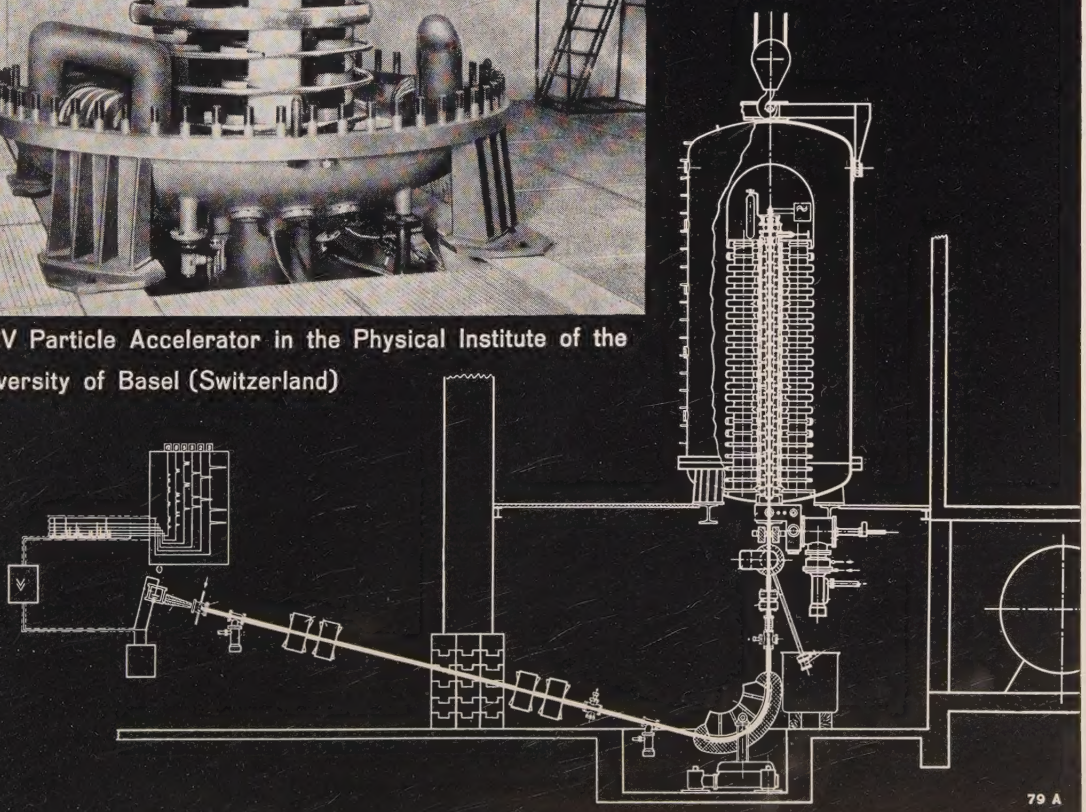

79 A

EMILE HAEFELY & CO LTD BASEL-SWITZERLAND

Elcor inc.
1225 W. BROAD ST.,
FALLS CHURCH, VA.

MODEL A 309
CURRENT INDICATOR AND INTEGRATOR

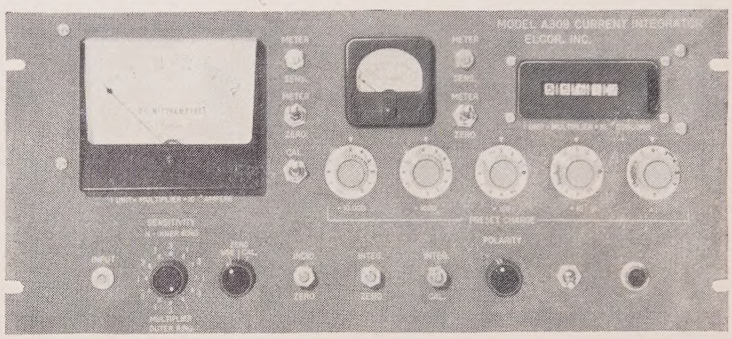

MODEL A 309 A

FEATURES

- Wide current range: 1 x 10^{-3} to 3 x 10^{-9} amp. in 12 switch settings.
- High accuracy: 1% of full scale.
- Internal calibrating current source to check proper operation.
- Front panel switch allows instrument to be used with current of either polarity.
- Pre-setting feature provides means of safeguarding against over-exposure.
- Developed especially for use with Van de Graaff and other high-voltage accelerators.
- Permits many experiments with particle accelerators that would otherwise be difficult or impossible.
- Register readout gives digital accuracy on charge measurement.

The versatility and accuracy of two instruments in one!

1. Measures currents from 1 milliampere to 3 milli-microamperes.
2. Integrates input current and registers accumulated charge.

GENERAL DESCRIPTION—The Model A309 Current Indicator and Integrator is a sensitive current indicator that also measures the total charge collected in a given length of time. Developed especially for use with high-voltage particle accelerators such as the Van de Graaff generator, the instrument is also ideally suited for other applications requiring the measurement of accumulated charge or the integration of a variable current.

The full-scale sensitivity of the instrument can be varied from 1 milliampere to 3 milli-microamperes in twelve ranges. For convenience in checking the performance and accuracy of the instrument, an internal calibrating current source is provided for each range. The accumulated charge is indicated on a 5-decimal digit register. Any number up to 99,999 can be preset into the instrument, and upon reaching the corresponding charge a relay closes to actuate a warning device or control auxiliary equipment. In applications where X-rays are being generated, this feature affords protection against accidental over-exposure.

Input current of either polarity can be measured and integrated, and a front panel switch enables the instrument to be immediately changed from one polarity to the other. Advanced circuit techniques have been employed to achieve low input impedance, negligible drift, and a high overall accuracy and reliability.

Two models are available with the same specifications except for the method of presetting. In the Model A309A the presetting means consists of five front-panel switches. Presetting in the Model A309B is accomplished by manual adjustment of five presetting wheels that are accessible through the hinged cover of the register used in this model.

SPECIFICATIONS

1. Input current for full-scale meter deflection — 1 x 10^{-3} to 3 x 10^{-9} ampere in twelve switch settings.
2. Polarity of input current — positive or negative, controlled by front-panel switch.
3. Current indicating means — 4½" meter.
4. Charge indicating means — 5-decimal-digit register and 2½" meter
5. Maximum charge indicating capacity — 99,999 units.
   Note: Each unit is equal to one coulomb multiplied by the numerical value of the full-scale current.
6. Maximum integrating time — 28 hours.
7. Integrating rate for full-scale current — 1 unit per second.
8. Method of presetting:
   Model A309A — five front-panel switches.
   Model A309B — five presetting wheels in register.
9. Accuracy (Indicating and integrating accuracy, based on full-scale current) — 1%.
10. Maximum drift — .01% per hour.
11. Maximum input voltage for full-scale current — 2 millivolts.
12. Minimum signal-source impedance for 1% accuracy — 1 ohm divided by numerical value of full-scale current.
13. Calibration — Internal reference current provided for each current range.
14. Power Input — 110–125 volts, 50-60 cps.
15. Dimensions — 19" wide x 8¾" high x 13¼" deep.
16. Mounting — standard 19" relay rack.
17. Weight — approximately 25 lbs.
18. Price: Model A309A — $1674.00.
    Model A309B — $1524.00.

ELCOR,—INC. • 1225 W. BROAD STREET • FALLS CHURCH, VA.
Telephone JEfferson 2-7718
A subsidiary of Fairfax Manufacturing Co., Inc.
Bulletin No. 24-1258

★ DIGITRON

TYPE DISPLAY

NOW MINIATURISED

FOR INSTANTANEOUS CLOSE-RANGE READOUT

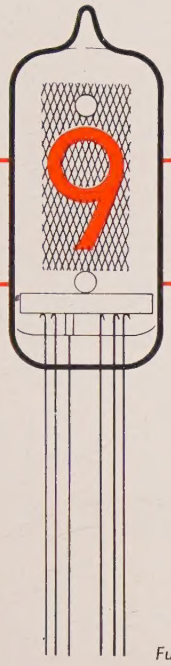

Full Size

THE GR. 10. W

In many digital applications it is often wasteful of valuable equipment space to employ the larger types of numerical indicators. The equipment design may call for a much more personalized type of display such as that required for control consoles, desk equipments, and similar layouts.

It is with these applications in mind that we introduce a newcomer to the DIGITRON range.

Whilst retaining the basic construction of the standard GR.10.G numerical indicator tube, the GR.10.W, being wire ended, can be soldered directly into the circuit and enables the designer to make full use of the display area by mounting these miniatures immediately adjacent to each other. This represents a considerable improvement in the readout facility at close range.

Like previous DIGITRONS, the numerical design of the GR.10.W is "human engineered" to eliminate readout error and again numbers are visible over wide viewing angles.

The miniature side-viewing GR.10.W with its robust construction, vivid presentation and its "no base" facility represents a big step forward in miniature display techniques.

Full Size

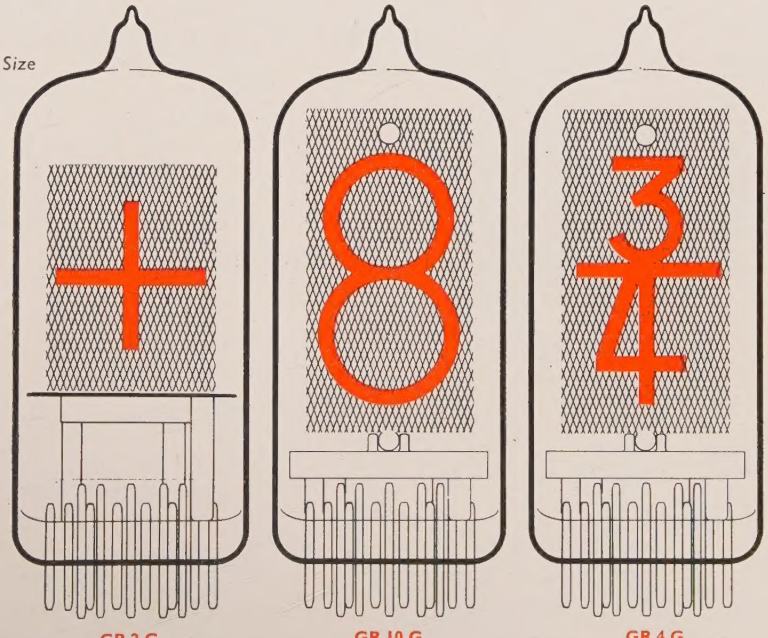

GR.2.G GR.10.G GR.4.G

OTHER SIDE-VIEWING DIGITRONS INCLUDE:

DIGITRON GR.2.G

Designed to display "plus" or "minus", this tube will find many applications in digital equipments requiring unambiguous sign display.

DIGITRON GR.10.G

The original DIGITRON—providing a clear numerical readout up to 50 feet over wide viewing angles. Ideal for audience readout.

DIGITRON GR.4.G

A recent introduction to the DIGITRON range, the GR.4.G displays $\frac{1}{4}$, $\frac{1}{2}$, $\frac{3}{4}$, or 1 in vivid numbers styled for easy readout. Suitable for applications concerned with monetary display.

May we send you full information on the DIGITRON range of display tubes. Write to: TECHNICAL SERVICE DEPT.

ETELCO

TUBE DIVISION
BEESTON, NOTTINGHAM

T E L ENGLAND

★ *Digitron is an Ericsson trade mark*

ETELCO LIMITED · HEAD OFFICE · 22 LINCOLN'S INN FIELDS LONDON W.C.2

NEW FROM TEXAS NUCLEAR CORP.

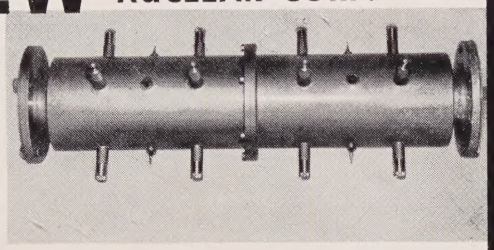

- For focusing an ion beam at large distances from the accelerator
- Cancels astigmatism produced by analyzing magnet
- Increases useful ion beam intensity

TEXAS NUCLEAR CORPORATION

P. O. Box 9267 Austin 17, Texas

WRITE DEPT. E

FOR SCINTILLATION & PROPORTIONAL COUNTING

Non-overloading Linear Amplifiers

MODELS 108 and 108 p

* GAIN–40,000, continuously variable
* RISE TIME–0.2 microsecond
* ACCEPTS + AND — PULSES

Tremendous Dynamic Range

EXCEEDS 1,000,000 (0.1 mV to 100 V)

Excellent linearity for small pulses in the presence of tremendous overloads that paralyze other amplifiers.
Model 108 P includes precision trigger type Pulse-Height Selector.

Model 413 Mercury relay precision sliding Pulser

The **one** pulser that fills **every need** of the Nuclear Physics Laboratory
0 to 100 Volts

10 full scale ranges from 1 mV to 100 volts
Fast rise and exponential decay of 1, 3, 10. 30, and 100 microsec simulate pulses from scintillation, proportional and Geiger counters.
Incorporates both manual control and precision motor drive.
The ideal instrument for precise calibration and test of pulse-height analyzers and other nuclear instrumentation.

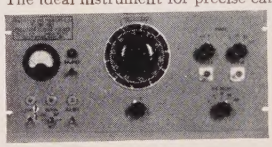

Window widths are determined AUTOMATICALLY, 10 × more ACCURATELY, 40 × FASTER than with conventional pulsers.

Model 108 Amplifier . . . . . $ 545.00
Model 108 P Amplifier (includes pulse-height selector) $ 595.00
Model 413 Precision Sliding Pulser . . . . . $ 630.00
Prices f.o.b. Silver Spring. Md.

RADIATION INSTRUMENT CO.

P.O. BOX 733 SILVER SPRING, MARYLAND, U.S.A.

NORTH-HOLLAND BOOKS

Analytical and Canonical Formalism in Physics

by

ANDRÉ MERCIER

Head of the Department of Theoretical Physics, University of Berne

6 × 9″ VIII + 222 pages Guilders 20.00 (40 s.)

THE CONTENTS

i LAGRANGIAN FORMALISM
ii LAGRANGIAN DENSITY
iii CANONICAL FORMALISM
iv CANONICAL FORM OF ELECTRODYNAMICS
v HAMILTONIAN DENSITIES
vi TRANSFORMATIONS
vii CANONICAL FORMALISM WITH VANISHING JACOBIAN DETERMINANT

Sole Agency for U.S.A.: Interscience Publishers Inc. – New York

NORTH-HOLLAND PUBLISHING COMPANY — AMSTERDAM

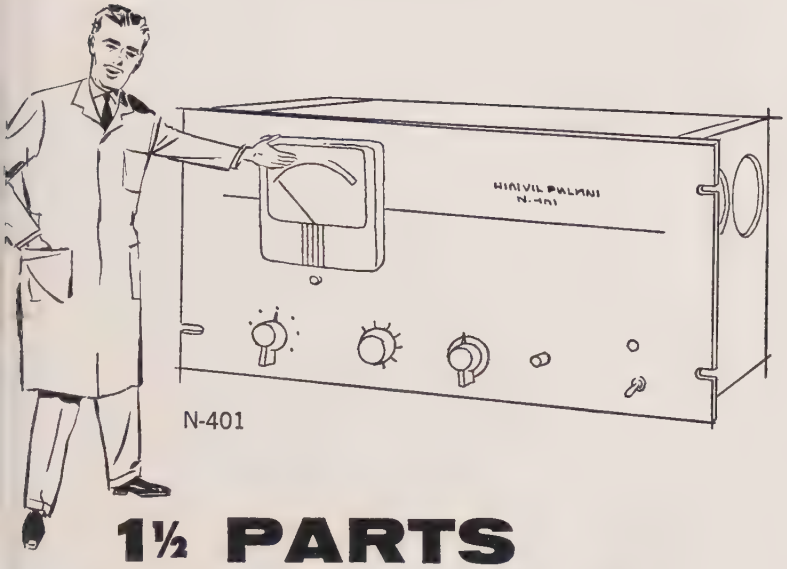

N-401

1½ PARTS PER MILLION LONG TERM STABILITY*

In Hamner's N-401 High Voltage Power Supply, stability is unexcelled, yet its measurement for the purpose of laying down specifications posed a great problem. The measurement was made by a leading university noted for their precision measurements of atomic constants by X-ray methods. The results obtained indicated a basic long term stability of *approximately 1½ parts per million per day — actually more stable than batteries. In the experiment, resistances used to attenuate the N-401's output had been aged and their values studied for over 50 years. Temperature was held constant to within .05°C.

Voltage:	500-1800 V, dual polarity
Current:	0-5 ma
Noise and Ripple:	Less than 1 mv rms at full output

The N-401 has been designed for use in scintillation and proportional counting systems, where other systems components offer the same degree of stability.

Some of Hamner's other instruments are described at the right. Each instrument has been designed to operate as an independent unit or in a system with other Hamner instruments.

Send For This Informative, Short-Form Catalog.

Hamner

Electronics Co., Inc.

Dept. 2, P.O. BOX 531, Princeton, N. J.
PEnnington 7-1320

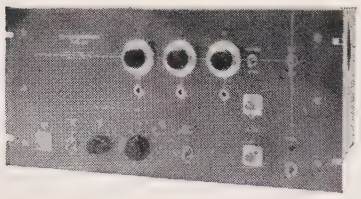

N-303 Amplifier with Single Channel Pulse Height Analyzer and Integral Discriminator

Amplifier

Gain:	10,000 at 2½ mc bandwidth
Gain Stability:	.25%/day
Hum and Noise:	Less than 2V peak to peak at full gain
Linearity:	Better than .1%, 0-100V, into 10K

Analyzer

Resolving Time:	1.3μs
Window Width Stability:	10mv/day, 0-10V width
Base Line Stability:	50mv/day, 0-100V
Linearity of Base Line:	Better than .1%, 0-100V

Both analyzer and discriminator may be operated simultaneously to record pulse height distribution and at the same time monitor background noise.

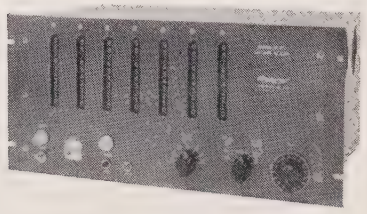

N-270 Scaler for High Speed and Automatic Systems

Resolution:	1 μs for pulse pairs
Preset Count:	10, 10^2, 10^3, 10^4, 10^5, 10^6, 10^7, 10^8
Discriminator:	—.25 to —5V or —50 to +100 volts

The N-270 may be used with a digital recorder for data print-out and can be gated on and off, recycled, etc., by the N-801 timer.

N-801 Electronic Timer

Accuracy:	.1%
Preset Time:	0.5, 1, 2, 5, 10, 20, 50, 100, 200, 500, or 1000 secs.

Timer will provide signals for gating N-270 scaler.

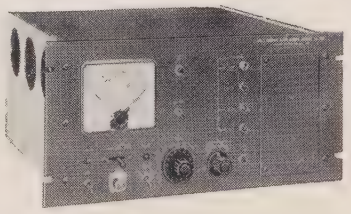

N-701C Log Count Rate Meter

Range:	1 to 10^5 CPS in 4 scales
Discriminator:	—50 to +100V or —.25 to —5 volts
Accuracy:	± 1% of log of count rate

Besides other models of the above mentioned units, Hamner also offers a complete line of GM, proportional and scintillation detectors with suitable preamplifiers for a variety of applications.

FIELD REPRESENTATIVES

RAYTRONICS COMPANY
Massachusetts,
New England States

A. B. EDWARDS
Eastern Pennsylvania

BEN Z. RUBIN CO.
Michigan, Indiana,
Ohio, Northern Illinois,
Wisconsin

W. A. BROWN & ASSOCIATES
Alabama, Delaware,
Florida, Georgia,
Kentucky, Maryland,
North & South Carolina,
Tennessee, Virginia,
Washington, D. C.

EARL LIPSCOMB ASSOCIATES
Texas, New Mexico,
Oklahoma, Arkansas,
Louisiana, Mississippi

H. E. RANSFORD CO.
Pennsylvania,
Northern West Virginia

LANDFEAR ENTERPRISES
Met. New York,
New Jersey

R C TESTING & CONTROL SYSTEM
Ontario, Quebec,
New Brunswick, Canada

McCARTHY ASSOCIATES
Arizona, California,
Nevada

EXPORT DEPT. 202 East 44th St., N. Y. C.
Cable: Henleysale RCA Teletype 210, N. Y. C.

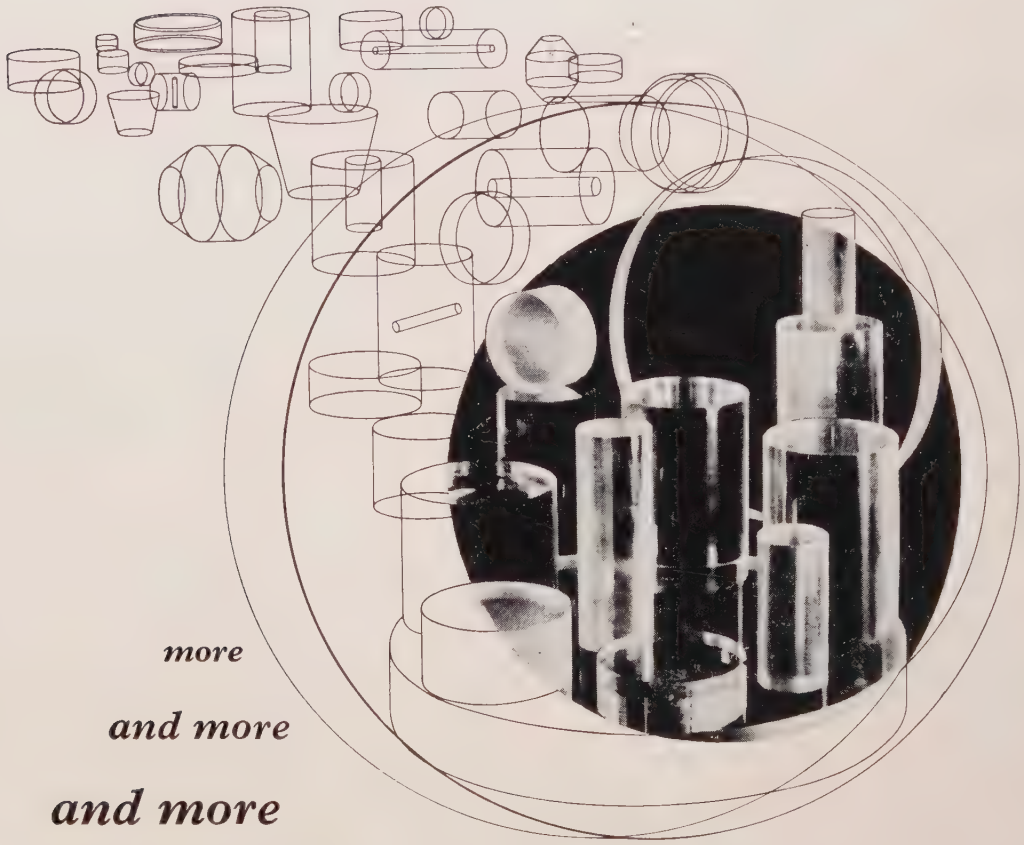

more

and more

and more

Scintillators

Nash & Thompson have now added Sodium Iodide, Caesium Iodide and Neutron Detectors to their extensive range of scintillators.

ORGANIC CRYSTALS. Anthracene, Stilbene, Terphenyl, in discs and cylinders.

PLASTICS. NATON-11 and NATON-136, high sensitivity, high transmission, based on either polyvinyl toluene or polystyrene. Available in discs, cylinders, ingots, foils, and filaments.

LIQUIDS. Ready made, sealed in glass containers to your specification, or in scintipaks

SCINTIPAKS. Accurately mixed dry constituents sealed in polythene envelopes, ready for dissolving in a suitable solvent as required.

CHEMICALS. Scintillation purity for making your own phosphors.

SODIUM IODIDE. Highest resolution, ready canned, in sizes up to 4″ dia × 3″ high, or 5″ dia × 2″ high.

CAESIUM IODIDE. In blocks up to 3″ dia × 3″ high.

Write or telephone for full information

Nash & Thompson LTD

Hook Rise, Tolworth, Surbiton, Surrey. Elmbridge 5252.

JSP 5689

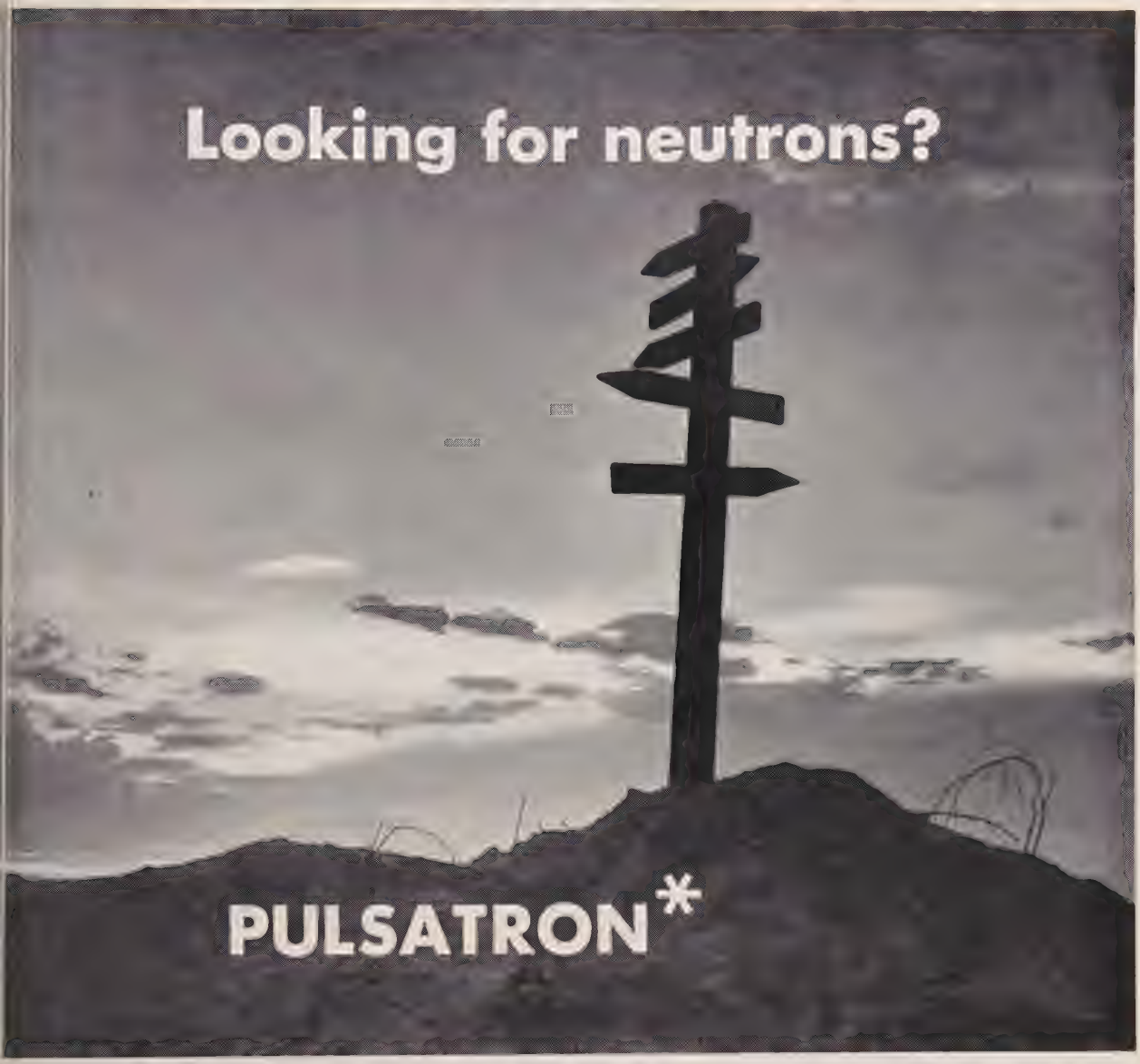

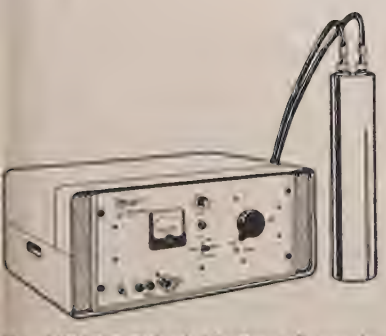

* the Kaman neutron source

small - lightweight - portable

10^7 neutron/pulse - nominal.
5 microseconds — pulse length.
Adjustable - 1-10 pulses/sec.
H^3 (d, n) He^4 reaction.
Accelerator Unit — 4" OD x 18" long.
Control Unit — 21¾" x 15¼" x 10½".

The NT-60-8 Pulsed Neutron Generator Assembly . . . an Exclusive Development by

KAMAN NUCLEAR
COLORADO SPRINGS, COLORADO
A Division of the Kaman Aircraft Corporation

Research and Development in Nuclear Weaponry and Instrumentation.

COMPACT 100 CHANNEL PULSE HEIGHT ANALYZER

The C.D.C. KICKSORTER

developed by Atomic Energy of Canada and manufactured by Computing Devices of Canada Limited

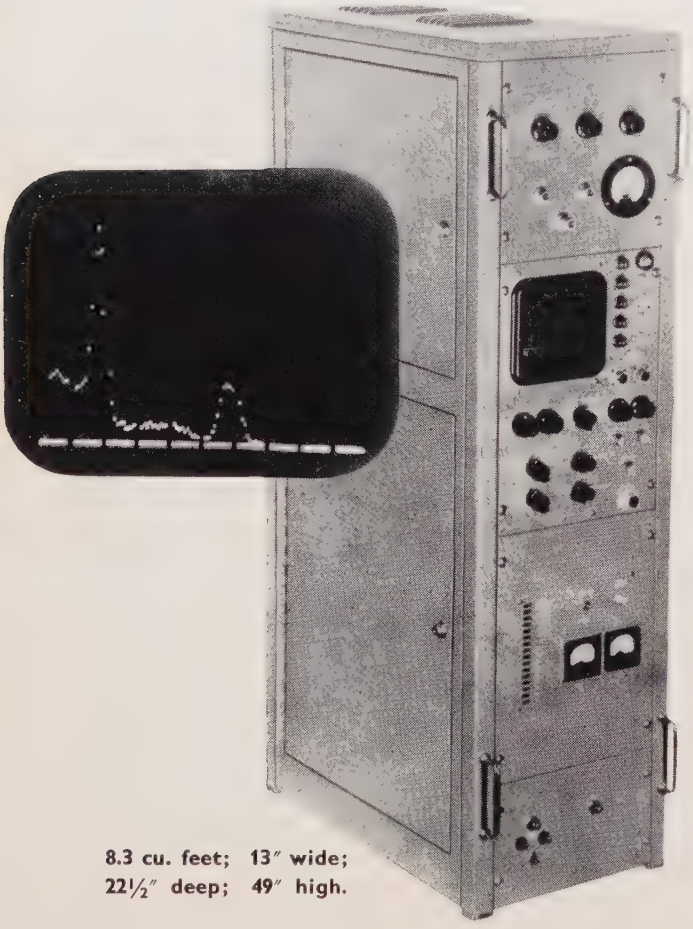

8.3 cu. feet; 13″ wide; 22½″ deep; 49″ high.

88% Transistorized

- Printed Circuitry
- Low Maintenance—High Reliability
- Compact—Semiportable
- Low Power Consumption—120 watts
- No Ventilation or Cooling problems

Highly Versatile

- Oscilloscope display
- Binary manual count readout allows the count on any channel to be displayed in digital form
- Accessory readout devices: photo recording camera, strip chart recorder, punch tape
- Magnetic core memory—65,535 counts can be stored per channel
- Permanent count storage—sixteen magnetic cores for each of the 100 channels

Bendix International

The "Chalk River Kicksorter", recently developed and based on designs and specifications prepared by Atomic Energy of Canada Ltd. is an extremely fast, accurate and versatile instrument.

The "Kicksorter" is designed to span random pulses of various amplitudes and shapes, sort them out according to amplitude into 100 channels, and store a record of the counted pulses in a magnetic core memory. A simple computer with its magnetic core memory and versatile data display system make it possible to observe the pulse amplitude spectrum as it accumulates or after it has accumulated.

In addition to its wide use in gamma spectroscopy, it has many applications in the fields of medical research, neutron time-of-flight studies, radioactive fallout studies, shielding studies, oil well and uranium logging, neutron activation analyses, measuring of radioactivity in humans and other uses.

The analyzer is designed so that information accumulated may be displayed or read out in various ways. Data may be observed on the oscilloscope, or information already accumulated in the memory core may be displayed on the screen, plotted on a strip chart recorder, or printed out in decimal form on an automatic printer.

Since the unit is highly versatile, it can be modified to accommodate most applications which require additional features.

For additional information, wire or write to:

Bendix International

DIVISION OF BENDIX AVIATION CORPORATION

205 E. 42ND ST., NEW YORK 17, N.Y., U.S.A. Cable Address: "BENDIXINT"

Sales Representatives for Great Britain

NUCLEAR ENTERPRISES (G.B.) LTD.

BANKHEAD MEDWAY, SIGHTHILL; EDINBURGH 11, SCOTLAND

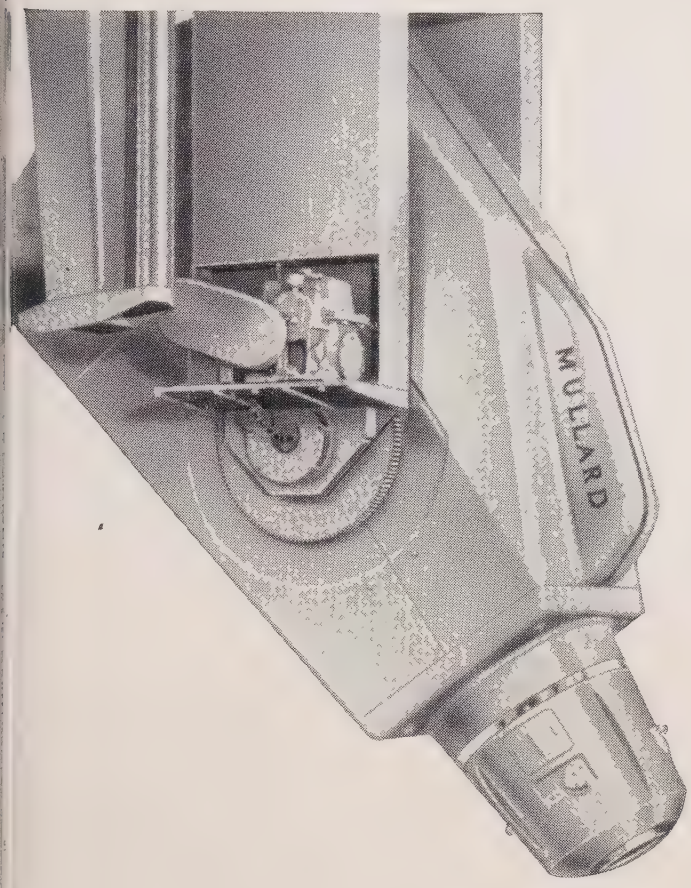

electron linear accelerators for research, industry and medicine

by Mullard Equipment Limited

Electron Linear Accelerators manufactured by Mullard Equipment Ltd. are the logical result of wide and detailed experience in this field. Machines for all types of applications are available, from the standard 4.3 MeV model to equipments specially built to meet individual requirements with electron beam energies up to 50 MeV.
The units are designed for continuous operation, ease of control and high reliability.

STANDARD MACHINE OPERATING AT 4.3 MeV

Mean power output at 500 pulses per second	850 W (electrons)
Maximum pulse repetition frequency.....	500 p.p.s.
Electron pulse length.....	1.65 microseconds
When used as an X-Ray source maximum X-Ray output is approximately.....	600 röntgens per minute at 1 metre

MULLARD EQUIPMENT LIMITED

Mullard House · Torrington Place
London W.C.1 · Tel: LANgham 6633

RESEARCH Now regarded as indispensable in many research laboratories Linear Accelerators can be fitted with supplementary heads to provide X-Rays or neutrons. Present day applications include investigation of properties of irradiated materials; preservation of food; basic studies on structure of organic molecules; modification of the properties of plastics.

INDUSTRIAL RADIOGRAPHY The compact accelerator design with wide range of movements and precision positioning enables radiographs of complicated heavy metal sections to be taken with minimum setting-up times. The high X-Ray output gives short exposure time and the extremely small (2mm) focal spot gives the highest possible definition. Penetration is sufficient to radiograph steel sections up to 12 inches thick.

MEDICAL THERAPY The use of Linear Accelerators for X-Ray and Electron Medical Therapy is well established. These machines give rapid treatment times with precisely defined fields and negligible 'penumbra' effects. Skin and exit dosages are minimised.

ME 664

INTERNATIONAL

advertise

YOUR NUCLEAR PRODUCTS IN

sell

YOUR NUCLEAR PRODUCTS

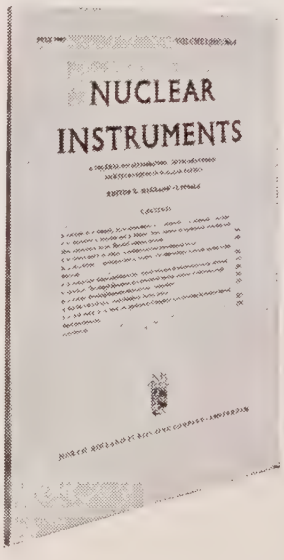

reap

YOUR NUCLEAR SALES
REWARDS

world wide

KEY NUCLEAR MANAGEMENT
NUCLEAR SCIENTISTS
NUCLEAR ENGINEERS
NUCLEAR PRODUCTION
PERSONNEL

SUBSCRIBE TO

you reach

THE WHOLE
NUCLEAR SALES WORLD IN

Entirely international in scope Nuclear Instruments and Methods is the one nuclear scientific journal that has an established subscription clientele throughout the whole world-where-ever nuclear men are at work—they want your nuclear products—they need your nuclear products—advertise in Nuclear Instruments and tell them WHAT – HOW – WHERE they can get your nuclear products

GO INTERNATIONAL WITH YOUR SALES PROGRAM TODAY WRITE

WILLIAM F. BAARS - ADVERTISING MANAGER NORTH-HOLLAND PUBLISHING COMPANY

P.O. BOX 103 – AMSTERDAM, HOLLAND

INTERNATIONAL

RIDL presents

the Complete Line of Nuclear Instrumentation

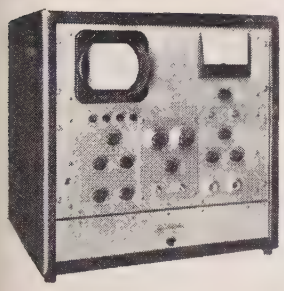

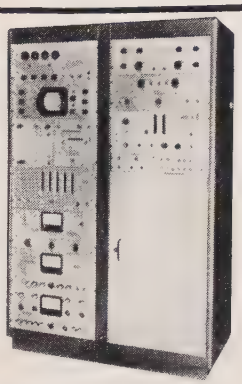

Analyzers Multi-Channel

RIDL offers the most complete line of Multi-Channel Analyzers ever offered by any manufacturer. From 100 channels to 2000 channels – from vacuum tube units to transistorized models, these are all STANDARD items. RIDL Multi-Channel Analyzers are presently in use in all AEC National Laboratories and other major nuclear research centers in the United States and abroad.

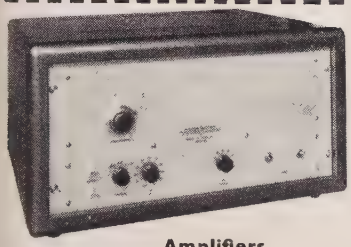

Amplifiers

From basic models to deluxe units with discriminators and high voltage power supplies, RIDL offers an amplifier that will fill your every requirement. Whether you want an Argonne, Brookhaven or Oak Ridge design, these are all manufactured by RIDL.

Scintillation Counters

RIDL offers a full line of scintillation counters designed to fit every requirement from basic probes to deluxe guaranteed resolution models. These units may be used to detect any type of radiation by simply inter-changing crystals.

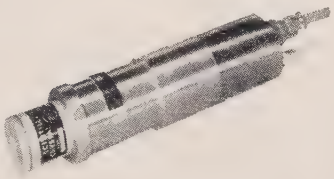

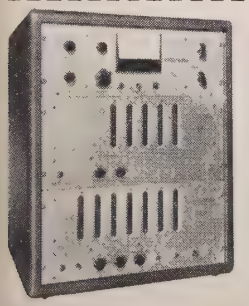

Scalers

RIDL manufactures the most complete line of scalers on the market today. From conventional vacuum tube units to completely transistorized models – from simple utility scalers to fully automated printing scaler systems, these are all STANDARD production items.

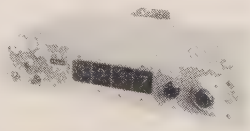

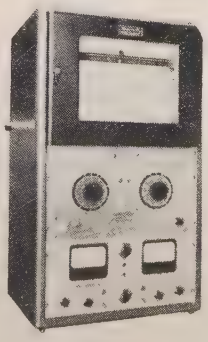

Spectrometers

A complete family of scintillation spectrometers is available from RIDL. From portable models to completely automatic recording systems, RIDL is the recognized leader in the design and manufacture of these units.

ALSO - -

- End Window Counters
- Gas Flow Counters
- Gas Sample Counters
- Cosmic Ray Counters
- PreAmplifiers
- Coincidence/Anti-Coincidence Analyzers
- Single Channel Analyzers
- Count Rate Meters
- Plug-In Counting Units
- Electronic Sweeps
- High Voltage Supplies
- Low Level Counting Systems
- Radiation Monitors
- Printers
- Recorders
- Reactor Control Instruments
- Pulse Generators
- Automatic Sample Changers
- Custom Equipment
- Electronic Timers
- Shields

RIDL is proud to present the most complete line of radiation detecting and measuring equipment ever offered by any manufacturer. From simple end-window Geiger tubes to deluxe guaranteed resolution scintillation detectors—from basic laboratory instruments to completely automated instrument systems, these are all STANDARD production items.

Whatever your radiation laboratory requirement may be, RIDL has the solution. Our staff is always available to answer your inquiries. Write today to Department MB for complete information.

RIDL INC.

Radiation Instrument Development Laboratory, Inc.

5737 South Halsted Street, Chicago 21, Illinois USA TRiangle 3-2345

Represented by: **INTERTECHNIQUE - 81, Rue Escudier - Boulogne-Billancourt (Seine)**

The place of the Particle Accelerator in Basic Research...

Radiation Effects in the Gaseous Phase—IX

Widespread study of the effects produced in organic and inorganic gases by high-energy particle bombardment is providing a better understanding of reaction kinetics, revealing new methods for chemical synthesis, and contributing to the new field of missile technology.

Organic Research

Complex organic molecules have been irradiated at low pressures to determine the number of dissociations per unit-energy input and to measure the lifetime of the resultant ions and free radicals. From such information, one can estimate the most probable location of the dissociation in long-chain hydrocarbons. Locating specific reactive groups at the ends of these chains permits the study of energy transfer along the chain. There is some evidence that random interactions will migrate to a weak molecular bond where chemical reaction occurs. Studies comparing ionic and free-radical mechanisms for energy transfer show that the ionic lifetimes are surprisingly long.

In addition to the gaseous phase alone, heterogeneous systems of gases or liquids and solids have been studied in relation to the catalysis of organic reactions. In such systems, these reactions occur under conditions where the reactive component is highly dispersed on a mineral support. It is believed that the products of the radiolysis of hydrocarbons may be changed under such conditions and the studies are bringing to light new methods of chemical synthesis.

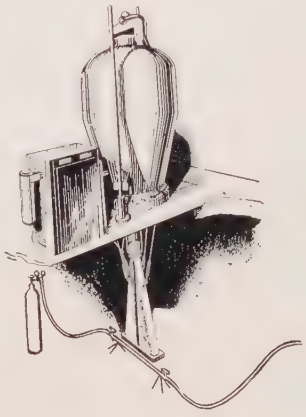

Inorganic Studies

In the inorganic field, studies of plasmas and gaseous reactions have been carried out by particle bombardment at pressures ranging from thousands of atmospheres down to near vacuum. The understanding of interactions between activated gases and of plasma stability at low ion concentrations is of extreme importance in a number of fields.

Recently, interest has grown in the possibility of using heavy-ion bombardment for producing moderate electron densities in gases to investigate reactions between plasmas and solid surfaces. This is of great importance in the missile field, since these missiles travel with sufficient velocity in the rarified upper atmosphere to produce a surrounding sheath of ions that can react with the missile skin to produce surface damage.

The study of reaction kinetics in gases by means of radiation is contributing to our understanding of industrial chemical processes based on gas-phase reactions. It also appears that knowledge of gaseous reactions may contribute to our presently incomplete understanding of liquid-state phenomena.

The Van de Graaff as a Radiation Source

One of the most versatile sources of radiation used in these studies is the Van de Graaff® particle accelerator. It can accelerate electrons, protons, and heavier ions, and it produces intense beams that are very homogeneous in energy and variable over a wide range of energies. Continuous or pulsed operation can also be provided, with pulses ranging in width from millimicroseconds to thousands of microseconds.

The beam intensities produced permit the use of these machines in studies requiring a high yield of reaction products. Because the energy and type of particle can be varied, it is possible to investigate linear energy transfer in a gas. The energy definition, considerably better than that obtainable with any other type of accelerator in the same energy range, and the applicability of pulsing techniques, make the Van de Graaff a precision instrument for the study of chemical reaction kinetics and the lifetime of the reactive components.

You are invited to visit the HIGH VOLTAGE ENGINEERING *exhibit at the 2nd International Exhibition on Peaceful Uses of the Atom, Geneva, Switzerland. On display: a 5.5-Mev Van de Graaff positive-ion accelerator; model of new Tandem Van de Graaff; and photomurals showing uses of* HIGH VOLTAGE *equipment.*

HIGH VOLTAGE ENGINEERING CORPORATION

BURLINGTON MASSACHUSETTS

High Voltage Servicing Company, Ltd.
London, England

High Voltage Engineering (Europa) N.V.
Amersfoort, The Netherlands

NUCLEAR INSTRUMENTS AND METHODS 6 (1960) 289–295; NORTH-HOLLAND PUBLISHING CO.

ENERGY DEPENDENT INSTRUMENTAL TIME DELAYS IN MILLIMICROSECOND DELAYED COINCIDENCE EXPERIMENTS

EKBAL BASHANDY†

Institute of Physics, Uppsala, Sweden

Received 13 November 1959

An experimental study of energy dependent time delays present in delayed coincidence measurements has been performed. The most important factor was found to be due to the time lag between the excitation of the scintillator and the appearance of the first few photoelectrons used to trigger the coincidence circuit. These time delays are of the order of 10^{-10} sec and may introduce serious systematic errors when submillimicrosecond lifetimes are to be measured by the centroid displacement method. It is shown that these errors can be eliminated by making use of an electron-electron coincidence spectrometer.

1. Introduction

The delayed coincidence technique is the most general method for the measurement of short nuclear lifetimes. But the lifetime of short lived excited states can also be determined from the electromagnetic transition probabilities for the inverse transition, measured by Coulomb excitation or by nuclear resonance scattering processes. These methods are complementary to the delayed coincidence technique, because, they are most suitable for large transition probabilities corresponding to very short lifetimes. However, the delayed coincidence technique is the only method that can be applied in the case of unstable isotopes.

In the last few years the delayed coincidence technique has been much improved, after the introduction of photomultiplier tubes having excellent light collection properties, high gain and reduced transit time spread. These tubes permit the use of shorter resolving times. Furthermore scintillators have been recently produced with shorter decay constants and improved light conversion efficiencies. By making use of these components, it is now possible to obtain resolving times less than 1 mμs. It will be shown below that lifetimes of the order of $\frac{1}{2}\tau_0$ of the resolving time can be measured with reasonable accuracy. This means that lifetimes $\geqslant 5 \times 10^{-11}$ sec are within the reach of the present day, delayed coincidence technique, at least for not too low transition energies.

When the lifetime of the excited nuclear level is comparable to or larger than the resolving time of the coincidence circuit, the shape of the delayed coincidence curve obtained by plotting the coincidence counting rate versus time delay, has a pronounced difference from a prompt coincidence curve. In such a case the halflife can generally be accurately determined from the exponentially decaying slope of the curve. Lifetimes shorter than the resolving time, can be determined from a careful comparison between the centroid position of the delayed coincidence curve for the cascade under investigation with respect to the centroid of the comparison delayed coincidence curve. This comparison curve should be obtained under identical conditions and the lifetimes should be known or known to be negligibly short (prompt curve). It may be shown that[1]) the difference between the time coordinate of the centroid positions corresponds to the difference in mean lifetime of the two nuclear levels involved i.e.

$$c - c_0 = \tau - \tau_0$$

† On leave from the Egyptian Atomic Energy Commission, Cairo, Egypt.

[1]) Z. Bay, Phys. Rev. **77** (1950) 419.

where c is the time coordinate of the delayed coincidence resolving curve under investigation and c_0 is the corresponding coordinate of the comparison curve, τ is the meanlife of the intermediate level and τ_0 is the known (or negligibly short) comparison lifetime. In practice however, it is difficult to find a suitable comparison curve corresponding to the same transition energies. The so called self comparison method[2]) presents a possibility of circumventing these difficulties. The self comparison method implies that the delayed coincidence curve is compared with its own "inverse". The latter is obtained by interchanging the order of the two detectors, such that if in the first measurement detector 1 responds to transition A and detector 2 to transition B, the inverse curve will correspond to transition B recorded in detector 1 and transition A in detector 2.

Great care should be exercised whenever the centroid shift method is applied. In the general case the position of the centroid is influenced by other factors than the lifetime of the intermediate level. Unless these contributions to the centroid shift are not properly taken into account, systematic errors will appear. These may easily be of the same order of magnitude as the nuclear lifetime to be measured.

It is the purpose of this paper to review the various "instrumental" contributions to the centroid shift. It will be shown that experimental conditions can be arranged such that these instrumental shifts will not affect the final result, which means that the ultimate limitations of the delayed coincidence method are due solely to the finite resolving time of the scintillation detectors, and to the statistical accuracy of the measurement.

2. Factors Affecting the Centroid Position

Two conditions have to be fullfilled if the centroid shift method is to be safely applied without any further refinement.

(i) There should be no admixture of coincidences apart from those which are of interest in the experiment. It is assumed that the background of random coincidences is subtracted. This background is preferrably determined on both sides of the coincidence resolving curve by introducing sufficiently large timedelays in the two channels.

(ii) The comparison curve should be obtained under exactly the same experimental conditions. This means that the comparison curve should correspond to the same energies dissipated in the scintillation crystal.

In a practical case it is generally difficult to satisfy those two conditions. It is easy to see that all admixtures of unwanted coincidences prompt or delayed will disturb the curve and affect the centroid position. In a complex decay such admixtures can hardly be avoided, unless good energy resolution is provided in both channels. But also in a single cascade difficulties occur, when the two cascading transitions are of nearly the same energy. In this case the delayed coincidence curve will be mixed up with its own inverse. Again good energy resolution is important in order to distinguish between the initial and the proceeding transitions.

The poor resolution obtainable with organic scintillation crystals contributes a severe limitation in the delayed coincidence technique. The resolution is much improved if a pair of magnetic beta ray spectrometer (fig. 1) is used for the energy selection. These spectrometers should have good resolution and high transmission. With the coincidence spectrometer one can measure the lifetime of a specified level in the presence of other transitions, prompt or delayed.

It is generally not possible to find a suitable comparison source. The coincidence spectrometer technique, however, is well suited for the self-comparison method. The inverse curve is easily obtained by interchanging the current settings in the two beta-ray spectrometers.

The comparison method implies that the centroid of the curve should coincide with the centroid of the comparison curve if the lifetimes are equal. In other words the centroid of a prompt curve should coincide with its own

[2]) R. E. Bell, R. L. Graham and H. E. Petch, Can. Jour. Phys. **30** (1952) 35.

inverse. This will, however, generally not be the case if the cascading transitions correspond to different energies, because there are certain energy dependent instrumental time delays. These energy dependent time delays are:

constant of the scintillator. Recent investigations indicate that the simple exponential decay is a very crude picture, but our present experiments indicate that it is a sufficiently good approximation for our purpose.

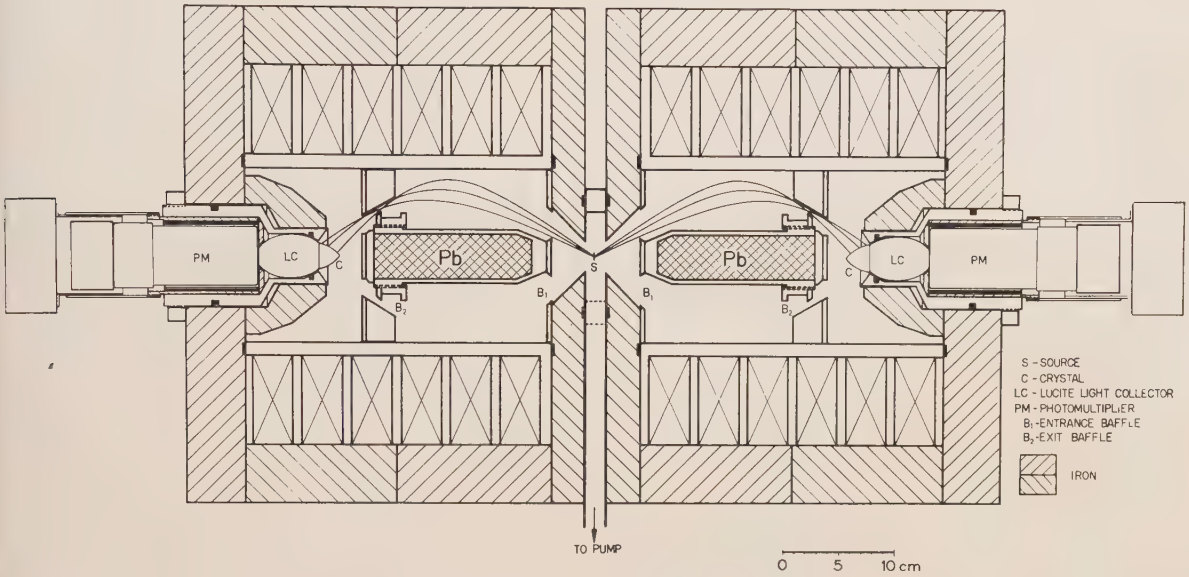

Fig. 1. Electron-electron coincidence spectrometer.

(a) The time lag between the absorption of the radiation or conversion electron in the crystal and the appearance of the first photoelectron.

If a magnetic spectrometer is used we have to consider two more contributions.

(b) The time of flight of the electron through the spectrometer and

(c) A possible influence of the magnetic field on the transit time of the photoelectrons through the photomultipliers.

In an earlier investigation[3]) we have shown that for our spectrometer (c) is negligibly small. This last factor will not be considered further.

Post and Schiff[4]) have derived an expression for the time elapsed between the excitation of the scintillator and the appearance of the first photoelectron. Their calculation is based on the assumption that the scintillation light flash can be expressed by a simple exponential decay

$$P_t = R\,(1 - \mathrm{e}^{-\lambda t})$$

where R is the total number of photoelectrons produced during the pulse, and λ is the decay

According to Post and Schiff one gets for the time lag t^1 between the excitation of the scintillator and the emission of the first Q photoelectrons

$$t^1 \approx \frac{Q}{R\lambda}\left[1 + \frac{Q+1}{2R} + \cdots\right].$$

Since $R >> Q$ we can neglect the second term within the brackets. Further $R \propto E$ and we may write

$$t^1 = \frac{Q}{R\lambda} = \frac{K}{E}.$$

An expansion in Taylor series give the difference in response time for the energies $E + \Delta E$ and E

$$t^1\,(E + \Delta E) - t^1\,(E) = -\frac{\Delta E}{E}\frac{K}{E} + \left(\frac{\Delta E}{E}\right)^2 \frac{K}{E} \quad (1)$$

where the constant K becomes

$$K = \frac{EQ}{R\lambda} = \frac{Q}{N\Omega\varepsilon\lambda}$$

[3]) J. Lindskog, E. Bashandy and T. R. Gerholm, to be published.

[4]) R. F. Post and L. I. Schiff, Phys. Rev. **80** (1950) 1113.

since $R = N\Omega\varepsilon E$ i.e. the average number of photons produced per keV absorbed in the scintillator (N), times the light collection efficiency of the light collector (Ω), times the photoelectric conversion efficiency (ε). The factor Ω has been experimentally determined to be 80 percent for the matched profile light collector system we use. Assuming for our plastic scintillator $N = 3$ photons/keV, ε equal to 5 percent and $1/\lambda = 3 \times 10^{-9}$ sec we get for K

$$K = Q \cdot 250 \times 10^{-10} \text{ sec.} \tag{2}$$

The values for N and ε are only approximate. Therefore the value of K can only be considered a rough estimate. We may assume that our coincidence circuit is triggered by the first few photoelectrons. But it is evident that for energies around a few hundred keV the centroid displacement due to the time delay expected by (2) will be range of 10^{-11} to 10^{-10} sec whenever the excitation energies differ by a few percent, it is therefore important to correct for, or eliminate these effects, which can be done to the first approximation with an interpolation (or extrapolation) method described below.

The second type of energy dependent instrumental time delays is due to the time of flight of the electrons through the spectrometer. The transit time of the electron can be written as

$$t_L(E) = \frac{L}{v} = \frac{L}{c} \frac{E_0 + E}{\sqrt{E^2 + 2E_0E}} \tag{3}$$

L is the length of the electron trajectory, v and E are the velocity and energy of the electron, c is the velocity of light. Thus the difference in transit time after applying the Taylor series for expansion is:

$$t_L(E + \Delta E) - t_L(E) = \\ = -\Delta E \frac{L}{c} \frac{E_0^2}{(E^2 + 2E_0E)^{\frac{3}{2}}} + \frac{\Delta E^2}{2} \frac{3E_0^2}{(E^2 + 2EE_0)^2} t_L(E) . \tag{4}$$

The first term in the right hand side of the equation can be eliminated in the case of interpolation (or extrapolation). However it is sometimes necessary to take even the second order term into consideration in case of short lifetimes[3]). The second order requires knowledge of the electron trajectory length which can be measured by the time of flight.

With the coincidence spectrometer one can also eliminate the effect of the energy dependent instrumental time delays by interpolation (or extrapolation) in the following manner. The method is slightly different in the case of comparison measurements and of self comparison measurements. Let us first consider comparison experiments. In this case two different sources are used, one of which has lifetime which is known or known to be negligibly short. One of the two cascading transitions is assumed to correspond to equal electron energies in the two cases. This applies for instance to beta-conversion electron cascades where a certain region of the beta spectrum is expected to lie within the momentum band pass of the spectrometer. It is then possible to select out of the continous beta spectrum an electron energy which is equal to the electron energy in the comparison experiment. In other words in one of the two channels the same current is used in both experiments, let this current setting correspond to an electron energy $E_{\text{const.}}$ Three coincidence resolution curves are now measured corresponding to the following combinations of electron energies

Same source $\begin{cases} E_{\text{const}} - E_1 \text{ centroid position } c'_1 \\ E_{\text{const}} - E_2 \text{ centroid position } c''_1 \end{cases}$

Comp. source: $E_{\text{const}} - E$ centroid position c_2 .

E_1 and E_2 are two different conversion electron energies corresponding to the same transition, e.g. K-conversion electrons and L-conversion electrons. let $E - E_1$ be ΔE_1 and $E - E_2$ be ΔE_2, ΔE_1 and ΔE_2 should be applied with signs. Let us further assume that the spectrometer accepting the first electron is connected to the negative side of the delay line while the opposite channel is connected to the positive side. It is easily seen that with this definition, the lifetime will have a positive sign. A negative experimental value means that the line cascading transitions take place in the opposite order in time.

From the three time resolution curves we now get the following two expressions for the differences in the time coordinates of the centroids:

$$c'_1 - c_2 = \tau_1 - \tau_2 - 2\Delta E_1 \left\{ \frac{1}{c} \frac{E_0^2}{(E^2 + 2E_0E)^{\frac{3}{2}}} + \frac{K}{E^2} \right\} + \\ + 2(\Delta E_1)^2 \left\{ \frac{3E_0^2}{2(E^2 + 2E_0E)^2} t_L + \frac{K}{E^3} \right\} \quad (5)$$

$$c''_1 - c_2 = \tau_1 - \tau_2 - 2\Delta E_2 \left\{ \frac{1}{c} \frac{E_0^2}{(E^2 + 2E_0E)^{\frac{3}{2}}} + \frac{K}{E^2} \right\} + \\ + 2(\Delta E_2)^2 \left\{ \frac{3E_0^2}{2(E^2 + 2E_0E)^2} t_L + \frac{K}{E^3} \right\}. \quad (6)$$

t_L is the transit time of the electron through the spectrometer and t_L is given by eq. (3). Thus finally we get:

$$\tau_1 - \tau_2 = \frac{(c'_1 - c_2)\ \Delta E_2 - (c''_1 - c_2)\ \Delta E_1}{\Delta E_2 - \Delta E_1} + \\ + 2\Delta E_1 \cdot \Delta E_2 \left\{ \frac{3E_0}{2(E^2 + 2E_0E)^2} t_L + \frac{K}{E^3} \right\}. \quad (7)$$

If one of the two τ's is known the second can be determined from (7). In the first order approximation we neglect the last term. In this approximation the result is independent of L and K. It sometimes becomes necessary to take into account the second order term. This correction, however, is quite small for reasonable values of $\Delta E_1 \cdot \Delta E_2$, and for this reason rough estimates of L and K are generally sufficient. Moreover, since L may be considered as known (see below) the equations above may be used to determine the appropriate value of K.

Let us now consider the closely related case of self comparison measurements. In this case we measure four resolution curves corresponding to

direct measurement $\begin{cases} E - E_1 \text{ centroid position } c_1 \\ E - E_2 \text{ centroid position } c_2 \end{cases}$

inverse measurement $\begin{cases} E_1 - E \text{ centroid position } c'_1 \\ E_2 - E \text{ centroid position } c'_2 \end{cases}$.

Expressions similar to (5) and (6) apply to $c_1 - c'_1$ and $c_1 - c'_2$ with the only exception that in this case $\tau_2 = \tau_1$ and we get

$$2\tau = \frac{(c_1 - c'_1)\ \Delta E_1 - (c_2 - c'_2)\ \Delta E_2}{\Delta E_1 - \Delta E_2} + \\ + 2\Delta E_1 \cdot \Delta E_2 \left\{ \frac{3E_0}{2(E^2 + 2E_0E)^2} t_L + \frac{K}{E^3} \right\}. \quad (8)$$

The self comparison method has the obvious advantage that it doubles the shift and therefore increases the accuracy and reduces the ultimate limitations. It is generally assumed that the position of the centroid of a curve can be determined to within $\frac{1}{10}$ of the full width at half maximum. The self comparison method thus allows us to determine lifetimes down to about $\frac{1}{20}$ of the half width.

3. Experimental Arrangement

In order to check the validity of the expressions above and to measure the value of K and L an electron-electron coincidence spectrometer[5]) was used. Magnetic momentum selection takes place in two halves of the spectrometer, and therefore good resolution is provided in both channels. For these measurements a coincidence arrangement[6]) of the fast-slow type was used. Pulses are taken from the photomultiplier anodes and are fed via equalizing circuits through a variable helical delay line to the fast coincidence unit. As detectors, RCA 6810 A photomultipliers were used, normally operated at 2000 volts. These are provided with plastic scintillators and lucite light collectors machined to a profile to obtain maximum light collection and minimum time spread of the photons. The source used was Hg^{203}, obtained from Harwell as a chloride. The active material after vacuum evaporation onto an aluminum foil 2 mg/cm² was covered with zapon film (15–20 μg/cm²) in order to prevent contamination in the spectrometer due to evaporation. Since the decay scheme concerned (fig. 2) is very simple, contributions due to other transitions are not present, for this reason the baffles of the spectrometers were opened to increase the counting rate. The resolution was 4% for the

[5]) T. R. Gerholm, Rev. Sci. Instr. **26** (1955) 1096.

[6]) R. E. Bell, Beta and Gamma ray spectroscopy (Editor Kai Siegbahn) (North Holland Publishing Company, Amsterdam, 1955) Ch. XV.

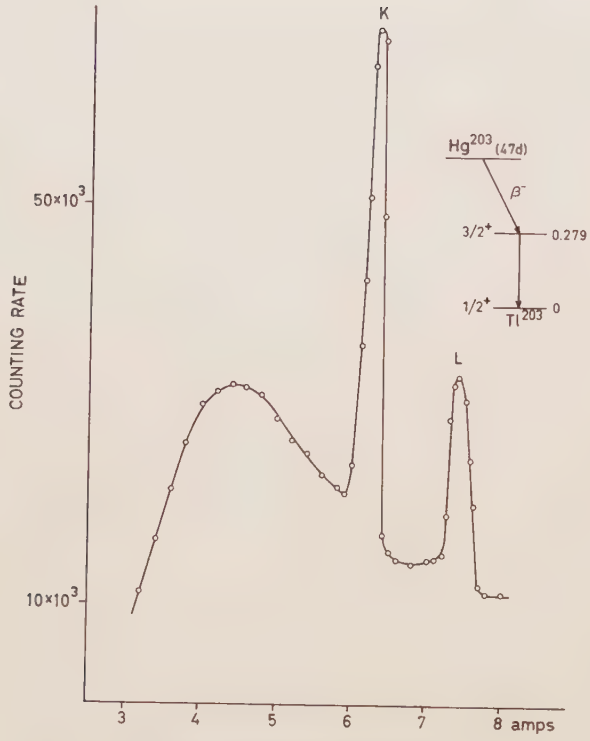

Fig. 2. Beta spectrum of Hg^{203}.

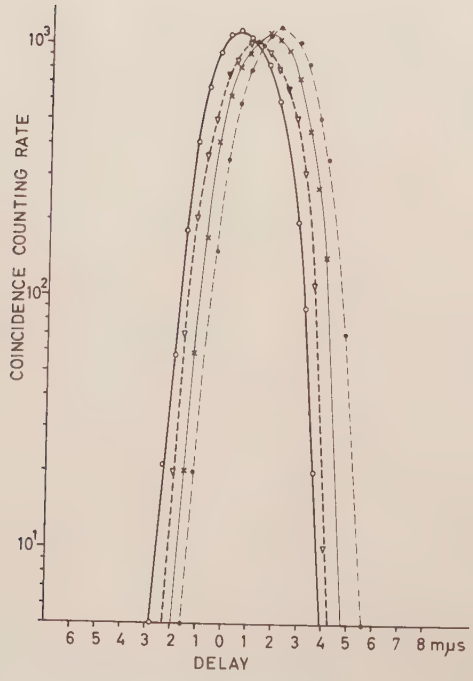

Fig. 3. Plot of delayed coincidences between electrons from different parts of the beta spectrum and the K-conversion electrons of the 279 keV transition in Tl^{203}.

K-conversion electron of the 279 keV and 3 coincidences per second were obtained. The resolving time of the coincidence unit was set to 3 mμs. Different energies from the β-transitions were focused in one half of the spectrometer, while the other half was triggered by the 279 keV conversion electrons. Typical resolution curves are shown (fig. 3). Throughout, the experiments were carried on under these conditions, and a large number of coincidence were recorded to secure a high degree of statistical accuracy. According to equations (1) and (4) the value of K was found to be 3100×10^{-10} keV sec and L 29 cm. This K value is substantially larger than the theoretical value given above. It was felt that the main reason for this discrepancy was due to bad light collection and to poor focusing of the photo electrons. A further indication that the detector system was not operated under optimum conditions was obtained from observations of the exceptionally bad resolution in the scintillation pulse height spectrum, for example, in the case of Cs^{137} K-conversion electrons we obtained a relative halfwidth of 40 percent. It was decided to improve the optical conditions and to adjust carefully the focusing potential in the photomultiplier tube. The use of a more transparent, high viscosity silicone oil together with a careful readjustment of the electron focusing voltage was quite effective in improving the resolution. We finally obtained a value of 17 percent for the caesium line. Another set of resolution curve determinations have been carried out under the conditions of the new arrangement, from which values for K and L were measured to be 840×10^{-10} and 29 cm respectively.

4. Conclusion

The experimental instrumental delay time due to various energy differences focused in the two spectrometer halves are summarized in fig. 4. The two curves were extrapolated to $\Delta E = 0$. Curve A gives the values $3133 \pm 310 \times 10^{-10}$ keV sec for K and 29.5 ± 1.2 cm for L, while curve B gives the values $840 \pm 90 \times 10^{-10}$ keV sec and 29.0 ± 1.5 cm for K

and L respectively. The values of electron trajectory in both experiments show good agreement and are also in agreement with direct measurement based on photographic ray tracing

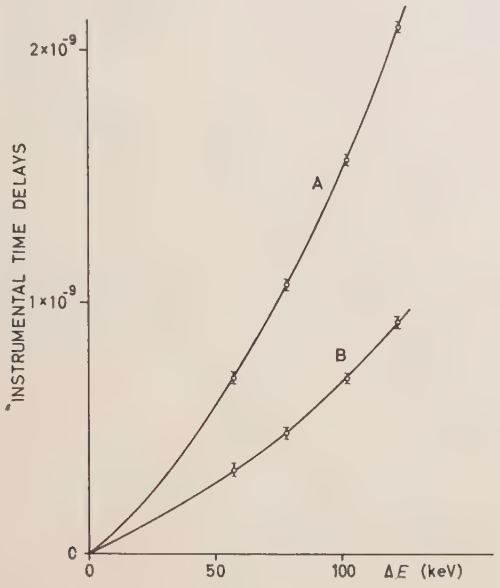

Fig. 4. The instrumental timedelay as a function of the energy difference between the electrons from different parts of the beta spectrum and the K-conversion electrons of the 279 keV transition in Tl^{203}.

of the electron trajectories in the spectrometer. (The source to detector distance is 23 cm.)

The large improvement in the value of K obtained after careful adjustment of the detector system illustrates the importance of these factors in delayed coincidence experiments. The lower value of K obtained experimentally should be compared to the theoretical estimate given in (2). Our experimental results indicate a value of Q of the order of 3, i.e. approximately three photoelectrons required to trigger the coincidence circuit. This is a quite reasonable value since the average number of photoelectrons produced during the "acceptance time constant" of the coincidence circuit, is of the same order of magnitude as may be seen as follows:

$$dp/dt = \lambda R\, e^{-\lambda t} . \qquad (9)$$

The acceptance time constant is the time interval under which the coincidence circuit when triggered on one side is ready to transmit a pulse presented in the opposite channel. This time is at 90 percent coincidence efficiency about $\frac{1}{3}$ of the resolving time (= full width at half maximum of the resolution curve). In our case we get for the acceptance time $\tau \approx 1$ mμs. From (9) we get by integration for the total number of photons produced during the time T_A

$$Q \approx 0.28\, R .$$

Using again $R = N\varepsilon\Omega E$ with the same values as before and for E about 100 keV as an average value for the energies used in the present experiment we get

$$Q = 0.28 \times 3 \times 0.05 \times 0.80 \times 100 = 3.4$$

in agreement with our experimental value for Q. Since

$$K = \frac{EQ}{R\lambda} = \frac{E \times 0.28\, R}{R\lambda} .$$

we get

$$K_{\text{theor.}} = 900 \times 10^{-10}\ \text{keV sec.}$$

The fact that our experimental results agree with the theoretical one shows that no energy dependent time delays other than these considered here are of importance. Our final conclusion is therefore that the origin and nature of the instrumental time delays is fully understood. The energy dependent instrumental time delays do not contribute to the errors in the measurements. Therefore the ultimate limitations in delayed coincidence measurements are set by the finite time resolution of the scintillation detectors and by the statistical accuracy.

Acknowledgment

The author is greatly indebted to Professor Kai Siegbahn for his encouragement and stimulating interest in this work. Grateful thanks to Docent T. R. Gerholm for his suggestions and discussions in all phases of the problem, and to fil. lic. J. Lindskog for his helpful participation.

NUCLEAR INSTRUMENTS AND METHODS 6 (1960) 296–300; NORTH-HOLLAND PUBLISHING CO.

UNTERSUCHUNGEN AN EINER ANORDNUNG ZUR MESSUNG DER NUKLEONENKOMPONENTE DER KOSMISCHEN STRAHLUNG

W. LOTZ†, A. SITTKUS und W. HASSLER

Physikalisches Institut der Universität Freiburg, Freiburg im Breisgau

Received 16 November 1959

A description is given of the Neutron Intensity Monitor on the Schauinsland near Freiburg im Breisgau, Germany. By adding 60 boron-10-detectors to the Standard-Pile-Geometry designed by Simpson *et al.* it was possible to reduce the statistical error from 0.46 to 0.29% for the hourly mean. The barometric pressure coefficient was $0.755 \pm 0.010\%$ mbar^{-1} in 1957 and 0.73 ± 0.02 in 1958. The median rigidity of the primaries is estimated to be 18 GV. A method is suggested by which it should be possible to shift the median to lower rigidities.

1. Beschreibung der Apparatur

Im Rahmen des Geophysikalischen Jahres wurde 1957 auf dem Schauinsland bei Freiburg im Breisgau (8° E, 48° N, geomagnetische Breite 49° N, 1200 m, 880 mbar) eine Apparatur zur Registrierung der Nukleonenkomponente der kosmischen Strahlung gebaut (Fig. 1). Die mittlere Zählrohrlage und die Bleianordnung entsprechen dem Simpson'schen Standard[1]), doch wurde durch Einbau weiterer 60 Zählrohre ober- und unterhalb des Bleiabsorbers die registrierte Teilchenzahl erhöht[2]).

† Jetzt im Max-Planck-Institut für Physik und Astrophysik, München.

Verwendet wurden Bortrifluorid-Zählrohre mit angereichertem Bor-10 (96%). 56 Glaszählrohre mit Graphit-Aussenkathode stellten wir selbst her[3]), 16 Messingzählrohre wurden von N. Wood, Chicago, bezogen[1]). Die Glaszählrohre haben folgende Daten (Messingzählrohre in Klammern): Aussendurchmesser 35 (38) mm, Innendurchmesser 33 (36.5) mm, aktive Zählrohrlänge 100 (87) cm, Zähldraht-

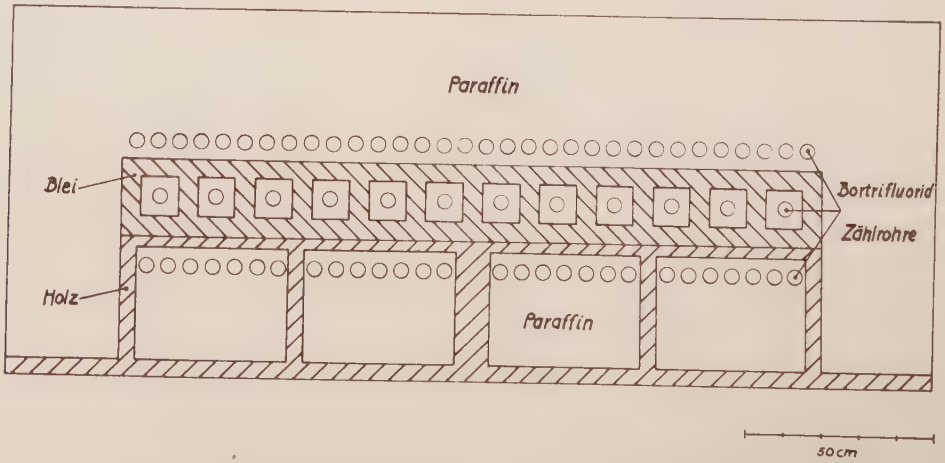

Fig. 1. Längsschnitt durch den erweiterten Blei-Paraffin-Messblock.

[1]) J. A. Simpson, Cosmic Radiation Neutron Intensity Monitor (University of Chicago, 1955).

[2]) W. Lotz, Dissertation. Universität Freiburg iBr. (1957).

[3]) W. Lotz, Diplomarbeit. Universität Freiburg iBr. (1956).

Tabelle 1

Gemessene Zählrate I_m in Abhängigkeit von der Totzeit des Zählgerätes. Nur 6 Glaszählrohre der mittleren Zählrohrlage sind eingeschaltet (Nulleffekt 1.64 s^{-1}).

Totzeit ± 2%	28	42	61	130	280	590	1300	3000	μs
Gemessene Impulszahl	13.20	12.95	12.69	12.12	11.52	10.90	10.61	10.40	s^{-1}
Neutronenzählrate	11.57	11.32	11.06	10.50	9.92	9.33	9.11	9.10	s^{-1}
Relative Neutronenzählrate	1.270	1.244	1.215	1.154	1.090	1.026	1.001	1	
Mittlere Lebensdauer der Neutronen	138	149	206	279	250	218			μs
Wahrscheinlicher Fehler der mittleren Lebensdauer	7	10	12	25	30	100			μs

durchmesser 25 (25) μm, Fülldruck 600 (450) Torr bei 0° C, Ansprechwahrscheinlichkeit für thermische Neutronen 26 (21)%, Nulleffekt 16 (< 1) min^{-1}.

2. Bestimmung der statistischen Schwankung

Durch die Erweiterung der Standard-Anordnung hat sich die Impulszahl bei 28 μs Totzeit um einen Faktor 4 erhöht. Da ein Primärteilchen im Blei einen Schauer von Verdampfungsneutronen erzeugt[4]), wird wegen der endlichen Lebensdauer der Neutronen und der grossen Zahl der Zählrohre die Wahrscheinlichkeit hoch, dass von einem Schauer mehr als ein Neutron registriert wird. Die mittlere Lebensdauer dieser Neutronen in kleinen Paraffinblöcken mit einzelnen Zählrohren wurde von verschiedenen Autoren zu 140 bis 160 μs bestimmt[4–8]), für einen unendlich ausgedehnten Paraffinblock sind etwa 210 μs zu erwarten[9]).

Zur Bestimmung der Zahl der kohärenten (nicht statistisch unabhängigen) Neutronen wurde die Totzeit des Zählgeräts variiert und die in Tab. 1 wiedergegebene Messreihe erhalten. Dabei wurden mit Hilfe eines parallel laufenden Zählgeräts mit konstanter Totzeit die Impulszahlen in erster Näherung auf zeitliche Schwankungen korrigiert. In Zeile 2 ist der erhaltene Mittelwert für jeweils 45 min Messzeit angegeben. Die Impulszahlen wurden mit $N = n \exp(NT)$ auf Zählverluste an inkohärenten Teilchen korrigiert (N = wahre Zählrate, n = gemessene Zählrate, T = Totzeit) und der Nulleffekt abgezogen (Zeile 3). Bei 3 ms nimmt die Neutronenzählrate nicht mehr ab, die dann noch registrierten Neutronen sind also inkohärent.

In einem homogenen Medium sollte die kohärente Neutronenintensität I exponentiell mit der Zeit t abnehmen

$$I = I_0 \exp(-t/\tau) \qquad (1)$$

(τ = mittlere Lebensdauer der Neutronen). Sei J_i die integrale kohärente Zählrate bei einer Totzeit T_i, so ist

$$J_i \propto \int_{T_i}^{\infty} I \, dt = I_0 \tau \exp(-T_i/\tau) \, . \qquad (2)$$

Da Ereignisse mit 3 und mehr kohärenten Neutronen seltener als solche mit 2 kohärenten

[4]) M. A. Collins, Nuovo Cimento **10** (1958) 428.

[5]) G. Cocconi, V. Cocconi-Tongiorgi and M. Widgoff, Phys. Rev. **79** (1950) 768.

[6]) G. Cocconi and V. Cocconi-Tongiorgi, Phys. Rev. **84** (1951) 29.

[7]) K. W. Geiger, Canad. J. Phys. **34** (1956) 288.

[8]) K. W. Geiger and D. C. Rose, Canad. J. Phys. **32** (1954) 498.

[9]) S. Glasstone and M. C. Edlund, The Elements of Nuclear Reactor Theory (D. Van Nostrand Co, Princeton, (1957).

TABELLE 2

Gemessene Zählraten für verschiedene Zählrohrkombinationen bei 28 μs Totzeit des Zählgerätes. Die relative Neutronenzählrate ist bezogen auf die jeweilige Zählrate bei 3 ms Totzeit. I_o: 16 Glaszählrohre mit 4.36 s^{-1} Nulleffekt; I_m: 6 Glaszählrohre mit 1.63 s^{-1} Nulleffekt; I_u: 14 Glaszählrohre mit 3.81 s^{-1} Nulleffekt.

Kombination	I_o	I_m	I_u	I_{om}	I_{ou}	I_{mu}	I_{omu}	
Neutronenzählrate	17.37	11.80	13.32	27.54	29.57	23.63	38.62	s^{-1}
Relative Neutronenzählrate	1.381	1.270	1.318	1.524	1.521	1.485	1.662	
Inkohärente Neutronen	72	79	76	66	66	67	60	%

Neutronen sind[4]), vernachlässigen wir die Tatsache, dass auch auf das zweite Neutron eine Totzeit T_1 folgt. Man erhält aus (2) die mittlere Lebensdauer

$$\tau = \frac{T_2 - T_1}{\ln (J_1/J_2)}. \qquad (3)$$

Die nach dieser Formel berechneten Werte wurden in Zeile 5 der Tab. 1 eingetragen, die kohärente Zählrate J_1 ist dabei gleich der relativen Zählrate minus 1. In der letzten Zeile ist der wahrscheinliche Fehler der so errechneten "effektiven Lebensdauer" angegeben. (Innerhalb der Fehlergrenzen ergeben sich für die drei Zählrohrlagen gleiche effektive Lebensdauern.) Da die effektive Lebensdauer wegen des inhomogenen Aufbaus stark variiert, ist es nicht möglich, die Anzahl der kohärenten Neutronen für sehr kleine Totzeit zu extrapolieren.

Die mit der Apparatur gemessenen Neutronenzählraten sind in Tab. 2 wiedergegeben. Dabei bedeutet I_o, I_m, I_u die Zählrate in der oberen, mittleren bzw. unteren Zählrohrlage. Sind obere und mittlere Zählrohrlage zusammengeschaltet, so ist die Zählrate mit I_{om} bezeichnet, entsprechend ergeben sich I_{ou}, I_{mu} und I_{omu}. Die Messzeit betrug wieder 45 min, eine Korrektur auf Schwankungen der Intensität war nur begrenzt möglich. Die Zahl der inkohärenten Neutronen in Prozent ist gleich dem Reziproken der relativen Neutronenzählrate, die auf die korrigierte jeweilige Zählrate bei 3 ms Totzeit bezogen ist. Die Summe $I_o + I_m + I_u$ ist grösser als I_{omu}, dasselbe gilt für beliebige andere Kombinationen. Bei sehr kleiner Totzeit ist zu erwarten, dass sich bei allen Kombinationen stets die Differenz 0 ergibt.

Durch Wahl einer geeigneten mittleren effektiven Lebensdauer (50 μs) für den Totzeitbereich von 0 bis 28 μs gelingt es, alle Differenzen innerhalb der zweifachen Standard-Abweichung (1.6%) zu 0 zu machen (Tab. 3).

Die Erweiterung des Standard-Messblocks von 12 Messingzählrohren auf 56 Glas- + 16 Messingzählrohre brachte eine Erhöhung der Neutronenzählrate bei 28 μs Totzeit von 18 auf 77 s^{-1}, während die Zahl der in den Zählrohren absorbierten Neutronen von 21 auf 100 s^{-1} zunahm. Dagegen wurde die Zahl der registrierten inkohärenten Ereignisse nur von 14

TABELLE 3

Berechnete Zählraten für verschiedene Zählrohrkombinationen bei sehr kleiner Totzeit (0 μs) des Zählgeräts. Die mittlere Lebensdauer der Neutronen für den Totzeitbereich von 0 bis 28 μs wurde zu 50 μs angenommen.

Kombination	I_o	I_m	I_u	I_{om}	I_{ou}	I_{mu}	I_{omu}	
Berechnete Zählrate	21.0	13.7	15.7	34.6	37.2	29.4	50.2	s^{-1}
Standard-Abweichung	0.1	0.1	0.1	0.2	0.2	0.2	0.3	s^{-1}
Relative Neutronenzählrate	1.667	1.472	1.556	1.917	1.912	1.848	2.160	
Inkohärente Neutronen	60	68	64	52	52	54	46	%

auf 46 s^{-1} erhöht, das entspricht einer statistischen Schwankung des Stundenmittelwertes von 0.45 bzw. 0.25%. Eine direkte Bestimmung der statistischen Schwankung durch Vergleich der beiden Apparaturhälften ergab 0.46 bzw. 0.29%[10]).

Durch Einbau weiterer Zählrohre lässt sich die statistische Schwankung nicht mehr nennenswert herabsetzen. Geht man von der Zählrate I_{ou} aus und schaltet die mittlere Zählrohrlage dazu, so ergibt sich, dass nur 29% von I_m inkohärent zu I_{ou} sind (Tab. 3). Da der Prozentsatz der inkohärenten Neutronen mit wachsender Zahl der Zählrohre abnimmt, können weitere Zählrohre noch mit maximal 29% ihrer Zählrate zur Verbesserung der Statistik beitragen. Wenn die Zahl der Zählrohre verdoppelt wird (auf 144 Stück), so kann sich die Zählrate höchstens ebenfalls verdoppeln, die Zahl der inkohärenten Ereignisse aber wird nur wenig zunehmen und die statistische Schwankung kann um maximal 10% kleiner werden.

Auch eine Verstärkung des Blei-Absorbers ist nicht sehr wirkungsvoll. Im Messblock reagieren etwa 70% der einfallenden Nukleonen mit dem Absorber. Durch eine Verdopplung ohne Vergrösserung der Grundfläche des Messblocks liesse sich die Zahl der erfassten Teilchen bestenfalls um 30% erhöhen, die statistische Schwankung würde sich höchstens um 10% verkleinern lassen.

3. Der Barometereffekt

Nach Simpson *et al.*[11–13]) ist die mittlere Absorptionslänge der Nukleonenkomponente in Luft für atmosphärische Tiefen $x > 700$ g cm^{-2} in erster Näherung unabhängig von dieser und von der geomagnetischen Breite gleich 140 g cm^{-2}. Daraus folgt, dass der Barometereffekt innerhalb dieser Näherung unabhängig vom Ort gleich 0.728 ± 0.015% $mbar^{-1}$ ist. Eine Zusammenstellung von Webber[14]) ergibt dagegen, dass der Breiteneffekt bei einer unteren Grenze der magnetischen Steifigkeit von 2 bzw. 15 GV von 1.74 auf Meeresniveau (1030 g cm^{-2}) auf 2.41 bei $x = 680$ g cm^{-2} ansteigt. Daraus folgt eine Breitenabhängigkeit der mittleren Absorptionslänge (und damit auch des Barometereffekts) von 13%, während diese Breitenabhängigkeit nach Simpson[12]) bei $x = 650$ g cm^{-2} schon kleiner als etwa 7% sein sollte und zu grösseren Tiefen hin noch kleiner wird.

Da also mit einer starken Abhängigkeit des Barometereffektes vom Messort zu rechnen ist, muss er für jede Apparatur neu bestimmt werden. Eine normale Korrelationsrechnung zu seiner Bestimmung führt nicht mit der gewünschten Genauigkeit zum Ziel[11]), da die Primärintensität während der Messzeit 1957 und 1958 wegen der Sonnentätigkeit stark schwankt. Wir haben deshalb die Tagesmittelwerte der Zählrate näherungsweise mit 0.73% $mbar^{-1}$ logarithmisch korrigiert und dann die Differenzen aufeinanderfolgender Tage mit den entsprechenden Druckdifferenzen linear korreliert[10]). Bei diesem Verfahren wirkt sich ein zufälliger Gleichlauf zwischen dem Druck und der Neutronenintensität nicht so stark aus wie bei der konventionellen Rechenmethode.

Für 1957 erhielten wir auf diese Weise 0.755 ± 0.010% $mbar^{-1}$ (12 Messingzählrohre in Standard-Anordnung) und 0.73 ± 0.02% $mbar^{-1}$ für 1958 (erweiterte Anordnung mit Glaszählrohren). In der Fehlerangabe für 1958 ist der wahrscheinliche Fehler des Nulleffekts der Glaszählrohre enthalten.

4. Abschätzung des Median-Wertes der magnetischen Steifigkeit der Primärteilchen

Unter der Voraussetzung, dass die mittlere Absorptionslänge unabhängig von der atmosphärischen Tiefe und der magnetischen Breite ist, lässt sich zeigen, dass die "mittlere wirksame Steifigkeit" der Primärteilchen für eine Neutronenapparatur in grossen Tiefen der Atmosphäre unabhängig von dieser ist[2]). Für unsere Apparatur bei $x = 900$ g cm^{-2} können wir dann auf

[10]) W. Hassler, Dissertation. Universität Freiburg iBr (1959).

[11]) J. A. Simpson, W. Fonger and S. B. Treiman, Phys. Rev. **90** (1953) 934.

[12]) J. A. Simpson and W. C. Fagot, Phys. Rev. **90** (1953) 1068.

[13]) W. H. Fonger, Phys. Rev. **91** (1953) 351.

[14]) W. R. Webber and J. J. Quenby, Phil. Mag. **4** (1959) 654.

die bei $x = 680$ und 1030 g cm^{-2} einigermassen bekannten Ausbeutefunktionen S zurückgreifen[14]).

Für die Angabe einer "mittleren wirksamen Steifigkeit" scheint der Medianwert ein geeignetes Mass zu sein. Er ist definiert durch die Gleichung

$$\int_{P_\lambda}^{\overline{P}} Sj \, dP = \int_{\overline{P}}^{\infty} Sj \, dP \qquad (4)$$

(j = differentielles Primärspektrum, P = Steifigkeit, $\overline{P}$ = Median der Steifigkeit, P_λ = untere Grenze der Steifigkeit, λ = wirksame geomagnetische Breite). Der normale Mittelwert (mean) ist hier unbrauchbar, weil das entsprechende Integral divergiert.

Freiburg hat eine geomagnetische Breite von 49° N. Aus Tabellen von Pfotzer[15]) und Quenby[16]) entnimmt man $P_\lambda = 3.2 \pm 0.2$ GV. Aus den Tabellen von Webber[14]) ergibt sich dann für 1954/55 der Median

des Primärspektrums zu	5.5 ± 0.4	GV,
des wirksamen Spektrums ($x = 680$) zu	12.4	GV,
des wirksamen Spektrums ($x = 1030$) zu	21.2	GV.
Durch Interpolation ergibt sich für unsere Apparatur bei $x = 900$:	18 ± 3	GV.

Die Fehlerabschätzung stützt sich auf die in Abschnitt 3 herausgestellten Unstimmigkeiten. Nach der Methode von Fonger[13]) (Mittelwert von $1/P$) ergibt sich für unsere Apparatur ein Mittelwert von 12.7 ± 1.5 GV.

In unserem erweiterten Messblock erfassen die obere und die untere Zählrohrlage zusammengenommen etwa die gleiche mittlere Steifigkeit wie die mittlere Zählrohrlage, auf die sich unsere obigen Überlegungen bezogen, denn die Verdampfungsneutronen werden isotrop abgestrahlt und der Messblock ist symmetrisch aufgebaut.

Durch eine überschlägige Rechnung und durch Vergleich mit Collins[4]) kann die Ansprechwahrscheinlichkeit unseres erweiterten Messblocks für im Blei erzeugte Verdampfungsneutronen zu $(8 \pm 3)\%$ abgeschätzt werden. Es ist wenig sinnvoll, die Ansprechwahrscheinlichkeit noch weiter zu erhöhen, um die statistische Schwankung zu verkleinern (Abschnitt 3). Bei hoher Ansprechwahrscheinlichkeit gibt es jedoch eine interessante Möglichkeit, den Median des wirksamen Spektrums zu kleineren Steifigkeiten hin zu verschieben:

In einer Messanordnung mit 100% Ansprechwahrscheinlichkeit, die also jedes im Blei erzeugte Neutron auch registriert, würde jedes Primärteilchen seiner Multiplizität m entsprechend auch m-fach registriert werden. Ist die Totzeit der Apparatur jedoch wesentlich grösser als die Lebensdauer dieser kohärenten Neutronen, so kann sich jedes Primärteilchen nur mit einem einzigen Impuls bemerkbar machen, d.h. die Ausbeutefunktion S würde wesentlich flacher verlaufen, da die hohen Steifigkeiten benachteiligt werden. Der Median des wirksamen Spektrums würde sich (bei 3.2 GV Mindest-Steifigkeit) von 18 GV vielleicht in die Nähe von 5.5 GV verschieben lassen.

Wir danken Herrn Prof. W. Gentner für seine freundliche Unterstützung. Die Anlage wurde aus Mitteln der Deutschen Forschungsgemeinschaft errichtet.

[15]) G. Pfotzer, Nuovo Cimento Suppl. **8** (1958) 220.
[16]) J. J. Quenby and W. R. Webber, Phil. Mag. **4** (1959) 90.

NUCLEAR INSTRUMENTS AND METHODS 6 (1960) 301–308; NORTH-HOLLAND PUBLISHING CO.

THE ACTION OF FAST SPHERICAL IONIZATION CHAMBERS

R. D. CONNOR

Physics Department, University of Manitoba, Winnipeg, Canada

Received 21 September 1959

Theoretical equations are presented representing the formation of pulses in fast spherical ionization chambers, with special reference to pulse height as a function of the position of the ionizing event in the chamber. The calculations are extended to ionizing tracks of finite length and it is seen that the pulse height is relatively independent of the position of the track.

Wall effects and the performance of a hydrogen filled chamber under neutron irradiation are discussed in detail.

1. Introduction

In a "slow" pulse ion chamber, the pulse size is proportional to the total number of ions produced and does not depend on the position of formation of the ions in the chamber, but the RC time-constant required to permit of the collection of the positive ions is very long and is often > 0.01 second. Further, the amplifier response must be good down to low frequencies. These two conditions limit the speed of counting and make the system highly microphonic. In recent years the advantages of using a "fast" chamber have been clearly expressed[1,2]). With such chambers the time-constant is long compared with the electron transit time, but very much shorter than the ionic transit time, and the pulse size is determined by the motion of the electrons alone. Disadvantages are that the chamber gas must be rigorously free from electron-attaching impurities, such as oxygen and water vapour, and that the independence of position of the ionizing event is lost, but microphony is removed, counting is rapid, and the low-frequency response of the associated amplifier need not be so good.

Fast chambers using electron collection have been examined theoretically and experimentally for parallel-plate and cylindrical geometries[1,2]). Spherical chambers have also been employed experimentally[3,4]) but a detailed analysis of their properties has yet to appear in the literature. It is the purpose of this present paper to give the theory of the action of the spherical chamber, firstly from the point of view of the electrostatics of pulse formation and the dependence of pulse height on the position of the ionizing event, and secondly by considering the performance of the chamber under certain special conditions.

2. Pulse Formation

Consider an ideal chamber consisting of two concentric spheres of radii a and b, $(a \ll b)$, filled with a gas in which electron attachment processes yielding negative ions are negligible. The inner sphere is insulated; the outer sphere is earthed. We wish to evaluate the change in potential of the inner sphere following the production of an ion pair in the gas and the collection of the electron. It will be assumed that the positive ion remains stationary for a time comparable with the collection time of the electron and that the voltage pulse is amplified in a distortionless amplifier whose differentiating time-constant is a few times the electron transit time but is very short compared with the transit time of the positive ion.

[1]) D. H. Wilkinson, Ionization chambers and counters (Cambridge University Press, 1950).

[2]) B. B. Rossi and H. H. Staub, Ionization chambers and counters (McGraw-Hill, 1949).

[3]) C. A. Barnes, J. H. Carves, G. H. Stafford and D. H. Wilkinson, Phys. Rev. 86 (1952) 359.

[4]) G. Bishop and R. Wilson, ed. K. Siegbahn "Beta and Gamma Ray Spectroscopy" (North-Holland Publ. Co., 1955).

Consider the situation in the chamber (a) before the formation of the ion pair and (b) after the collection of the electron. Let the ion pair be formed at a distance r from the centre of the chamber. In the first situation consider an infinitesimal conductor without charge at this point. The charges on the inner and outer spheres are $+Q$ and $-Q$ respectively. The potential of the inner sphere is V, that of the infinitesimal conductor $V(r)$, and that of the outer sphere zero. In the second situation the charge on the inner sphere is $Q - e$, that on the infinitesimal conductor $+e$, and $-Q$ on the outer sphere while their respective potentials are $V + \Delta V$, T (say) and zero. Applying Green's reciprocal theorem, $\Sigma q_1 V'_1 = \Sigma q'_1 V$ gives

$$Q(V + \Delta V) = V(Q - e) + eV(r)$$

where $V(r)$ is

$$\frac{b - r}{b - a}\frac{a}{r}V .$$

Thus

$$\Delta V = -\frac{Ve}{Q} + \frac{e}{Q}\frac{b - r}{b - a}\frac{a}{r}V = -\frac{Ve}{Q}\frac{b(r - a)}{r(b - a)} .$$

The greatest potential change possible from one electron is

$$\Delta V_{\max} = -\frac{Ve}{Q}$$

and occurs when the ion pair is formed in the gas just inside the outer sphere.

Hence the actual pulse height as a fraction of the greatest is

$$P = \frac{b(r - a)}{r(b - a)} = \frac{1 - a/r}{1 - a/b} \qquad (1)$$

which gives the dependence of pulse height on the position of the ionizing event. This is shown in fig. 1 as a function of r/b for two values of b/a, viz. 10 and 50. Also shown are the corresponding graphs for a cylindrical chamber whose ratio of radii is 500 and 10^4.

It will be seen from fig. 1 that for even moderate values of b/a the pulse size is nearly independent of the position of the ionizing event in the chamber. In this respect the spherical chamber is vastly superior to the ungridded parallel plate chamber, where the pulse size is directly proportional to the distance of the ion pair from the collecting electrode; moreover, a given degree of independence of position is attained for a very much smaller ratio of radii than that needed in the cylindrical

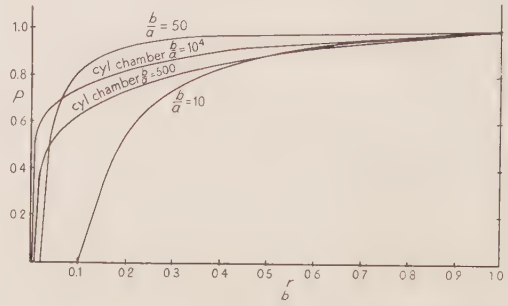

Fig. 1. Pulse size as a function of distance from the centre of the chamber to the position of the ionization.

chamber. This result makes a spherical chamber a practical proposition, and the "self gridding" action of such a chamber is reasonably complete.

We now find the probability, $p(P)\,dP$, of obtaining a pulse height in the range P to $P + dP$, (the maximum pulse height being taken as unity), for a uniform distribution of ionizing events in the gas such as occurs in the idealized case of such a chamber filled with boron trifluoride and subject to slow neutron irradiation. It will be assumed that the (n,α) reaction in boron yields tracks which can be considered as being all of equal ionization and effectively of zero length, and we let $q(r)\,dr$ be the probability that the ionizing event will occur between radii r and $r + dr$. Then

$$q(r)\,dr = \frac{4\pi r^2\,dr}{\frac{4}{3}\pi(b^3 - a^3)} ,$$

hence

$$q(r) = \frac{3r^2}{b^3 - a^3} .$$

Now

$$p(P)\,dP = q(r)\,dr$$

so

$$p(P) = \frac{3r^2}{b^3 - a^3}\frac{dr}{dP} = \frac{3r^4}{ab(b^2 + ab + a^2)} =$$

$$= \frac{3}{(b/a)[(b/a)^2 + b/a + 1][1 - P(1 - a/b)]^4} \qquad (2)$$

using the result (1). This function is shown graphically in fig. 2 for $b/a = 10$ and 50, being

normalized to unity at $P = 1$ for the sake of clarity while the corresponding function for a cylindrical chamber having $b/a = 500$ and 10^4 is also shown. A parallel plate chamber yields a rectangular distribution.

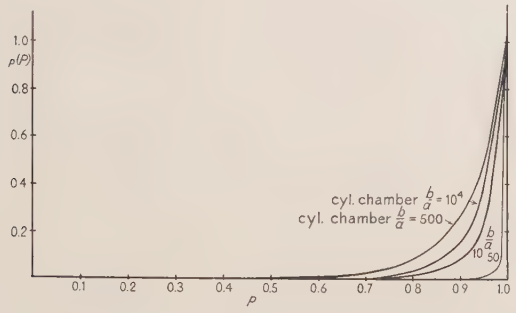

Fig. 2. Probability of obtaining a pulse of size P as a function of P.

The bias curve for this condition, i.e. the probability of obtaining a pulse $\geqslant P$ is given by

$$B(P) = \int_p^1 p(P)\,\mathrm{d}P =$$

$$= \frac{1}{(b/a)^3 - 1}\left[\left(\frac{b}{a}\right)^3 - \frac{1}{[1 - P\,(1 - a/b)]^3}\right]. \quad (3)$$

This function is shown graphically in fig. 3 for the same b/a values. It is seen that for moderate values of b/a a very good approximation to a rectangular bias curve is obtained.

These considerations require some modification when extended to ionization tracks in the gas instead of point charges. For a parallel

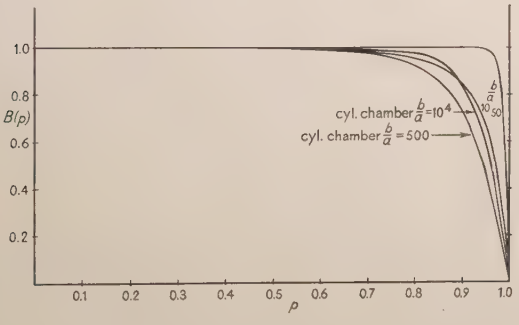

Fig. 3. Integral bias curve for spherical chamber.

plate chamber the pulse height obtained from a track of finite length is identical with that from the same total charge located at the "centre of gravity" of charge. This simple substitution does not hold for a cylindrical chamber nor, as will be seen presently, for a spherical chamber.

We shall for the moment assume that there is no wall effect and shall further postulate that the total ionization produced is proportional to the particle energy and that Geiger's relation holds, viz. $E \propto (\text{Residual range})^{\frac{2}{3}}$, E being the particle energy.

Let us consider a track of length R_0 beginning at a distance r_0 from the centre of the chamber and making an angle θ with the inward directed radius. Considering an element of track situated R from the point of origin and r from the centre of the chamber, we have

$$\frac{\mathrm{d}E}{\mathrm{d}\,(R_0 - R)} = K\,(R_0 - R)^{-\frac{1}{3}}$$

and

$$r = (R^2 + r_0^2 - 2Rr_0\cos\theta)^{\frac{1}{2}}.$$

The pulse from the extended track is therefore proportional to

$$\frac{K}{1 - a/b}\int_0^{R_0}(R_0 - R)^{-\frac{1}{3}} \times$$

$$\times\left[1 - \frac{a}{(R^2 + r_0^2 - 2Rr_0\cos\theta)^{\frac{1}{2}}}\right]\mathrm{d}R =$$

$$= \frac{K}{1 - a/b}\left[\tfrac{3}{2}R_0^{\frac{2}{3}} -\right.$$

$$\left. - a\int_0^{R_0}\frac{\mathrm{d}R}{(R_0 - R)^{\frac{1}{3}}(R^2 + r_0^2 - 2Rr_0\cos\theta)^{\frac{1}{2}}}\right]. \quad (4)$$

The integral has to be evaluated numerically along the track, but as the Geiger relation diverges as $(R_0 - R)$ tends to zero, we shall evaluate the integral between 0 and $(R_0 - h)$ using Simpson's rule for eleven ordinates putting the last ordinate equal to zero, h being the interval between the ordinates.

The results for a chamber with $a = 0.25$ cm and $b = 12.5$ cm are as follows, where X is the ratio of the pulse given by the extended track to that given by the same total charge located at a distance of $\frac{2}{5}R_0$ from the end of the track, i.e., at the "centre of gravity" of charge.

It will be seen that if the "centre of gravity" of charge is not close to the inner sphere the ratio is approximately unity, but is considerably

greater than one when the "centre of gravity" is in the vicinity of the inner electrode.

Point of origin (r_0)	Range	θ	X	Y
$\frac{1}{2}b$ (i.e. 6.25 cm)	2 cm	30°	1.003	0.968
	8 cm	30°	1.006	0.983
b (i.e. 12.5 cm)	12.25 cm	0°	0.975	0.944
	20 cm	5°	1.603	0.955

However, if we compare the pulse from the track with the pulse obtained from the same total charge located at a point at distance b from centre of the chamber, i.e. located at the inner surface of the outer sphere, which produces the maximum pulse, we get the values listed in column Y. It is apparent, therefore, that the pulse produced by an extended track is equal to the greatest pulse producible by the total ionization in this chamber to within a few per cent.

To examine this point further, eq. (4) is evaluated for $R_0 = 2$ cm and $\theta = 0°$ from $r_0 = b$ to $r_0 = a + 2$ cm in order to obtain the pulse height dependence on position for a 2 cm track directed inwards along the radius. The results are shown in fig. 4, for $b = 12.5$ cm and $a = 0.25$ cm.

It should be remembered that a track of given length radially directed inwards from a given point of origin yields the smallest pulse and any other orientation will give a larger one.

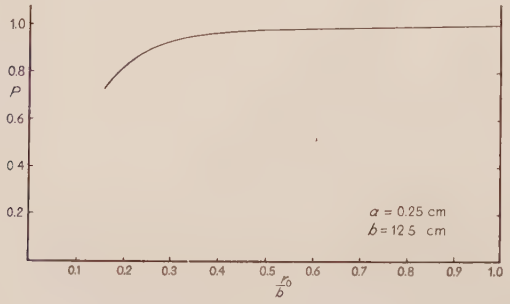

Fig. 4. Pulse produced by α-particle track 2 cm long inwardly directed along a radius.

A case of interest occurs when the inner sphere is coated with a thin α-emitting source, e.g. polonium and the gas pressure is adjusted so that the range of the particles is just $b - a$. It is easy to show, using the known specific ionization curve for these α-particles and neglecting straggling, that the total spread in pulse size is 10% of the greatest for $b = 5$ cm, $a = 0.5$ cm and 2% for $b = 12.5$ cm, $a = 0.25$ cm.

Thus, provided we are not concerned with ionization produced quite near the centre of the chamber we can to a good approximation consider the pulse obtained from a given amount of ionization as being independent of its position in the chamber. This is a result frequently invoked for cylindrical chambers and from what has gone before it would have been reasonable to suppose that it held, at least to the same degree of approximation for spherical chambers.

3. Wall Effects

In what follows the volume of the inner sphere and the dependence of pulse height on the position of the ionization in the chamber will be ignored.

For a spherical and a cylindrical chamber of the same radius operating under similar conditions it is easy to show that the ratio of their respective electron transit times is about 2 and for an isotropic distribution of tracks the respective wall effects are in the ratio $\frac{3}{2}$. Again, with a cylindrical chamber the wall effect can be further reduced if the tracks are generally directed along the axis of the chamber; the spherical chamber does not offer this possibility. These considerations reveal disadvantages—but only slight disadvantages—in the spherical form.

To illustrate the wall effect in a spherical chamber, consider the filling gas to be argon containing some radon.

Consider an atom of radon located at A, distant β from the centre of the chamber. The solid angle as a fraction of 4π in which an α-particle would traverse a path $\geq r$ is $\frac{1}{2}(1 - \cos\theta)$. Take a spherical shell of radius β and thickness $d\beta$. If n is the number of disintegrations in unit time in the chamber then N, the number of pulses per unit time from α-particles having tracks $\geq r$ is given by

$$N = \frac{n}{\frac{4}{3}\pi b^3} \int 4\pi\beta^2 \tfrac{1}{2}(1 - \cos\theta)\,\mathrm{d}\beta$$

between appropriate limits. Now

$$\cos\theta = \frac{\beta^2 + r^2 - b^2}{2\beta r}.$$

So $$N = \frac{n}{\frac{4}{3}\pi b^3} \int \frac{\pi}{r}(\beta b^2 - \beta(r-\beta)^2)\,\mathrm{d}\beta\,.$$

If $r > b$, the limits of integration are b and $r - b$. So

$$N = \frac{n}{2}\left[2 - 3\left(\frac{r}{2b}\right) + \left(\frac{r}{2b}\right)^3\right]. \qquad (5)$$

If $r < b$, as is the usual condition, part of the volume of the chamber, viz., $\frac{4}{3}\pi(b - r)^3$ possesses unit solid angle for tracks $\geqslant r$. In it easy to see that in this case

$$\frac{4}{3}\pi b^3 \frac{N}{n} = \frac{4}{3}\pi(b - r)^3 +$$

$$+ \frac{\pi}{r}\int_{b-r}^{b} (\beta b^2 - \beta r^2 + 2\beta^2 r - \beta^3)\,\mathrm{d}\beta \qquad (6)$$

which yields the same result as before, viz., eq. (5). Let G be the energy spent in the chamber by an α-particle in moving a distance r from its parent atom and let R be the total range and E the total energy of the α-particle. Then, if Geiger's relation holds,

$$E = kR^{\frac{2}{3}}$$

and

$$G = k\,[R^{\frac{2}{3}} - (R - r)^{\frac{2}{3}}]$$

or

$$r = R\left[1 - \left(1 - \frac{G}{E}\right)^{\frac{3}{2}}\right].$$

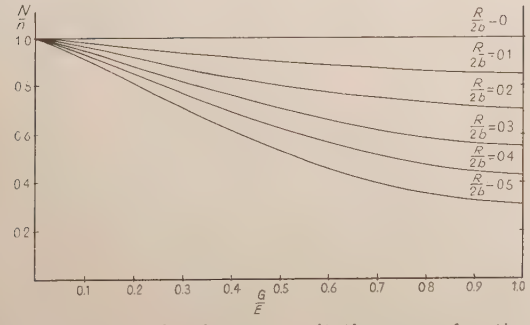

Fig. 5. Number of pulses per unit time as a function of energy spent in the chamber.

Substituting this last value for r in eq. (5) yields N/n as a function of G/E which is shown graphically in fig. 5 for various values of $R/2b$.

4. Neutron Irradiation of a Chamber Filled with Hydrogen

The last example of operation of these chambers which will be considered here is the important case of a hydrogen filled chamber subject to neutron irradiation.

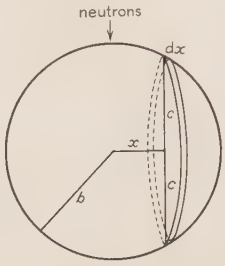

Fig. 6. Section through chamber undergoing irradiation by a parallel beam of neutrons.

We consider here the case in which a parallel beam of monoenergetic neutrons is incident on a chamber containing gaseous hydrogen. In practice it is not customary to use hydrogen alone, but rather a mixture of argon and hydrogen owing to the smallness of the stopping power of the latter and pressures in excess of one atmosphere are common. For example, Allen[5]) used successfully a mixture of 3.02 atmospheres of argon and 0.68 atmospheres of hydrogen to shorten the track length in a cylindrical chamber and so reduce the wall effect. We shall have occasion to consider this matter later.

The corresponding case for the cylindrical chamber has been evaluated by Skyrme[6]) employing a neat analytical method, and here the same considerations are applied to the spherical chamber. It is known that the energy distribution of "knock-on" protons in hydrogen produced by monoenergetic neutrons of not too high energy is rectangular from zero energy up to that of the incident neutron. Therefore, the probability of a collision producing a proton in the energy interval E to $E + \mathrm{d}E$ is $\mathrm{d}E/E_0$ where E_0 is the neutron energy. Let there be A n–p collisions per unit volume, this number being assumed constant throughout the volume.

[5]) W. D. Allen, British Atomic Energy Project Report B.I. (1945) 93.

[6]) T. H. R. Skyrme, British Atomic Energy Project Report M.S. (1944) 94.

Take a plane section of the sphere distant x from the centre (fig. 6), and of thickness $\mathrm{d}x$, parallel to the direction of the neutron beam.

Let $\mathrm{d}S$ be a small element in this section. The number of protons originating in the element of volume $\mathrm{d}S\,\mathrm{d}x$ having energies between E and $E + \mathrm{d}E$ is

$$A\,\mathrm{d}S\,\mathrm{d}x\,\frac{\mathrm{d}E}{E_0}$$

where E_0 is the energy of the incident neutron, and the number scattered in a wedge of angle $\mathrm{d}\phi$ is

$$A\,\mathrm{d}S\,\mathrm{d}x\,\frac{\mathrm{d}\phi}{2\pi}\,\frac{\mathrm{d}E}{E_0}\,.$$

The number of protons of initial energy between E and $E + \mathrm{d}E$ formed in the chamber which traverse a path $\geqslant r$ is found by integrating this expression over all elements $\mathrm{d}S$ in the section such that the path from $\mathrm{d}S$ to the chamber wall inclined at an angle θ to the direction of the incident neutron is $\geqslant r$, the angle θ being defined by the equation $E = E_0 \cos^2\theta$ [7]), and the expression is then integrated with respect to x between the limits 0 and b, and with respect to ϕ from 0 to 2π.

The plane section of the spherical chamber has a circular perimeter. Let the radius be

$$c = (b^2 - x^2)^{\frac{1}{2}}\,.$$

A little consideration will show that the number in question will be obtained by considering proton recoils restricted to the section chosen and by evaluating the area of the section in which a range $\geqslant r$ is possible, then integrating with respect to ϕ and then with respect to x between the limits 0 and

$$(b^2 - \tfrac{1}{4}r^2)^{\frac{1}{2}}$$

for there will be no contribution from the section if $r \geqslant 2c$. Consider for the moment $r < 2c$. The dead space at the bottom of the section in which a range $\geqslant r$ at an angle θ to the vertical is not possible is the area bounded by the arc ABC, being the bottom of the section, and the arcs AD and DC which are the loci of points (r,θ) from all points on the arc ABC (fig. 7).

[7]) J. C. Bower, E. Bretscher and C. W. Gilbert, Proc. Camb. Phil. Soc. **34** (1938) 290.

It is easy to show that these loci are arcs of circles of radius c and of centre $(-r\sin\theta, r\cos\theta)$ and $(r\sin\theta, r\cos\theta)$ with respect to the centre of the section taken as origin O.

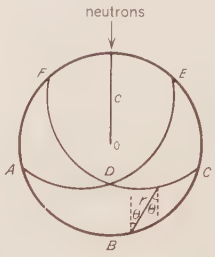

Fig. 7. Diagram of section of radius c shown in fig. 6.

The continuation of the circular arcs AD and DC to E and F respectively define the areas ADF and DCE in which only an inwardly directed proton can attain a range $\geqslant r$ while the area which remains, FDE, contains all points in which two directions of projection with range $> r$ are possible.

Hence the total area from the section which is to be considered is ADF + DCE + 2 FDE, i.e., area ADEFA + CEFDC or 2 (ADEFA).

ADEFA is the area common to two intersecting circles of radius c whose centres are r apart.

Hence the total area in question is

$$\left(4c^2 \arccos\frac{r}{2c}\right) - 2r\left(c^2 - \frac{r^2}{4}\right)^{\frac{1}{2}}$$

which vanishes when $r = 2c$ as is required.

Now suppose $r < 2b$. The number of protons scattered in the chamber having initial energies between E and $E + \mathrm{d}E$ and a range $\geqslant r$ in the chamber is

$$A\,\frac{\mathrm{d}E}{E_0}\int_0^{2\pi}\frac{\mathrm{d}\phi}{2\pi}\int_0^{(b^2-\frac{1}{4}r^2)^{\frac{1}{2}}}\left[\left(4c^2\arccos\frac{r}{2c}\right) - 2r\left(c^2-\frac{r^2}{4}\right)^{\frac{1}{2}}\right]\mathrm{d}x$$

$$= 4A\,\frac{\mathrm{d}E}{E_0}\int_b^{\frac{1}{2}r}\left[-\frac{c^3}{(b^2-c^2)^{\frac{1}{2}}}\left(\arccos\frac{r}{2c}\right) + \right.$$

$$\left. + \frac{rc}{2}\left(\frac{c^2-\frac{1}{4}r^2}{b^2-c^2}\right)^{\frac{1}{2}}\right]\mathrm{d}c = 4A\,\frac{\mathrm{d}E}{E_0}\,\frac{\pi}{2}\left[\frac{2b^2}{3} - \frac{r}{2}\,b^2 + \tfrac{1}{3}\left(\frac{r}{2}\right)^3\right]$$

$$= \tfrac{4}{3}\pi b^3 A\,\frac{\mathrm{d}E}{E_0}\left[1 - \tfrac{3}{2}\left(\frac{r}{2b}\right) + \tfrac{1}{2}\left(\frac{r}{2b}\right)^3\right]. \qquad (7)$$

As a check it is seen that when $r = 0$ the number

$$= \tfrac{4}{3}\pi b^3 A \frac{\mathrm{d}E}{E_0}$$

and when $r = 2b$ the number $= 0$, as is required.

If R is the total range of a proton of initial energy E, then, using the Geiger relation, the energy G spent in the chamber in r cm is

$$k\,[R^{\frac{2}{3}} - (R - r)^{\frac{2}{3}}]$$

and

$$E = kR^{\frac{2}{3}},$$

so

$$\frac{G}{E} = 1 - \left(1 - \frac{r}{R}\right)^{\frac{2}{3}}$$

or

$$r = R\left[1 - \left(1 - \frac{G}{E}\right)^{\frac{3}{2}}\right].$$

The number of protons in the energy range zero to E_0 which have a range $\geqslant r$ in the chamber is therefore

$$\frac{\frac{4}{3}\pi b^3 A}{E_0}\int_G^{E_0}\left\{1 - \frac{9}{16b}E^{\frac{3}{2}}\left[1 - \left(1 - \frac{G}{E}\right)^{\frac{3}{2}}\right] + \right.$$

$$\left. + \frac{27}{1024b^3}E^{\frac{9}{2}}\left[1 - \left(1 - \frac{G}{E}\right)^{\frac{3}{2}}\right]^3\right\}\mathrm{d}E = \psi\,. \quad (8)$$

This expression yields the bias curve, and is shown graphically (in fig. 8) for $E_0 = 2$ MeV using the empirical relation suggested by Allen[3]), (viz., $R = \frac{3}{4}E^{\frac{3}{2}}$, R being in cm where E is in MeV) for the cases $b = 12.5$ and $b = 5$ cm.

However, an examination of the range-energy relation[8,9]) for protons in air suggests the empirical relation $R = 2.15\ E^{1.7}$ as being superior to the $\frac{3}{2}$ power law. The bias curve, has therefore, been computed from (7) for $R = E^{1.7}$, a stopping power of 2.15 being readily attained for an argon-hydrogen mixture at moderate pressure. The final form of the expression is:

$$\psi = \frac{n}{E_0}\left\{E_0 - \frac{3}{10.8b}E_0^{2.7} + \frac{3}{10.8b}(E_0 - G)^{2.7} + \right.$$

$$+ \frac{1}{97.6b^3}[E_0^{6.1} - (E_0 - G)^{6.1}] - G +$$

$$+ \frac{3}{10.8b}G^{2.7} - \frac{1}{97.6b^3}G^{6.1} +$$

$$\left. + \frac{3}{16b^3}\int_G^{E_0}E^{5.1}(1 - G/E)^{1.7}[(1 - G/E)^{1.7} - 1]\,\mathrm{d}E\right\} \quad (9)$$

where $n = \frac{4}{3}\pi b^3 A$. The integral in this last expression has to be evaluated numerically, but its contribution turns out to be small for the case considered.

This function is also shown in fig. 8 for $E_0 = 2$ MeV and $b = 5$ cm together with the ideal bias curve ($b = \infty$). The differential bias curve is frequently used when a kick sorter is available and gives the number of protons which spend energy between G and $G + \mathrm{d}G$ in the chamber. This curve can be obtained by differentiating (8) or (9) with respect to G. Restricting our attention to the differentiation of (9) we have

$$\frac{\mathrm{d}\psi}{\mathrm{d}G} = \frac{n}{E_0}\left\{-\frac{3}{10.8b}2.7\,(E_0 - G)^{1.7} + \frac{6.1}{97.6b^3}(E_0 - b)^{5.1} - \right.$$

$$- 1 + \frac{3}{10.8b}2.7\,G^{1.7} - \frac{6.1}{97.6b^3}G^{5.1} +$$

$$\left. + \frac{3}{16b^3}\int_G^{E_0}E^{4.1}\left[1.7\left(1 - \frac{G}{E}\right)^{0.7} - 3.4\left(1 - \frac{G}{E}\right)^{2.4}\right]\mathrm{d}E\right\}. \quad (10)$$

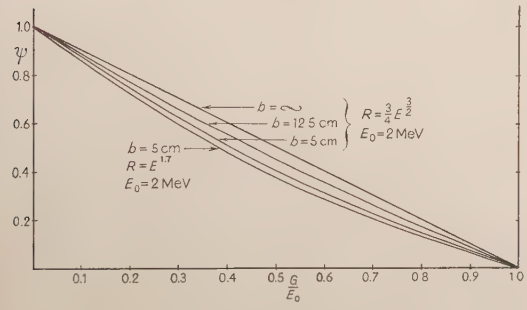

Fig. 8. Integral bias curve for spherical chamber irradiated with 2 MeV neutrons.

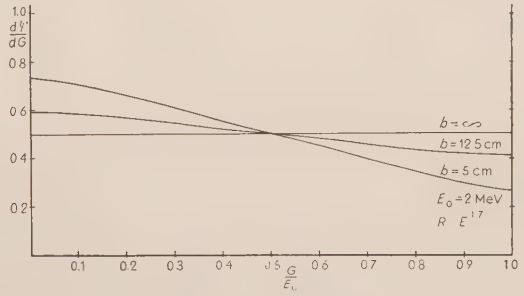

Fig. 9. Differential bias curve for spherical chamber irradiated with 2 MeV neutrons.

This function is shown in fig. 9 for $b = 5$ and 12.5 cm and $E_0 = 2$ MeV.

[8]) H. A. Bethe, Revs. Mod. Phys. 22 (1950) 213.

[9]) M. S. Livingstone and H. A. Bethe, Revs. Mod. Phys. 9 (1937) 1.

5. Practical Considerations

The equations given above represent an idealized situation. In practice the inner sphere must be supported, usually by a rod which necessitates an insulated entry in the outer wall. The field will no longer be radial especially in the vicinity of the probe and the pulse size distributions calculated here will apply only as a first approximation. We might expect that the actual distribution will resemble a superposition of that calculated here and those characterizing cylindrical chambers of low values of b/a. While an exact fit with the above calculations is not to be expected, the shape of the various distributions should be preserved.

Acknowledgements

The helpful criticism of the text of this paper by Professor N. Feather F.R.S. of the University of Edinburgh is gratefully acknowledged and thanks are due to Mr. M. K. Husain for assistance in the production of the figures.

NUCLEAR INSTRUMENTS AND METHODS 6 (1960) 309–322; NORTH-HOLLAND PUBLISHING CO.

ON THE MECHANISM OF MULTIPLE DISCHARGES IN SELF-QUENCHING GEIGER COUNTERS

O. J. ORIENT

Central Food Research Institute, Dept. for Radiology, Budapest

Received 15 September 1959

Multiple pulses occurring in the plateau and breakdown region of pure ethyl alcohol as well as ethyl alcohol-argon gas mixture filled counter tubes have been studied. A single sweep oscilloscope was used to investigate the shape and the time of appearance of multiple discharges. In pure ethyl alcohol filled tubes the plateau slope and the breakdown region were due to multiple pulses of the same order of magnitude as the "ordinary" pulses. These multiple pulses were produced always immediately after the recovery time. The same process has been observed for ethyl alcohol-argon gas mixture filled tubes. Pulses responsible for the breakdown region were much smaller and occurred after the dead time.

The two kinds of multiple pulses may be discriminated electronically and counted separately. These experiments too have shown only "high" pulses occurring in the plateau region whereas at the termination of the plateau region, in the breakdown section for ethyl alcohol-argon gas filling the number of "low" multiple pulses was much higher than that of "high" multiple pulses.

According to measurements the "high" multiple pulses result from processes occurring on the cathode surface while the "low" multiple pulses are due to processes in the gas volume. It is assumed that the "high" multiple pulses are caused by the decay of organic gas molecules returning to ground state in the vicinity of the cathode and the "low" ones may be attributed to the decay of metastable argon molecules remaining after the dead-time. The values calculated according to this theory for the plateau and breakdown region of our counters were in good agreement with our experimental results.

1. Introduction

The mechanism responsible for the occurrence of multiple pulses were first investigated by Korff and Present[1]). They assumed these spurious counts to be due to excited organic vapour molecules returning to the ground state near the cathode surface. Willard and Montgomery[2]) attributed this phenomenon to negative ions. According to Colli and Facchini[3]) the spurious counts in non-self-quenching counters are caused by photons bombarding the cathode. Wiser and Krumbein[4]) concluded from their measurements that the steep rise in the counting rate at the high voltage end of the plateau region was due to metastable atoms and molecules. Experiments and theoretical considerations reported in the literature seem to lead to disagreeing results and therefore we decided to investigate thoroughly the origin of multiple discharges occurring in selfquenching counters.

2. Measuring Apparatus

(a) In our counter tubes we used nickel cathodes and a 0.1 mm thick tungsten wire, with an effective length of 80 mm as anode; cathode cylinder diameter was 20 mm. The counter tube was encased in a glass envelope. Prior to sealing the cathode surface was carefully polished and cleaned as well as degreased. The tube casing and all other components were also thoroughly scourred before being assembled.

The process of evacuating and filling was performed as follows: In order to remove the adsorbed humidity, we heated the device for 6 hours to 450° C at 10^{-5} mm Hg vacuum pressure. The tubes were filled after cooling

[1]) S. A. Korff and R. D. Present, Phys. Rev. 65 (1944) 274.

[2]) D. Willard and C. C. Montgomery, Rev. Sci. Instr. 21 (1950) 520.

[3]) L. Colli and V. Facchini, Phys. Rev. 88 (1952) 987.

[4]) H. L. Wiser and A. D. Krumbein, Phys. Rev. 98 (1955) 303.

down. Argon gas of higher than 99.98 percent purity was used and the ethyl alcohol, serving as quenching gas was introduced only after careful dehydration and deaeration. The alcohol was free even from traces of water.

(b) The block diagram of the measuring circuit is shown in fig. 1.

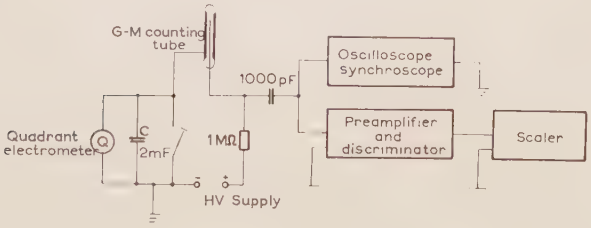

Fig. 1

The pulses counted by the tubes were investigated by means of a single-sweep oscilloscope. The horizontal sweep could be set approximately to 400, 800 and 1000 μsec and in addition a marker pip of 100, 20 and 10 μsec could be turned on.

The pulses of the counter were sent through a preamplifier and a differential discriminator to a scaler with a scaling factor of 1000. The preamplifier gain could be varied in the range 0–10 continuously. The discriminator threshold voltage could be preset from 5 to 55 V continuously with an error of less than 5 mV. The deadtime measured on the whole system consisting of preamplifier, discriminator and scaler, was less than 5 μsec.

We have provided for the continuous setting and measuring of high voltage. The cathode of the tube to be measured was connected through a well insulated 2 mF condenser to the negative pole of the high voltage supply. The voltage across the condenser was measured by a quadrant electrometer. It was possible to short circuit the two poles of the condenser by means of the switch shown in fig. 1. This apparatus was used (1) to measure the response characteristic of self quenching counters, (2) for oscilloscopic studies of multiple discharges, (3) to dertermine the deadtime and recovery time and (4) to measure the charge collected per pulse.

The charge per pulse was measured as follows: Measuring the time required for charging the condenser to 1 V while the short

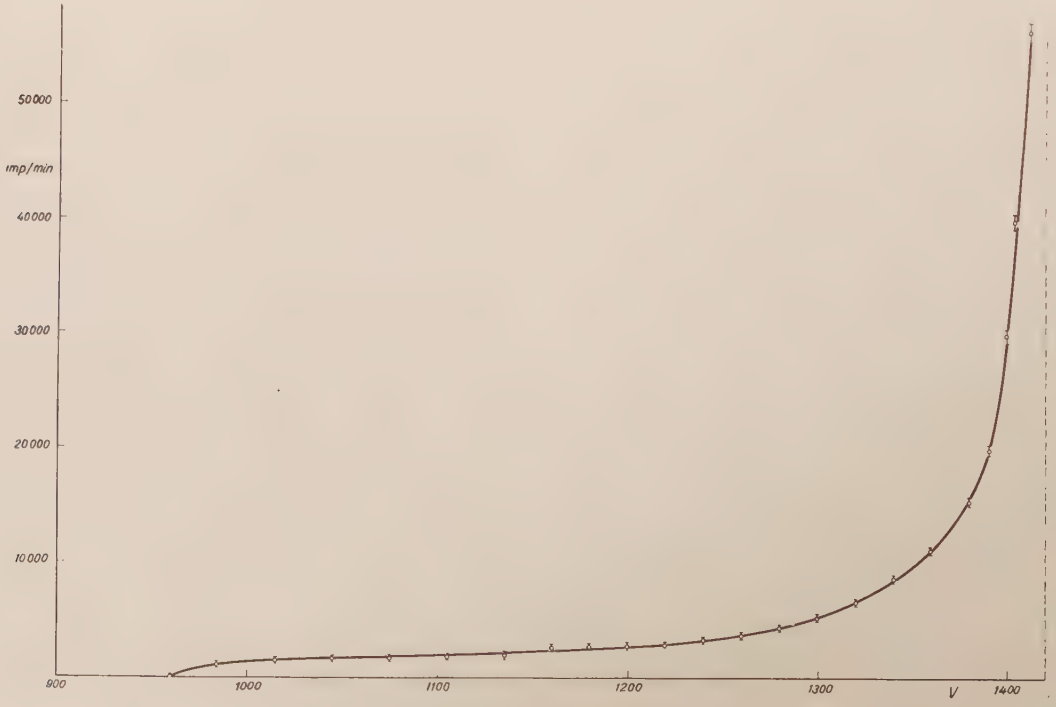

Fig. 2

circuiting switch was off, the number of discharges produced in the interval thus measured was counted by means of the scaler. Now, by knowing the capacity of the condenser, the voltage across the condenser and the number of discharges producing this voltage, the charge produced per discharge can be readily determined.

3. Results of the Measurements

3.1. INVESTIGATION OF THE MULTIPLE DISCHARGES

First, experiments with 15 mm Hg ethyl alcohol filled tubes were carried out. The characteristic plot for the operation of counters filled at this pressure is shown in fig. 2. The "plateau region" in the characteristic plot is followed by a first slowly but subsequently rapidly increasing breakdown section. The dashed line in fig. 2 (1420 V) represents the onset of continuous discharge.

The nature of multiple discharges was studied by means of a single-sweep oscilloscope. Irradiating the tube by a radioactive sample we photographed the pattern appearing on the oscilloscope screen (fig. 3a). This oscillogram is well known from the literature[5]). The time lag after the first pulse is the dead-time of the counter and the subsequent section consisting of increasing pulses, is the recovery time. With this setting the marker pip was about 10 μsec and the total horizontal sweep time about 400 μsec. The deadtime is seen to be 70 μsec and the recovery time 140 μsec.

The time of appearance of multiple pulses in relation to that of primary pulses can be studied by means of single sweep oscilloscope. Short time records were taken of the oscilloscope screen at low counting rates. The pictures obtained are to be seen in figs. 3b and 3c. The operating voltage for figs. 3a, 3b and 3c was 1160 V. For records 3b and 3c the marker pip was set at 100 μsec and the total horizontal sweep was about 1000 μsec. In fig. 3b it can be seen that in the case of double pulses the second pulse started immediately after the recovery time. The second pulse was initiated after a time interval corresponding to the sum of dead time plus recovery time, the components of the double pulse follow each other at intervals of 210 μsec. In fig. 3c a triple pulse is shown. The intervals between the components of the triple

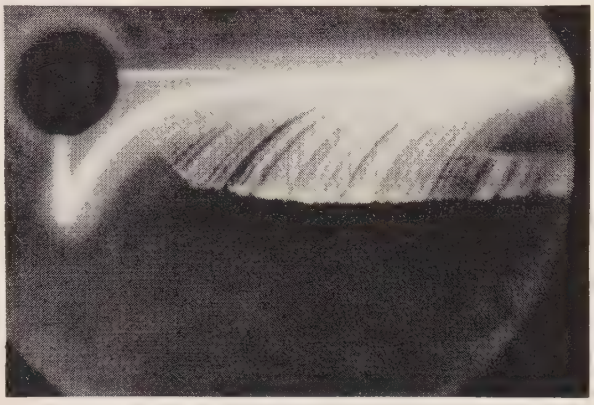

Fig. 3a

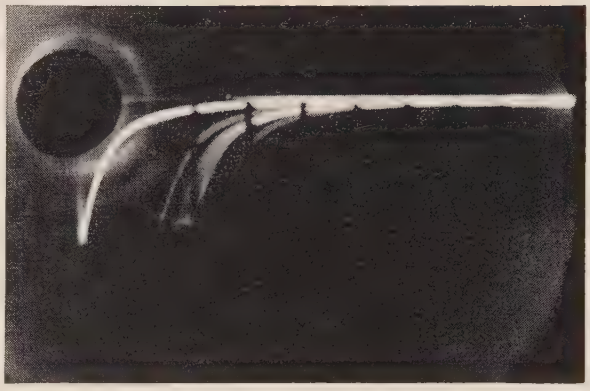

Fig. 3b

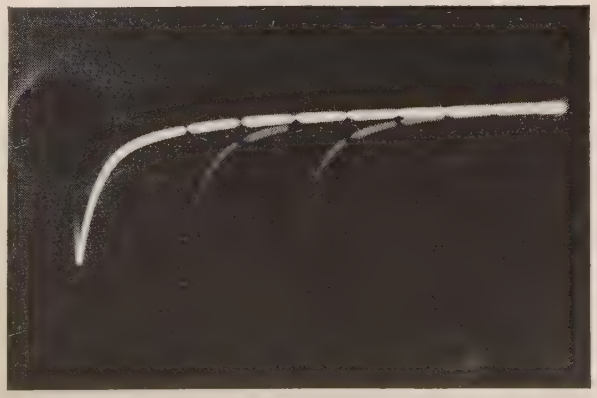

Fig. 3c

[5]) G. H. Stever, Phys. Rev. **59** (1941) 765.

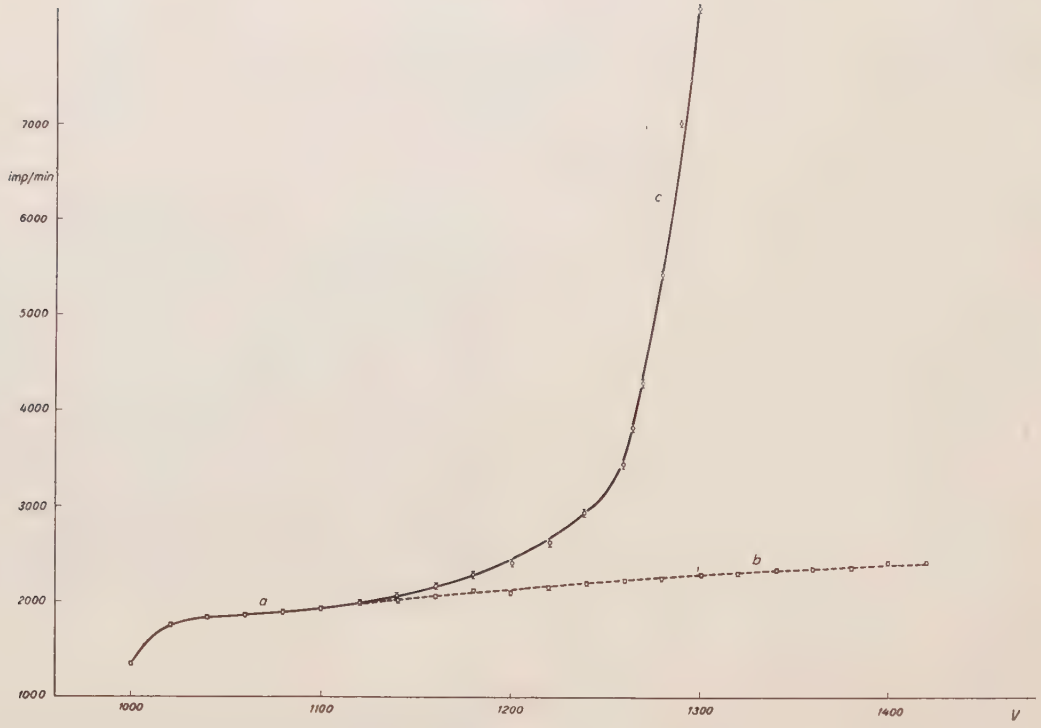

Fig. 4

pulse are 210 μsec. The multiple pulses consist of components of the same height since they are produced after the recovery time. With increasing voltage the multiple discharges have shown the same behaviour in the breakdown section of the characteristic plot as described above. They were initiated after a time corresponding to dead time plus recovery time and were of equal height.

The characteristic plot of 15 mm Hg ethyl alcohol and 100 mm Hg argon mixture filled tubes is shown in fig. 4 by the curve portion a–c.

The slope of the plateau region, similarly to that of 15 mm Hg pure ethyl alcohol filled tubes, is due to multiple discharges. In the breakdown region, however, multiple pulses of quite a different nature also occur. Dead time and recovery time of the counter at operating voltage of 1320 V are to be seen on the curve in fig. 5a. The other kind of multiple discharges,

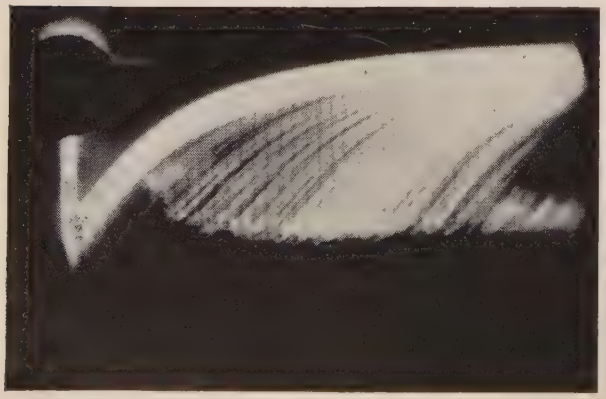

Fig. 5a

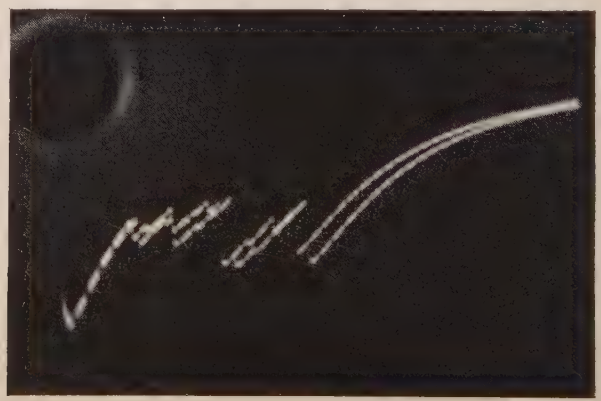

Fig. 5b

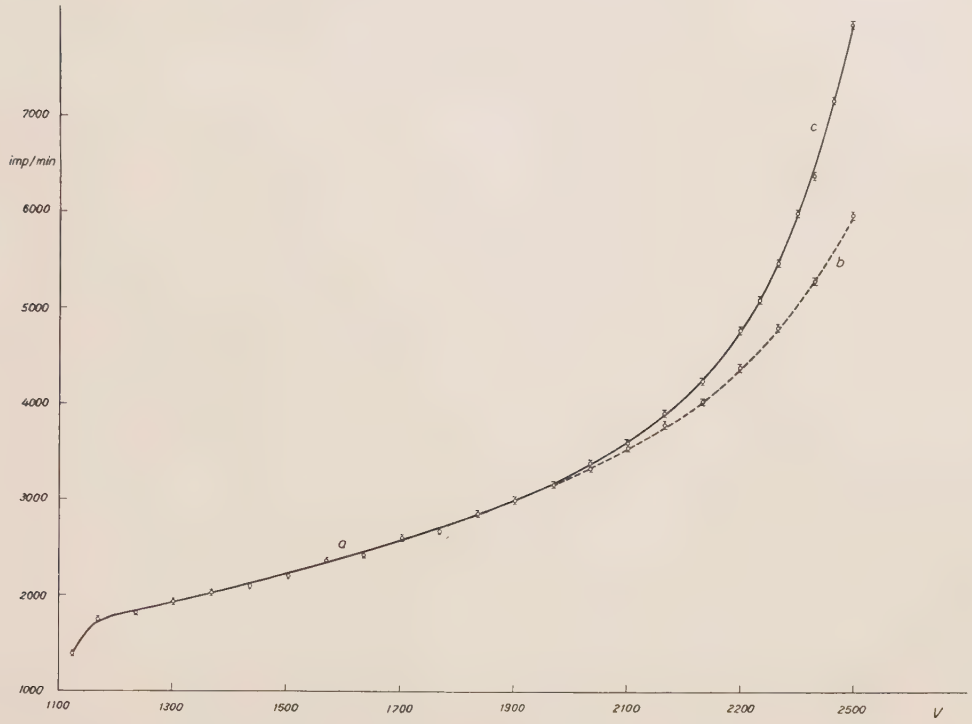

Fig. 6

appearing in the breakdown region (at 1320 V) are illustrated by the oscillogram in fig. 5b. (The oscillograms were recorded for a marker pip set at 20 μsec and total horizontal sweep time about 800 μsec.) The dead time amounts here to about 90 μsec. The single components of the multiple discharges appearing now already during the recovery interval immediately after the dead time are much lower than the "primary" pulses, they follow each other at irregular intervals each shorter than the dead time.

These "low" multiple discharges may be electronically discriminated from the "high" pulses preceding them. Therefore we plotted the operational characteristics also by using a differential discriminator. The discriminator was set to cut off the low multiple pulses. The counting rate in the plateau region was the same as measured without discriminator since in this region only "high" multiple pulses occurred (section a). In the breakdown region, however, the curve shows different trends when measured with discriminator as it is to be seen in the section a–b. According to the measurements plotted in fig. 4 the steep rise in the slope of the breakdown region is caused by "low" multiple pulses. The slope of the curve for "high" pulses shows only a slight increase in the breakdown region.

Tubes with 15 mm Hg ethyl alcohol and 300 mm Hg argon filling were also measured. The characteristic plot for the operation of counters filled at this pressures is shown in fig. 6.

Curve a–c corresponds to measurements without discriminator.

Operational characteristics in the plateau region give the same plot for measurement both with and without discriminator. The characteristic plot measured with discriminator for the breakdown region is indicated by section a–b in fig. 5.

Curve a in fig. 7 illustrates the increase in the number of "low" pulses per "high" pulse in the breakdown region with increasing voltage. For comparison we also plotted curve b (fig. 7) to show the same ratio in terms of voltage as measured in the breakdown region of counters

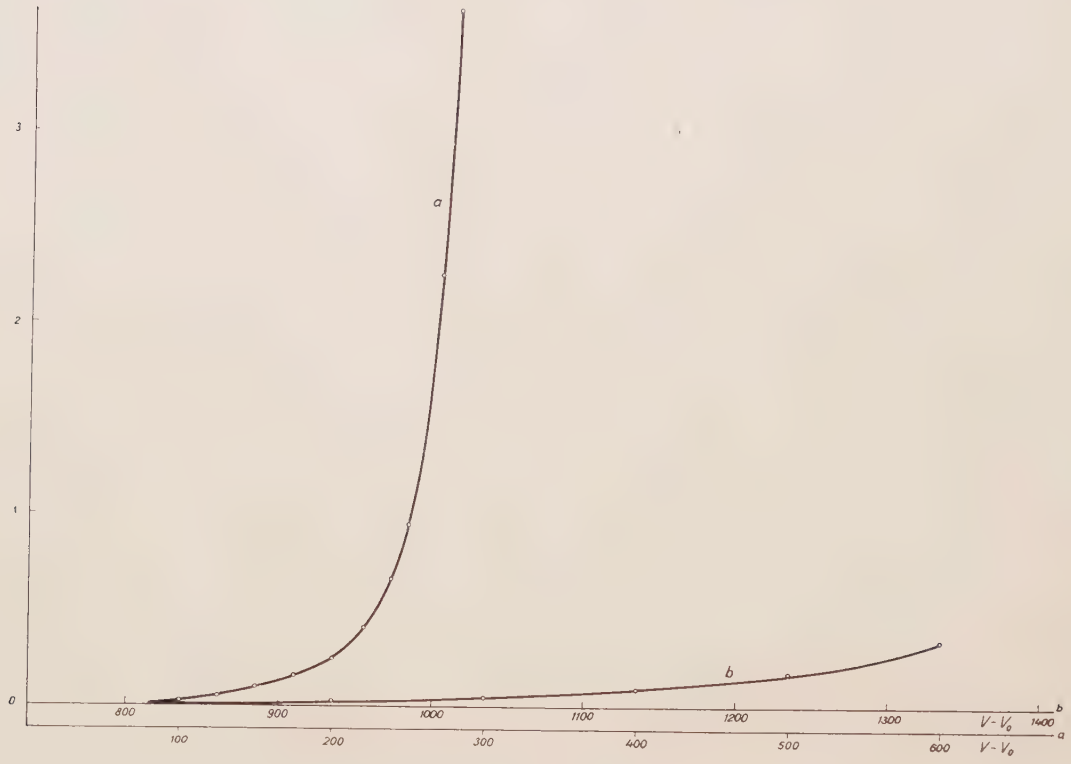

Fig. 7

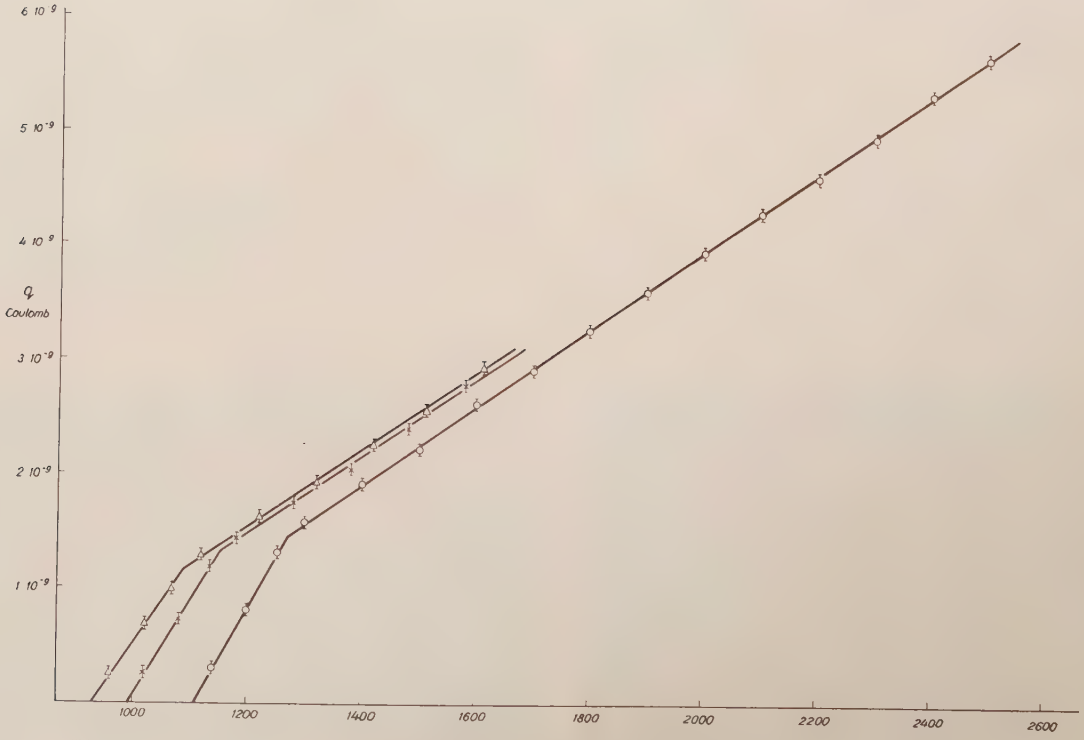

Fig. 8. △ = 15 mm Hg ethyl alcohol; × = 15 mm Hg ethyl alcohol 100 mm Hg argon; ○ = 15 mm Hg ethyl alcohol 300 mm Hg argon.

filled at higher pressures. It can be seen that for tubes filled at higher argon pressure the number of "low" pulses increased more slowly with increasing voltage than for those filled at lower argon pressure.

Following conclusion may be drawn from the results of our measurements on multiple discharges:

(1) In pure quenching gas filled tubes both the plateau slope and the breakdown are caused by multiple pulses appearing immediately after the recovery time. Thus the spurious counts are due to processes occurring on the cathode surface.

(2) In argon-ethyl alcohol mixture filled counters, too, multiple discharges resulting from processes on the cathode surface are responsible for the slope of the plateau whereas the steep rise in the breakdown section is due to other type of multiple discharges. These begin to appear already after the dead time and thus they are much smaller than the full-size pulses. Such "low" pulses produced in the recovery time are to be attributed to processes in the gas volume. Their particular feature is that the increase in their number with increasing voltage is more apparent for low argon pressure than for high argon pressure.

In further experiments charge produced per discharge versus voltage as well as dead time versus voltage were determined on counters with three different kinds of filling. Results of these measurements will be referred to in our conclusions.

3.2. MEASUREMENT OF THE CHARGE PRODUCED PER DISCHARGE

The charge collected in the tube per discharge was measured versus operating voltage by the method described in section 2. The respective plots for 15 mm Hg ethyl alcohol, 15 mm Hg ethyl alcohol—100 mm Hg argon and 15 mm Hg ethyl alcohol—300 mm Hg argon filled tubes are shown in fig. 8.

Above method can be applied for measuring the number of ions per discharge only in the absence of "low" multiple pulses. In argon-ethyl alcohol mixture filled tubes the discharge begins in the plateau as well as in the breakdown region with the formation of an ion sheath along the wire. This positive space charge proceeds towards the cathode. Upon termination of the dead time, the charge carried by the ion sheath will be increased by an additional charge resulting from the "low" multiple discharges. If we want to determine the charge produced only in the primary ion sheath we may proceed as follows: The time integral of the pulse recorded by a single-sweep oscilloscope and represented by the area below the curve is proportional to the charge. This area can be calibrated in the plateau region where no "low" multiple discharges occur, according to the absolute value of charge. Upon appearance of "low" multiple discharges the charge carried in the "high" discharge without the additional charge of "low" pulses may be determined by extrapolation that is by substituting the corresponding exponential section for the pulse recovery section like in fig. 9 and the area below the pulse thus plotted is evaluated as charge.

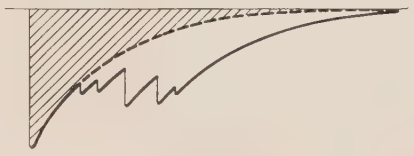

Fig. 9

The curves for the charge carried in the "high" pulse shown in fig. 8 are plotted for 100 mm Hg argon filled counters to over 1180 V and for 15 mm Hg–300 mm Hg argon filled counters in over 2000 V according to the procedure given above since it is past these voltages that the contribution of the "low" multiple pulses becomes appreciable.

The curves for charge versus voltage show two straight sections for each of the three kinds of fillings. The experimental data are in agreement with those given in the literature[6]). The theoretical interpretation of these results was given by

[6]) G. H. Stever, Phys. Rev. **61** (1942) 38.

Wilkinson[7]). If no discharge takes place in the counter, its charge is Q_0 which is due to the tube capacity. If the space charge in the tube is higher than Q_0. the slope of the curve for charge versus voltage will be about the half of that for $Q_0 < q$ and a deviation from the straight line is seen at Q_0. It has been shown by Wilkinson that the expected value of the ratio q/Q_0 did not depend on the gas filling or its pressure, only on tube geometry. This prediction has been verified by experiments carried out over a wide range of pressures[8]).

The ratio

$$\frac{q}{Q_0} = m$$

is shown in fig. 10 in terms of overvoltage (the overvoltage being equal to $V - V_0$ where V_0 is the starting voltage of the counter) for the three kinds of counter-fillings. The three curves have the same trend within error of measurement and thus it is seen that Wilkinson's theory holds not only for argon-alcohol mixture but for pure ethyl alcohol filled counters as well.

3.3. MEASUREMENTS OF DEAD TIME

Results of measurements as to the dependence of dead time on overvoltage for three different fillings are shown in fig. 11.

Theoretical considerations led Wilkinson[9]) to the conclusion that the dead-time decreased with increasing overvoltage like a hyperbola. This was verified by our experiments.

4. Conclusion

Let us now consider in each case the processes responsible for the "high" as well as the "low" pulses.

1. At pressures applied in our experiments on ethyl alcohol-argon gas mixture filled counters only organic vapour ions approach the cathode. Thus the theory proposed by Korff and Present applies to the origin of "high" multiple discharges. An electron is knocked out from the cathode surface by ions which remain in an excited state after this process. The major part of these excited vapour molecules will dissociate and the rest will return to the ground state by photon emission. These emitted photons in turn may release photoelectrons from the cathode surface. Now, these photoelectrons give rise to "high" multiple pulses.

Korff and Present's theory can be interpreted mathematically too. Let us introduce following symbols:

n is the number of all primary pulses initiated per unit time. (Assuming not too many primary pulses being produced per unit time, no correction is required for the deadtime.)

n_i is the number of pulses per discharge.

W_a is the probability that the excited quenching vapour molecules will return to the ground state.

W_f is the probability of photoelectron release.

All the ions reaching the cathode per discharge are organic vapour ions which, as it is known, release electrons from the cathode surface and remain in an excited state. The fraction of the excited molecules returning to the ground state is given by

$$n n_i W_a .$$

Each excited molecule decays to the ground state by photon emission. The number of photoelectrons released is written as

$$n n_i W_a W_f .$$

Assuming that there are no electro-negative impurities in the counter gas volume, each photoelectron initiates a further discharge. This produces a "high" double pulse.

In each discharge, thus in secondary discharges too, n_i ions are produced. Since the number of secondary discharges is $n\, n_i\, W_a\, W_f$, the total number of secondary ions has to be

$$n n_i^2 W_a W_f .$$

Now, the number of photoelectrons released from the cathode by secondary discharges may be expressed as

$$n n_i^2 W_a^2 W_f^2 .$$

This expression gives also the number of

[7]) D. H. Wilkinson, Phys. Rev. **79** (1948) 1472.

[8]) A. G. Fenton and E. W. Fuller, Proc. Phys. Soc. A **62** (1949) 32.

[9]) D. H. Wilkinson, Ionisation Chambers and Counters (Cambridge University Press, Cambridge, 1950) p. 206.

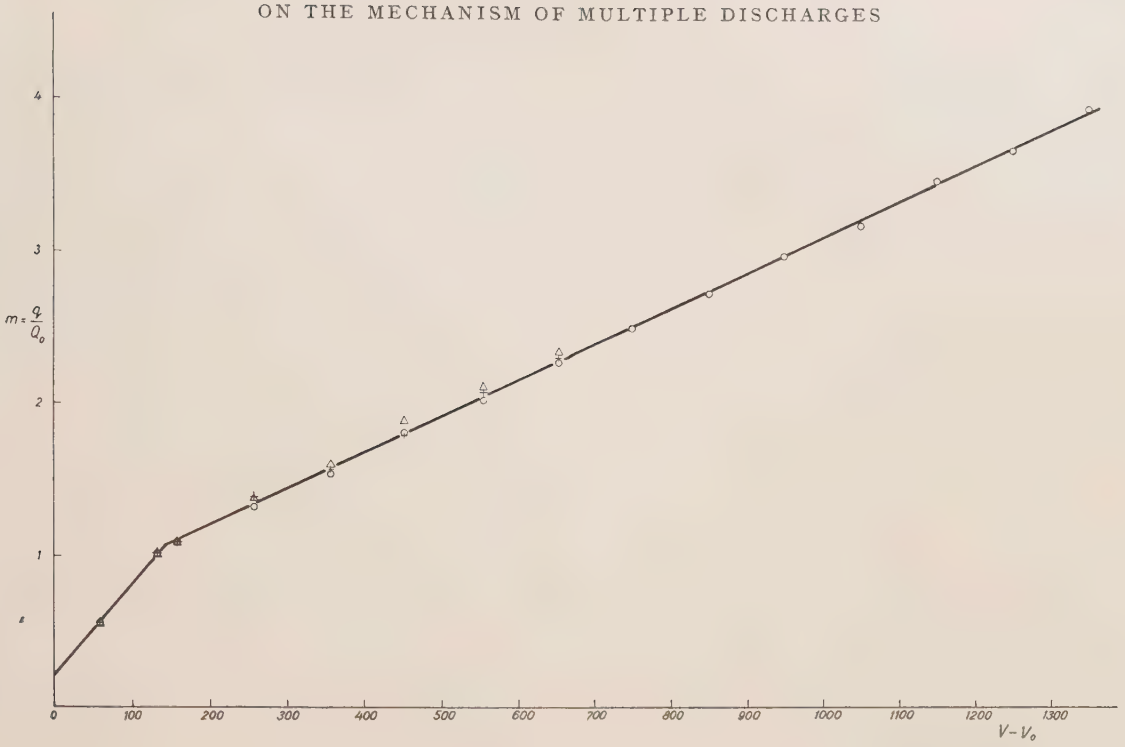

Fig. 10. △ = 15 mm Hg ethyl alcohol; + = 15 mm Hg ethyl alcohol 100 mm Hg argon; ○ = 15 mm Hg ethyl alcohol 300 mm Hg argon.

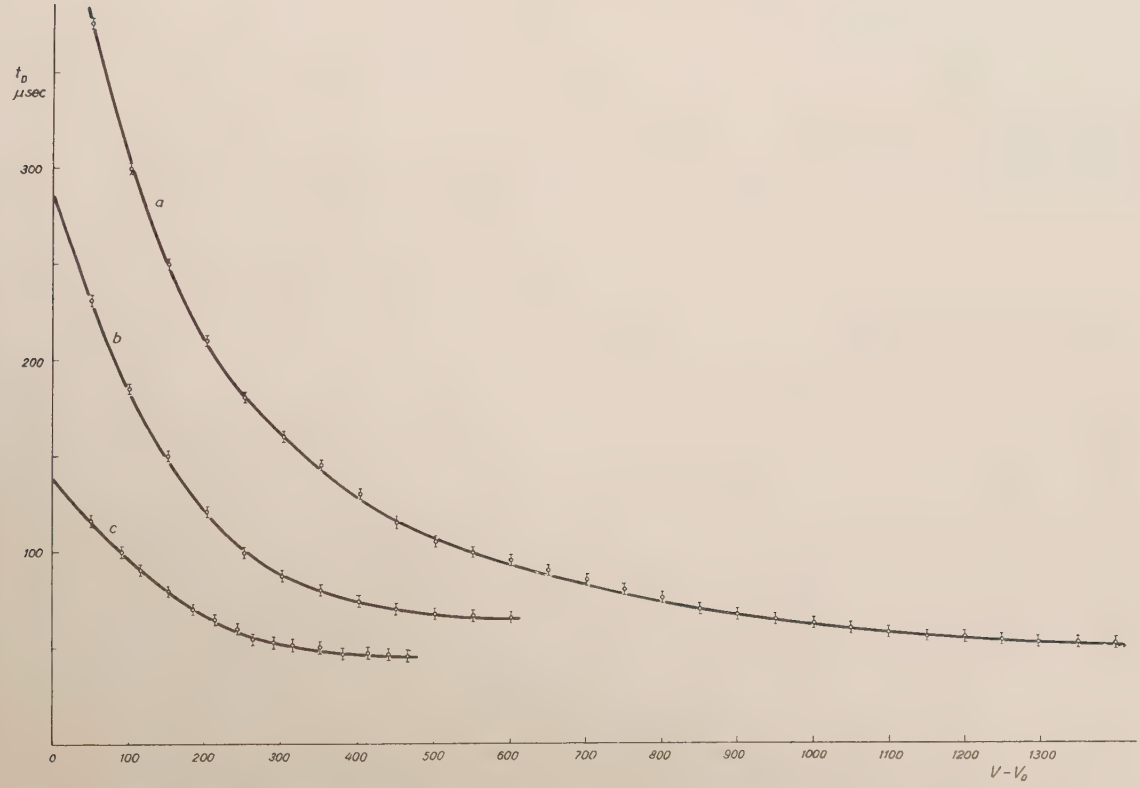

Fig. 11. a = 15 mm Hg ethyl alcohol 300 mm Hg argon; b = 15 mm Hg ethyl alcohol 100 mm Hg argon; c = 15 mm Hg ethyl alcohol.

tertiary discharges. We may obtain in the same way the number of fourth, fifth, etc. discharges that is the number of the fourth, fifth etc. pulses of multiples discharges. By summation we obtain the total number of "high" multiple pulses for n primary pulses. By adding now to this quantity the number of the primary pulses, the total number of "high" pulses is obtained as

$$N' = n + \\ + n n_i W_a W_f + n n_i^2 W_a^2 W_f^2 + \cdots + n n_i^s W_a^s W_f^s + \cdots .$$

Upon summing up, the expression leads to

$$N' = n \sum_{r=0}^{\infty} n_i W_a W_f .$$

This is an infinite geometric series. It is divergent for $n_i W_a W_f > 1$ and $N \to \infty$. In this case the tube ceases to operate as a counter and continuous discharge sets in. For self-quenching tubes above product is always less than unity, since the number of ions produced per pulse is about 10^{10}. The value of W is of the order of 10^{-6} and that of W_f about $10^{-4} - 10^{-5}$. For convergent series the sum is given by

$$N' = \frac{n}{1 - n_i W_a W_f} . \qquad (1)$$

The number of ions per discharge is obtained by dividing the charge $q(V)$ produced per discharge by the elementary charge ε, i.e.

$$n_i = \frac{q(V)}{\varepsilon} .$$

The product $W_a W_f$ represents the probability that the excited organic vapour molecule will decay to the ground state and the photon emitted in this process will release photoelectrons from the cathode surface initiating is the probability that a single ion will induce a secondary avalanche. In the following let us set $W_a W_f = W$. Substituting this into eq. (1) the dependence of N' on operating voltage may be obtained if the values of n and W as well as the charge in terms of voltage are known. Thus we find

$$N' = \frac{n}{1 - \frac{q(V)}{\varepsilon} W} . \qquad (2)$$

The interpretation of eq. (2) will be discussed later.

2. The "low" multiple pulses appear in the recovery interval, consequently they may be attributed to processes occurring in the gas volume. Metastable argon molecules produced around the wire are assumed to be responsible for the multiple pulses observed after the dead time. According to Kruithof[10]) the ratio of the number of ions to that of metastable atoms produced in the avalanche along the wire was found to be 1:1 for the range of E/p applied in the measurement. The number of ions in the avalanche can be determined, as seen above, from the expression given for the charge produced per pulse $(n_i = (1/\varepsilon) q(V))$. The number of metastable atoms at the time of their birth i.e. at the time of the formation of the ion sheath around the anode all along the wire, is equal to n_i. The dissociation rate of metastable atoms may be described by the following exponential law:

$$N_M = n_i^{-\beta t}$$

where N_M is the number of metastable atoms still existing at time t after their birth. β is defined by the following equation

$$\beta = A p + B p^2$$

where p is the argon pressure. Phelps and Molnar[11]) reported following values for the constants involved: $A = 40$ mm/sec and $B = 9/\text{mm}^2$ sec. Ap is the decay of metastable atoms while Bp^2 represents a metastable decay where metastable molecules result from metastable atoms.

For the argon pressures applied in our measurements, the term Ap may be neglected as compared to Bp^2. At these pressures metastable atoms result preponderantly in metastable molecules which decay emitting ultraviolet photons of a bout 1250 Å wavelength.

The decay of metastable atoms resulting in the formation of metastable molecules was investigated by Colli[12]). In the reported experiments it was found that the mean life τ_a of

[10]) A. A. Kruithof, Physica **7** (1950) 519.

[11]) A. V. Phelps and J. P. Molnár, Phys. Rev. **89** (1953) 1202.

[12]) L. Colli, Phys. Rev. **95** (1954) 892.

metastable atoms versus pressure is given as

$$\tau_a = \frac{1}{9p^2}$$

where p is the argon pressure in mm Hg. The mean life of metastable molecules was measured as $\tau_m = 3.4\ \mu$sec independently of pressure.

Knowing the values of τ_a and τ_m, the number of metastable molecules at any given time may be calculated. As a result we obtain

$$N_m = n_i \frac{\frac{1}{\tau_a}}{\frac{1}{\tau_m} - \frac{1}{\tau_a}} (e^{-t/\tau_a} - e^{-t/\tau_m}) .$$

In the decay of each metastable molecule an ultraviolet photon is emitted. The rate of photon emission is given by

$$\frac{dF}{dt} = \frac{1}{\tau_m} N_m .$$

Substituting the value of N_m and upon integrating from t to ∞, the total number of ultraviolet photons produced after time t is obtained as

$$F = \frac{n_i}{\tau_a - \tau_m} (\tau_a e^{-t/\tau_a} - \tau_m e^{-t/\tau_m}) . \qquad (3)$$

These photons are produced around the wire and only a fraction of them reaches the cathode seeing that some are absorbed in the meantime. Photons reaching the cathode may release photoelectrons from the cathode surface. Denoting by w_f the probabilities that a photon will impinge upon the cathode surface and by w_e that this will result in the release of a photoelectron, then the product $w_e w_f$ gives the probability that a secondary electron will be liberated on the cathode surface by a photon produced at the anode. The electrons released by the photons travel to the anode in a negligible time as compared to the motion of the ion sheath and induce there a further avalanche. Thus this process occurs in the recovery interval immediately after dead time.

The number of photons originating from metastable molecules surviving after dead-time is obtained from eq. (3) by substituting the dead time $t_D(V)$ for t. The number of "low" pulses produced by the photons is given by multiplying eq. (3) by w, that is

$$\frac{n_i}{\tau_a - \tau_m} (\tau_a e^{-t_D/\tau_a} - \tau_m e^{-t_D/\tau_m}) . \qquad (4)$$

Upon the formation of each "high" pulse, immediately after the dead time, the "low" multiple pulses due to the decay of metastable molecules, begin to appear in a more or less high number.

Consequently the total number of "low" pulses may be obtained by multiplying expression (4) with the number N' of all "high" pulses and introducing $(1/\varepsilon)(q(V))$ for n_i, thus we have

$$N'' = \frac{n_i}{1 - \frac{q(V)}{\varepsilon} W} \frac{\frac{q(V)}{\varepsilon} w}{\tau_a - \tau_m} (\tau_a e^{-t_D/\tau_a} - \tau_m e^{-t_D/\tau_m}) . \qquad (5)$$

The sum of the number of "high" and of "low" pulses gives the total number N of discharges per unit time. If the number of primary avalanches per unit time is n, then

$$N = N' + N'' . \qquad (6)$$

The equation (2) derived for the voltage dependence of "high" pulses represents an isosceles hyperbola. On plotting this equation with the voltage as abscissa and N' as ordinata we obtain for $N' = n$ the asymptote of the hyperbola parallel to the abscissa. The asymptote parallel to axis N' is at $V = V'$ where V' satisfies the equation

$$W = \frac{\varepsilon}{q(V')}$$

On increasing the voltage the value of function $N(V')$ increases first slowly. The curve shows a slight break at the same voltage at which a "break" has been observed on the curve for charge per discharge versus voltage. The slope becomes then more marked with increasing voltage and on approaching the asymptote N' increases rapidly. The portion of the hyperbola approximately parallel to the abscissa corresponds to the plateau region. If the counters measured are pure quenching gas filled tubes or if in the case of argon content the "low" pulses are being suppressed by means of a discriminator, the rapidly rising portion of the hyperbola represents the breakdown region. This means that at the voltage V' corresponding to the

asymptote parallel to the N' axis continuous discharge sets in. The slope of the hyperbola approximately parallel to the axis depends on the value of W, the slope varies according to the increase or decrease in the value of W. Moreover W determines also the position of the asymptote parallel to the ordinate, i.e. the voltage V' at which according to the theory the continuous discharge appears.

Eq. (5) gives the total number of "low" multiple pulses per unit time for argon-quenching gas mixture filled tubes. The value of N'' as given by eq. (5) is very low for values of V slightly above the starting voltage. With the increase in voltage $t_D(V)$ decreases while $q(V)$ linearly increases (see section 3. Results of the measurements), consequently N'' increases with increasing voltage more and more rapidly. The dependence of the number of "low" multiple pulses on pressure is implied in the quantity τ_a. As seen previously, τ_a is inversely proportional to the argon pressure. That is why the number of "low" pulses increases with voltage less rapidly for high argon pressures than for low ones.

Studying the behaviour of function (6) for $N' + N''$ for argon-alcohol filled counters, it becomes apparent that in the plateau region N' is preponderant and N'' seems to be negligible. Later on, however, N'' increases rapidly.

3. For 15 mm Hg ethyl alcohol filled counters the operational characteristics may be approached by eq. (2). The number of primary avalanches produced per unit time was measured in the approximately proportional region. The number of discharges per unit time measured in this region is equal to n since the probability of multiple discharges occurring in this region is negligible. n was found to be 1050 ± 33 as measured under conditions corresponding to the characteristic plot in fig. 2.

Function $N'(V)$ was plotted in fig. 12 for 15 mm Hg ethyl alcohol filled tubes. To evaluate the function we used values of $q(V)$ and of n as measured in the approximately proportional region. W was chosen as 6.25×10^{-11}. Also the experimental points are given in the figure. They fit well to the curve calculated for $N'(V)$. The asymptote of curve $N'(V)$ corresponds to the voltage (1420 V) as measured for the appearance of continuous discharge.

Also eq. (2) was used to plot the operational characteristics resulting from "high" pulses only for 15 mm Hg alcohol plus 100 mm Hg argon filled tubes. By measurements on the approximately proportional region n was obtained as 1710 ± 40 with $W = 1.92 \times 10^{-11}$. Curves I–II shown in fig. 13 were obtained for the function $N'(V)$.

The overall characteristic plot of operation of these counters including "low" pulses too, is given by eq. (6). To evaluate the term $N''(V)$ in eq. (6), w was chosen as 1.12×10^{-6} and by introducing the measured values for $t_D(V)$ the solution of eq. (6), yields section I–III of the curve to be seen in fig. 13. Experimental points for these three sections are also shown and again there is a good agreement between experimental and theoretical results with above values chosen for W and w.

Characteristic plots for the operation of 15 mm Hg alcohol — 300 mm Hg argon filled tubes based on eqs. (2) and (6) are shown in fig. 14. W and w were chosen here as 2.05×10^{-11} and 1.07×10^{-6}, respectively. Sections I–II show the variations in the number of "high" pulses, while that in the total number of pulses is represented by sections I–III. There is a satisfactory agreement between experimental and calculated results.

Table 1

	W	w
15 mm Hg ethyl alcohol	6.25×10^{-11}	
15 mm Hg ethyl alcohol 100 mm Hg argon	1.92×10^{-11}	1.12×10^{-6}
15 mm Hg ethyl alcohol 300 mm Hg argon	2.06×10^{-11}	1.07×10^{-6}

In table 1 values are listed as obtained for W and w with three different kinds of filling. The order of magnitude of secondary "high" pulses per ion (this corresponds to W) has been estimated by Korff and Present[1]).

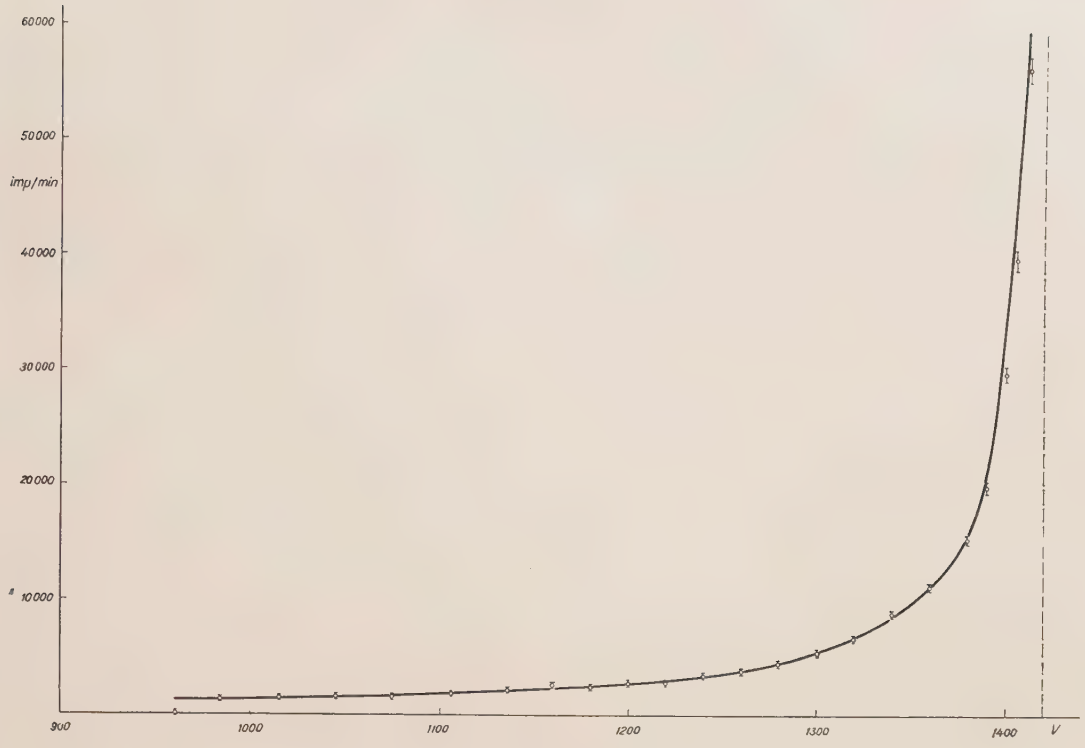
60000
50000
imp/min
40000
30000
20000
10000
900
1000
1100
1200
1300
1400
V

Fig. 12

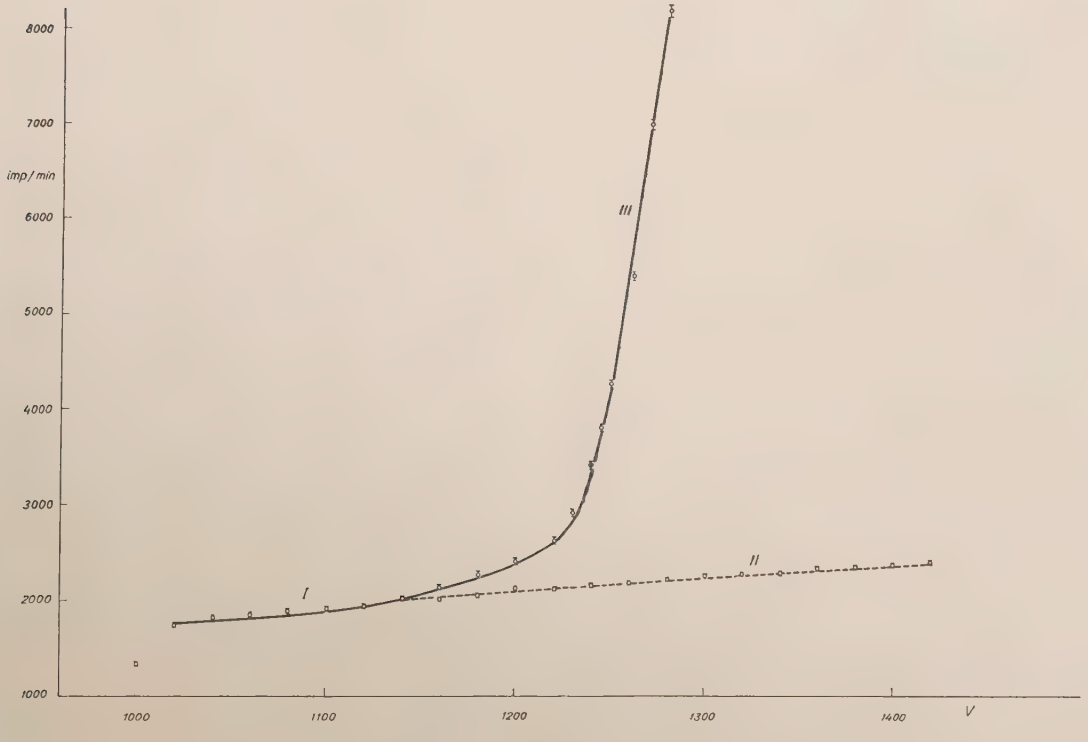
8000
7000
imp/min
6000
5000
4000
3000
2000
1000
1000
1100
1200
1300
1400
V
I
II
III

Fig. 13

As to the order of magnitude, the values calculated by them are in agreement with our results. Bretta and Rostagni[13]) obtained W as 3.33×10^{-11} for brass cathode tubes. Wiser and Krumbein[4]) reported counts of 1.8×10^{-11}–5×10^{-11} secondaries per ion. The value of W depends rather strongly on the condition and on the material of the cathode, consequently the tabulated data was observed in the values of W and w. For tubes refilled and measured under the same conditions or for new tubes of identical construction. This deviation may be attributed to the well known fact that even carefully handled metallic surfaces of identical material show a different behaviour in measurements of work function and photon release

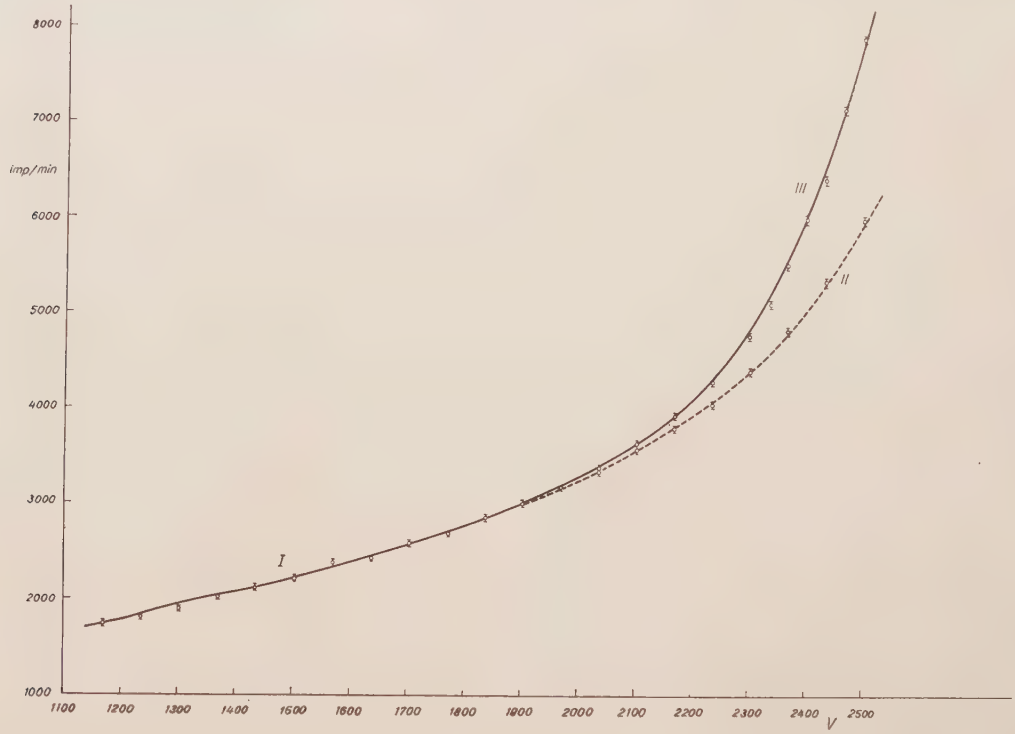

Fig. 14

the values obtained in our experiments do not show significant discrepancy from data given in the literature.

w is the product of two probabilities ($w_f w_a$). According to literary data, the value of w_a is of the order of 10^{-4}–10^{-5}. The probability that a photon produced at the anode from metastable decay will reach the cathode is about 10^{-1}–10^{-2}. This result was supported by the experiments of Huster and Siegler[14]). They obtained values of the same order of magnitude for the probability that photons emitted by excited atoms returning to the ground state at the anode will reach the cathode.

A maximum deviation of 10–15 percent from efficiency. The value of W was found to be, as a rule, much higher for pure quenching gas filling than for argon-ethyl alcohol mixture. It is very probable that photon release efficiency is affected by the nature of the filling gas. In the literature on photocells there are some indications to this effect. The value of w is approximately the same for tubes filled whether at 100 mm Hg or at 300 mm Hg argon pressure. This is plausible since it is the quantity of quenching gas which determines the photon absorption and owing to the same quenching gas pressures these quantities were identical in both cases.

[13]) E. Beretta and A. Rostagni, Nuovo Cimento **6** (1949) 391.
[14]) E. Huster and E. Ziegler, Zs. f. Phys. **146** (1956) 281.

NUCLEAR INSTRUMENTS AND METHODS 6 (1960) 323–330; NORTH-HOLLAND PUBLISHING CO.

MILLIMICROSECOND PULSING – ITS APPLICATION AND TECHNIQUE†

W. M. GOOD

Oak Ridge National Laboratory, Oak Ridge, Tennessee

Received 14 September 1959

A terminal pulsed Van de Graaff Generator is capable of delivering 500 μA and more peak currents in bursts 2–10 millimicrosecond time duration at arbitrary repetition rates. It is shown how millimicrosecond intervals of time relative to these bursts can be measured and recorded. Applications of such measurements to nuclear physics are given. Some of the problems encountered in producing bursts of ions at the terminal of a Van de Graaff are outlined by considering the application of a simple sinusoidally varying voltage to obtain bursts. It is shown that existing techniques can be improved substantially in a number of ways.

1. Introduction

The direct measurement of neutron velocity as a means of studying neutron energies and energy distributions has in recent years been a powerful incentive to the development of techniques for the production of millimicrosecond bursts of ions and the measurement of millimicrosecond intervals of time. The techniques associated with these two facets of the general problem have taken respectively the directions of pre-acceleration ion burst production, and multi-channel storage and presentation of measured time intervals. This paper is primarily concerned with the problem of pre-acceleration ion burst production as it applies to a Van de Graaff accelerator. Excepting in a schematic sense, the following discussions will not be concerned with the electronic problems relating to time interval measurement and display.

Since neutron velocity determination is not the only use of an instrument which combines millimicrosecond bursts of ions with time spectrometry, some general account will first be given of the general utility of such an instrument.

2. General Application of Pulsed Ion Beams

Fig. 1 is a representation of the type of instrument with which this paper is concerned. It consists of (a) pre-acceleration pulsed Van de Graaff, (b) fast detector, (c) time analyzer. The time interval to be measured is the difference between the burst arrival time at the target and the time of the detector response. The time duration of the bursts produced by the pre-acceleration pulsed Van de Graaff is presumed to be 2 to 10 $\times$ 10^{-9} sec at a repetition rate of 600 kc/sec to 5 Mc/sec with 500 μA or more peak current.

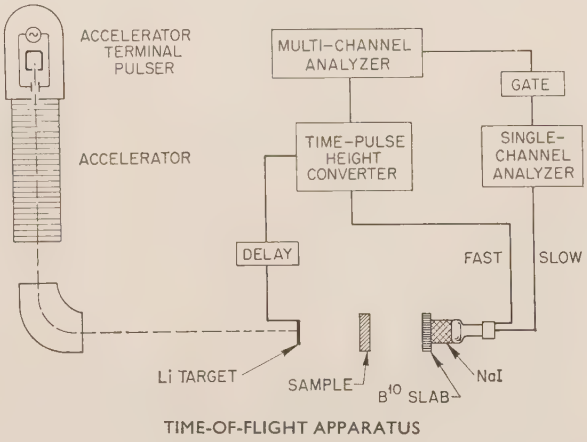

Fig. 1. Block diagram of pre-acceleration pulsed Van de Graaff and associated time analyzer.

The function of the time analyzer is, (a) to divide the range of times of particular interest between burst on target and signal from detector into 100 or more equal intervals, (b) to catalogue each measured time and store it in its proper

† Based on a talk given at the Accelerator Conference, High Voltage Engineering Corporation, Burlington, Mass., Oct. 14–16, 1958.

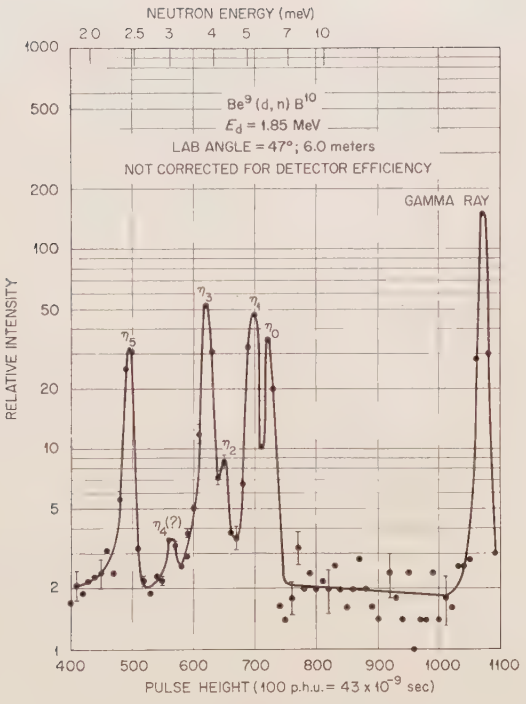

Fig. 2
Time spectrum of neutrons from the reaction $Be^9(d,n)B^{10}$.

interval. The clock which measures the time is a condenser which can be charged at a constant rate by turning on and off a constant current. The voltage change on the condenser is proportional to the time to be measured, and once time has been converted to a pulse height, the problem of multiple channel time storage is essentially solved.

For the purpose of discussing the applications of such an instrument, it is convenient to make the following classification as to use:

1. Time measurement: (a) nuclear events; (b) time-of-flight or energy measurement.

2. Event discrimination: (a) identification of nuclear events by characteristic times; (b) background discrimination, (i) time correlated, (ii) steady.

Consider briefly some examples of these applications. To begin with, there is the problem of the measurement of the lifetime of nuclear states, a significant number of which could be expected to lie in the range 10^{-9}–10^{-6} sec. Bloom[1]) and more recently Holland[2]) have searched for and measured such lifetimes. This is an example of what could conveniently be called timing nuclear events. A second timing application is the important one of energy measurement by time-of-flight. The method can be applied to ions as well as neutrons, but it is of especial importance to neutrons. The reason obviously is that since they possess no charge, it is not possible to bend them in order to measure their energy or momentum. Fig. 2 shows a primary neutron spectrum obtained from the $Be^9(d,n)B^{10}$ reaction. In this case the neutrons originate directly from the ions on the target. The example just given, in the terminology of the spectroscopist, is a line spectrum. Such spectra can be not only of primary origin but of secondary origin as well, as in the case of neutron inelastic scattering. In this case the ions strike target No. 1 which is the source of pulses of neutrons which then impinge upon target No. 2 which then becomes the source of secondary neutrons of various energies. Cranberg at Los Alamos[3]) has made extensive use of

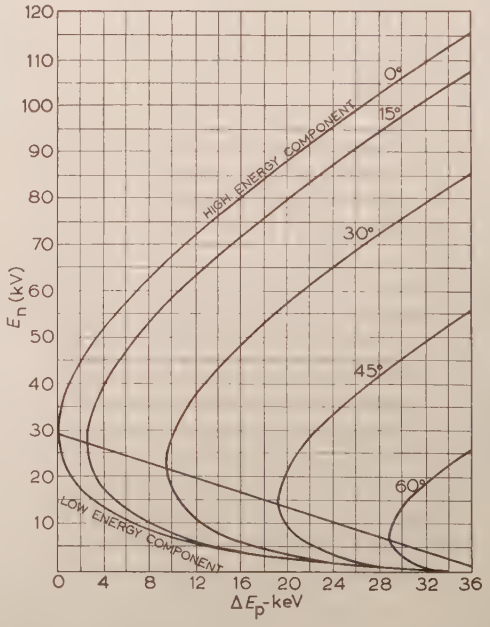

Fig. 3. Neutron energies from a thin lithium target as a function of the difference between the bombarding energy and the threshold energy for various angles of emission in the laboratory.

[1]) Bloom, Turner and Wilkinson, Phys. Rev. **105** (1957) 232.
[2]) Holland, Lynch and Hanna, Phys. Rev. **112** (1958) 903.
[3]) L. C. Cranberg and J. S. Levin, Phys. Rev. **103** (1956) 343.

this technique in the study of nuclear energy levels.

In the spectroscopist's terminology there are absorption spectra as well as emission spectra. To obtain optical absorption spectra, "white" light is incident on a sample, and black lines appear at the frequencies of absorption. The neutron analogue of this type of spectrometry is the measurement of neutron total cross sections. At Oak Ridge[4]), millimicrosecond time-of-flight is used to study neutron absorption spectra in the important kilo electron volt range of neutron energies. The source which provides the "white" neutron spectrum is the $Li^7(p,n)Be^7$ reaction. From fig. 3 it can be seen that, with a target of suitable thickness, this reaction can produce "white" neutrons without the use of moderation over the entire kilovolt range of energies. Let it be assumed that 10 mμs time resolution is available with adequate intensity for making measurements at 1 meter. Then 5 keV neutrons which require 1 μs to traverse 1 meter will have their velocity

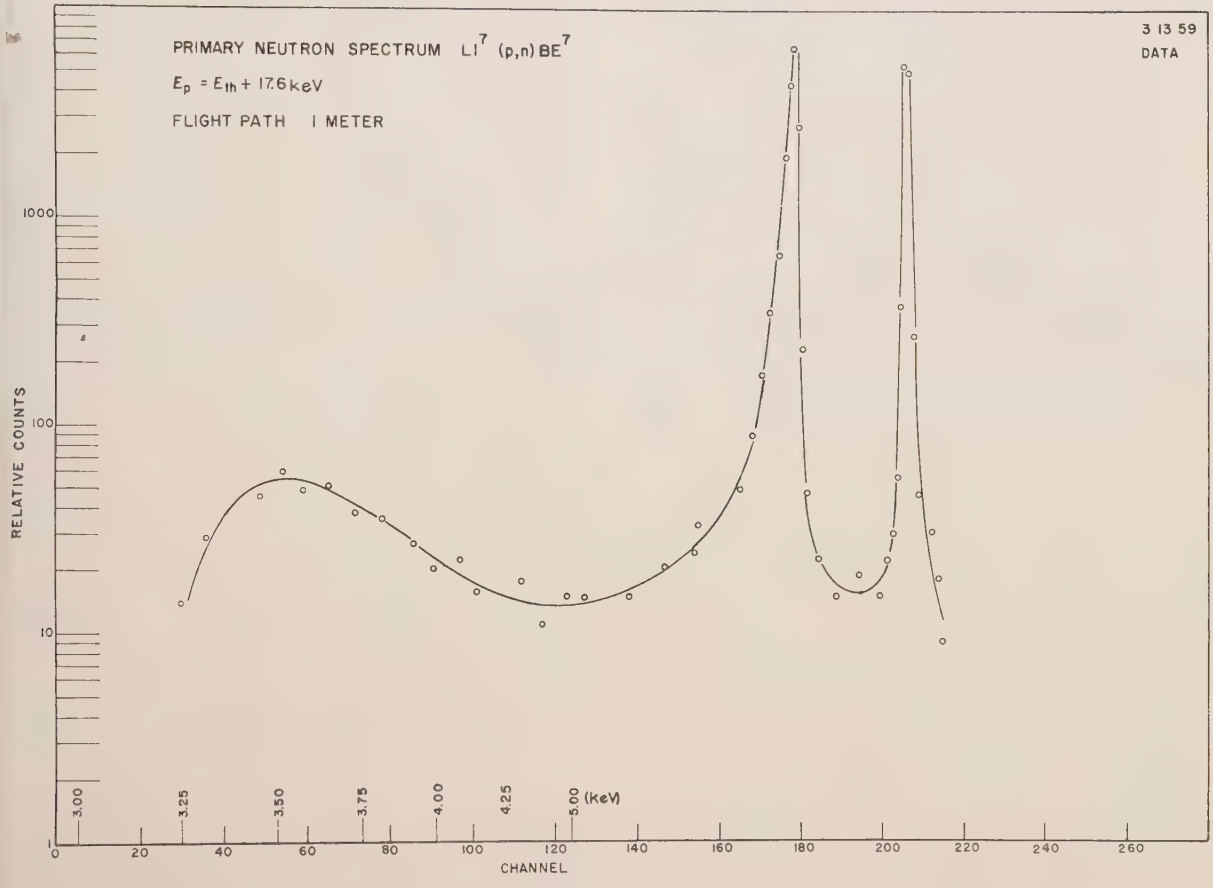

Fig. 4. Time spectrum at 0° and 1 meter that results from bombarding about a kilovolt thick Li target with proton 18 keV above p,n-threshold. From low to high channel numbers the groups are respectively low energy neutrons, high energy neutrons, target γ-rays.

determined to 1%, their energy to 2%. The dynamics of the $Li^7(p,n)$ reaction is such that, by appropriate choice of bombarding energy and flight path, neutrons from 2 keV to about 60 keV energy can be measured with the same precision as can neutrons of 5 keV energy. Fig. 4 shows on a compressed time scale an example of a complete time spectrum from the $Li^7(pn)$ reaction. An absorption spectrum is obtained when an absorber is introduced between target

[4]) Good, Neiler and Gibbons, Phys. Rev. **109** (1958) 926.

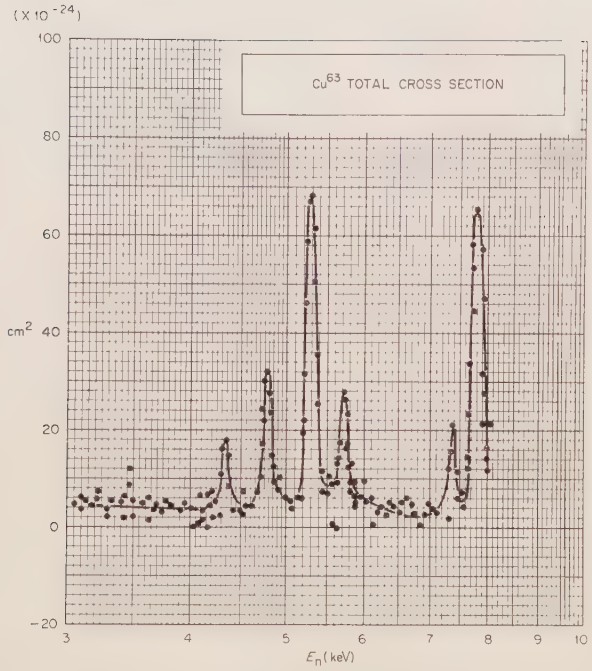

Fig. 5. Neutron total cross section of Cu^{63}.

and detector. Fig. 5. shows the results obtained on Cu^{63} with the absorption coefficient converted into cross sections.

Time discrimination designates those applications where the prior knowledge of characteristic times permits identifying events. One clear example is that of Diven[5]) at Los Alamos who uses pulse techniques to discriminate those γ-rays that are emitted after a simple neutron capture in uranium from those γ-rays that are emitted and then followed by fission subsequent to the neutron capture. The scheme is to observe the multiplicity of pulses that appear after the γ-pulse. If fission follows the γ-emission, then the γ-pulse will be followed by a sequence of neutron pulses corresponding to the multiplicity of prompt neutrons following fission. A somewhat similar type of discrimination is currently being employed by Macklin, Neiler, Gibbons and Miller at Oak Ridge to distinguish the neutron capture γ-rays from the scattered neutrons in the measurement of neutron capture cross sections.

Lastly, the pulsed beam permits effective background discrimination. It does this by virtue of the fact that if the detector knows precisely when to look for an event, spurious events can be ignored and the between event backgrounds ignored. Advantage can be taken of a 1% to 10% duty to raise the peak current 10 to 100 without raising the average current and thus gain 10–100 in signal to background.

3. Ion Burst Production by Beam "Chopping"

Before we discuss the subject of special interest here, viz., the problem of terminal pulsing a Van de Graaff, it is opportune to make a few comments on general requirements that may be different from those normally acceptable for a Van de Graaff. To begin with, it is not surprising that more terminal power is the first such requirement, the extra amount depending upon the peak current and the shortness of the "burst" that is required. The Oak Ridge pulsed Van de Graaff, for example, which is producing 500 μA bursts as short as about 4 mμs utilizes about 350 extra watts of power over and above that normally required. This power is consumed in a circuit for producing a periodic voltage for rendering the periodic bursts of ions, a circuit which permits the Van de Graaff to accept only a certain fraction of the periodic bursts, and at least one additional lens. A requirement of good general voltage stability is associated with the need for "zero time" information on each burst. The ion bursts themselves can be used to supply this information if the beam from the ion source does not vary in intensity by more than a few per cent. A high efficiency ion source may not perform suitably for more than, say, 200 hours of steady operation and one highly desirable future of the ion source, therefore, is good source-to-source reproducibility. In connection with this question of sources, it should be recognized that some sources are known to be inherently pulsed[6]) and there may be some special applications in which this fact can be utilized. However, for the degree of flexibility in application that is generally needed it seems

[5]) Diven, Terrell and Hemmendinger, Phys. Rev. **109** (1958) 144.

[6]) Phillips, Paul, Ferguson, Whitehead, Grjebine, Moreau and Olkowsky, Nuclear Instruments **3** (1958) 43.

necessary to first produce a steady beam, free of modulation, and then by some means "chop" this beam into bursts of the desired time-duration.

There are of course several approaches to this problem of producing pulsed beams; for example, there may be beam bunching, there may be beam chopping, or there may be a combination of the two. Or again, if "chopping" is to be used, there are different choices that can be made as to the form of the time-varying voltage that is employed, the separate choices being accompanied by differences in the properties of the bursts that are produced. A voltage varying sinusoidally with time is a particularly simple choice of time-varying voltage for the purpose, and this case will be briefly analyzed to give some general feeling for the problem.

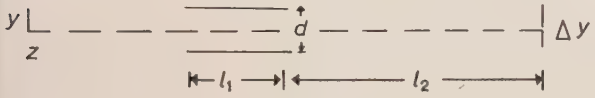

Fig. 6. Schematic of simple deflector plate ion beam pulser.

Consider a ray entering at $t = t_0$, $\dot{y} = 0$, $\ddot{y} = 0$. If the transit time through the deflector plates is a small fraction of a period, the voltage $V = V_0 \sin \omega t$ can be represented by $V = V_0 \omega t$ and it is then easy to show that

$$\Delta t_0 = \frac{4}{2\pi} \frac{E}{eV_0} \frac{\Delta y d}{l_1 (l_1 + 2l_2)} T \qquad (1)$$

in which E is the K. E. of the beam, e is the ionic charge. This formula can be written alternatively

$$\Delta t_0 = \frac{\Delta y}{\text{writing speed}} .$$

In this formula the writing speed is closely related to the steady beam deflection sensitivity

$$\frac{1}{4} \frac{e}{Ed} l_1 (l_1 + 2l_2)$$

to which it is indeed closely related in the case of the ramp function voltage $V = V_0 \omega t$. The aperture Δy is given approximately by $\Delta y \approx$ slit width + beam width. From formula (1) ion bursts of mμs and even shorter time duration would appear to be achievable.

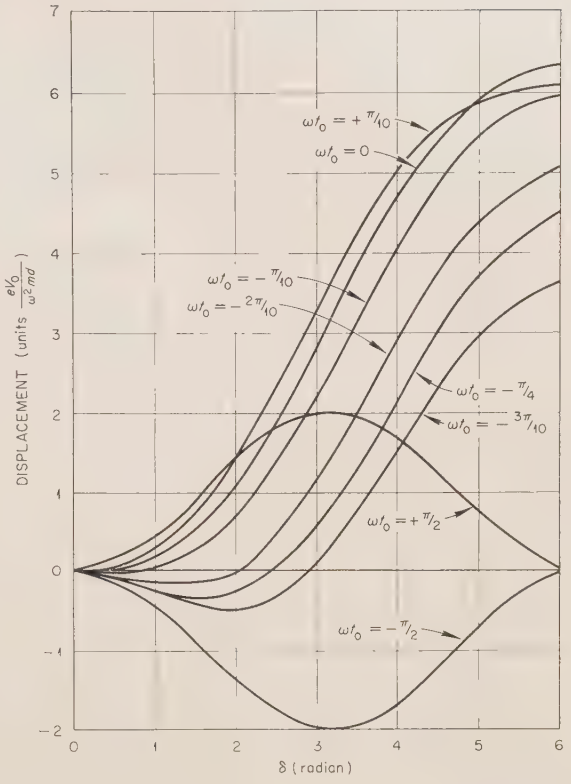
DISPLACEMENT (units $\frac{eV_0}{\omega^2 Md}$)
δ (radian)
$\omega t_0 = +\pi/10$
$\omega t_0 = 0$
$\omega t_0 = -\pi/10$
$\omega t_0 = -2\pi/10$
$\omega t_0 = -\pi/4$
$\omega t_0 = -3\pi/10$
$\omega t_0 = +\pi/2$
$\omega t_0 = -\pi/2$
Particle Displacement vs. Transit Angle Between Deflector Plates.

Fig. 7. Ion displacement as a function of entrance phase angle and transit phase angle in the case of a simple pair of deflector plates.

While this simple description within limits gives a reasonable estimate of the duration of a burst, it has to be extended to include (a) arbitrary transit angles, and (2) finite size of beam. The exact solution to the equations of motion of ions of mass M subjected to a transverse electric field established by a voltage $V = V_0 \sin \omega t$ and subject to the previous initial conditions is:

(a) $\dot{z} = \text{constant} = v_0$

$$\text{(b)}\ \dot{y}(l_1) = \frac{eV_0}{\omega M d} [\cos \omega t - \cos \omega t_0] \qquad (2)$$

$$\text{(c)}\ y(l_1) = \frac{eV_0}{\omega^2 M d} [\sin \omega t - \sin \omega t_0 - \cos \omega t_0 (t - t_0)] .$$

Fig. 7 shows the form of the trajectories between the deflector plates. At the position of the screen we have with the usual assumptions,

$$y_{\text{screen}} = y (l_1) + \tau_2 \dot{y}(l_1) \qquad (3)$$

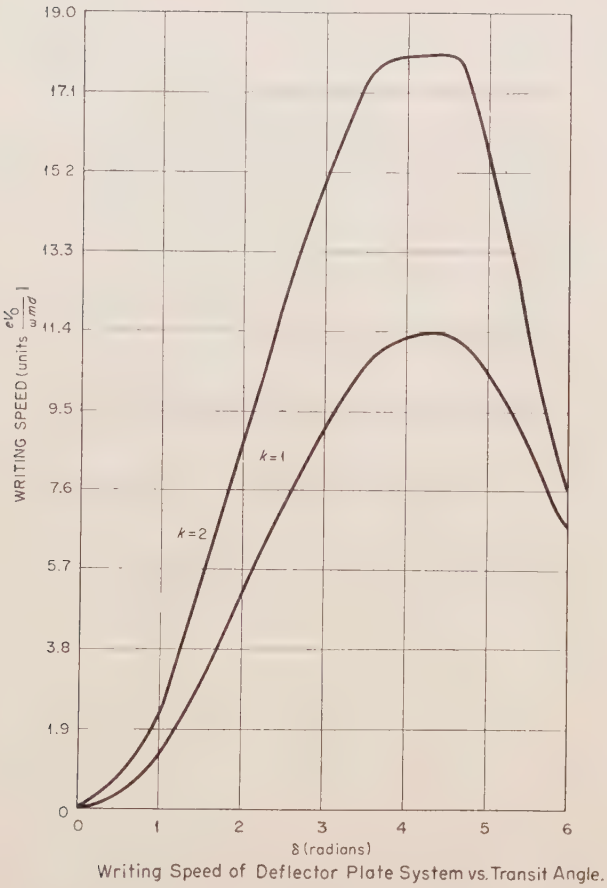

Fig. 8. Writing speed of a simple deflector plate system as a function of transit phase angle and of distance from deflector plates to screen, this distance expressed in units of deflector plate length.

where $\tau_2 = l_2/v_0 =$ transit time to screen from the end of the deflector plates. Eq. (3) can be written in the form.,

$$y_{\text{screen}} = \frac{eV_0}{\omega^2 Md}\,[B(\delta_1,k)\sin(\omega t_0 + \theta(\delta_1,k))]\,. \tag{4}$$

In this equation,

$$\delta_1 = \omega\tau_1 = \omega\frac{l_1}{v_0}$$

$$\delta_2 = k\delta_1$$

and

$$B(\delta_1,k) = \sqrt{\begin{array}{l}2 + \delta^2 + 2k\delta^2 + 2k^2\delta^2 \\ -2\,[1 + k\delta^2 + k^2\delta^2]\cos\delta \\ -2\,\delta\sin\delta\end{array}} \tag{5}$$

$$\theta(\delta_1,k) = \tan^{-1}\frac{\delta\,(1+k) - k\delta\cos\delta - \sin\delta}{1 - \cos\delta + k\delta\sin\delta}\,. \tag{6}$$

The form of $B(\delta_1,k)$ is shown in fig. 8. Differentiating eq. (4):

$$\frac{\Delta y_{\text{screen}}}{\Delta t_0} = \frac{eV_0}{\omega Md}\,[B(\delta_1,k)\cos(\omega t_0 + \theta)] \tag{7}$$

$\equiv$ writing speed $\cos(\omega t_0 + \theta)$.

Normally $y_{\text{screen}} = 0$ so that

$$\omega t_0 = -\theta(\delta_1,k) \tag{8}$$

$$\Delta t_0 = \frac{\Delta y_{\text{screen}}}{\text{writing speed}}\,. \tag{9}$$

Eq. (8) gives the entrance angle as determined by placing the aperture on the beam axis, i.e., by requiring $y = 0$. The relationship (8) is shown in fig. 9. Eq. (9) is the burst duration of a ray that enters the deflector plates on axis.

From eq. (4) it can be seen that $y_{\text{screen}} = 0$ is satisfied every half period; correspondingly eqs. (2) show for these two situations that the beam directions are relatively reversed with respect to the y-axis. The consequence of the latter fact is that it is possible for two different images to appear at the target and these may have different pulse length characteristics at the timing circuits. Observe here that the symmetry mentioned above

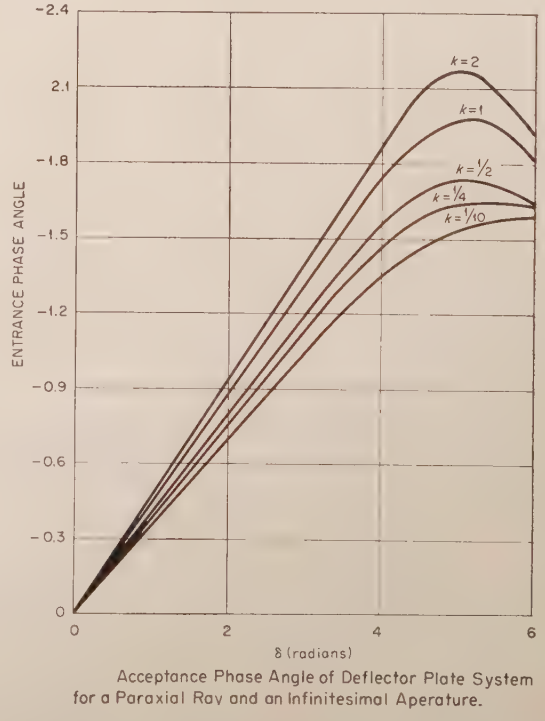

Fig. 9. The relationship for a simple pair of deflector plates between entrance phase angle and transit phase angle.

can be removed by adding a constant term A to $B(\delta_1,k)\sin(\omega t_0+\theta)$. This can be done by splitting the deflector plates and placing a D.C. bias on one or both. In fact, it can be managed that for one of the rays $\dot{y}(l_1)=0$, $\dot{y}(l_1)=0$. Now the time at the screen as measured with reference to the periodic sweep voltage is

$$t_{\text{screen}} = t_0 + \tau_1 + \tau_2 \,. \tag{10}$$

If we consider an infinitesimal aperture at the screen, there will exist a spread of times at this aperture if the initial ions have a spread in energy ΔE. For this infinitesimal aperture

$$\Delta t\,(\text{energy}) = \Delta t_0 + \Delta\tau_1 + \Delta\tau_2 \,. \tag{11}$$

Now very approximately from (7)

$$\mathrm{d}t_0 \approx -\tfrac{1}{2}\,\mathrm{d}\tau_1$$

so

$$\Delta t\,(\text{energy}) \approx (\tfrac{1}{2}+k)\,\mathrm{d}\tau_1 \quad \text{where} \quad k=\tau_2/\tau_1 \,. \tag{12}$$

Furthermore,

$$\mathrm{d}\tau_1 = -\frac{1}{2}\frac{\Delta E}{E}\tau_1 \,. \tag{13}$$

If we note that the spread in time at an infinitesimal aperture given by (12) constitutes a lower limit of achievable burst duration from this type of pulser, we see the importance of a high quality beam from the ion source.

The process of "chopping" a beam introduces energy spreads in addition to those already present before chopping. It should be said that these introduced energy spreads posses time correlations by consequence of which the limit (11) might be expected not necessarily to apply. These correlations are too involved to consider here, and care has to be used because of them. Nevertheless, for a good ion source the intrinsic energy spread may be 80 volts while that introduced by the beam deflector may be 200 to 400 volts. It is evident then, that this latter energy spread is the important one.

The problem of producing pulses of ions as described in formulae (5) through (10) appears very much related to that of the fast oscilloscope, as indeed it is[7]). However, there are two facets of the problem of special importance to the problem of producing bursts of particles that deserve further emphasis. The first facet relates to the fact that it is desirable to have the burst duration independent of repetition rate. Since the writing speed which governs the duration of the ion bursts is proportional to ωV_0, a simple means that presents it self of securing this independence is to have ω and V_0 both variable. This is true, but experience has shown that more sophistication eventually becomes necessary. The second facet has already been touched upon, viz., the fact that the "trace" and "retrace" sweeps are distinguishable. This distinguishability shows up in two ways: (a) the time displays are different for the two bursts, and (b) the two bursts are geometrically separated at the target. Both these features are undesirable, but fortunately it is easy to get rid of this situation and at the same time halve the repetition rate for a given writing speed by eliminating the "retrace". It has already been shown that a split pair of biased deflector plates permits preserving a kind of axial symmetry for either the "trace" or "retrace" burst and it is only necessary to insert an appropriate baffle then to remove the remaining burst. Turner and Bloom[8]) have in fact employed essentially this solution to the problem. Another system, employed at Oak Ridge, is that of sidestepping the retrace beam. Both systems of course require an extra set of deflector plates. Each of these systems has its advantages and dis advantages.

The foregoing discussion and analysis serve to illustrate by a specific example the general problems that will be encountered in the production of bursts of ions by "chopping" a steady beam, and the implication is that as more power and space are available, shorter bursts can be obtained. The peak current by this "chopping" approach is almost entirely the domain of the ion source. It is a fortunate circumstance that there has been noteworthy advancement in recent years in ion source technology, first in the original development by Von Ardenne of

[7]) H. E. Hollmann, Zeits. für Tech. Phys. **9** (1938) 259.
[8]) C. M. Turner and S. D. Bloom, Rev. Sci. Inst. **29** (1958) 480.

the Duo Plasmatron[9]), and more recently in the adaption of the original source by Moak, Banta, Thurston, King and Johnson[10]) of Oak Ridge National Laboratory to the specific needs of pre-acceleration pulsing.

A discussion of terminal pulsing would not be complete without some consideration of klystron bunching, since this is feasible in the terminal of a Van de Graaff generator, but the scope of this paper permits only a few brief observations. Apart from limitations of space charge, which has so far been completely omitted from the discussion, klystron bunching affords the opportunity of achieving shorter bursts simultaneously with higher peak currents. Of course, the quality of the beam is reduced in the process, but as has been shown, beam clipping also reduces the quality of a beam, that is introduces energy and/or angular spread. While klystron bunching has been successfully applied to a few hundred kilovolt ions[11]) no corresponding success has been reported for Van de Graaff beams. Continued effort in this direction is certainly justified. This approach is worth effort and is doubtlessly being persued in numerous places.

There is another approach to bunching which is in a somewhat different category from klystron bunching because it is a post-acceleration method rather than pre-acceleration. This is the magnetic bunching proposed by Mobley[12]) by which it is possible to sum a large number of elementary bursts produced exterior to the accelerator, each of a given burst duration, to achieve a corresponding increase in peak current. This method, which is under development at various laboratories, has value in two ways, viz.: it permits post-acceleration pulsing when pre-acceleration pulsing is not feasible; alternatively it permits raising the peak current available from a pre-acceleration pulsed accelerator. These benefits are bought at the expense of increased angular divergence of the beam at the target which is a fact that may under some circumstances require consideration.

In very brief summary, this paper has sought to show some of the applications of millimicrosecond bursts of ions, and to demonstrate by an example the nature of the problems involved in producing such ion bursts. It is indicated that very great improvements are possible in the existing techniques. Certainly the applications warrant the efforts in this direction.

Acknowledgments

The author gratefully acknowledges the use of unpublished contributions from the following individuals: C. D. Moak on ion sources, general principles of pulsing and ion optics, C. H. Johnson on the mechanics of pulsing and the sources of energy spread, and J. H. Neiler on time spectrometry.

[9]) M. Von Ardenne, Tabellen der Electronen Physik Ionen Physik and Übermikroskopie (Deutscher Verlag der Wissenschiften, Berlin, 1956).

[10]) Moak, Banta, Thurston, Johnson and King, Rev. Scient. Instr. **30** (1959) 694.

[11]) N. N. Flerov and E. A. Tamanov, Atomnaya Energiya **3**, No. 7 (1957) 44.

[12]) R. C. Mobley, Phys. Rev. **88** (1952) 360.

NUCLEAR INSTRUMENTS AND METHODS 6 (1960) 331–336; NORTH-HOLLAND PUBLISHING CO.

DETECTION OF LOW ENERGY NEUTRONS WITH A NaI(Tl) CRYSTAL AND TIME OF FLIGHT

R. BALLINI

S.R.N.B.E., C.E.N., *Saclay*

and

S. M. SHAFROTH†

Northwestern University, and Saclay

Received 27 October 1959

A NaI(Tl) crystal has been substituted for a plastic scintillator in conventional neutron time of flight apparatus. The characteristics of this neutron detection system have been studied using pulsed low energy neutrons from the $Li^7(p,n)$ reaction. Neutron groups have been resolved down to 30 keV with reasonable efficiency. The method should prove useful in studying low energy neutron spectra resulting from nuclear reactions.

1. Introduction

Conventional neutron time of flight apparatus with plastic scintillators works well for neutrons which are more energetic than about 500 keV. Various methods have been devised to push the minimum energy down to as low as 250 keV; for example, two photomultipliers in coincidence which view the same scintillator permit higher dynode voltages without increasing the background exceedingly[1]). Millimicrosecond neutron time of flight measurements have also been made[2]) in the range from 2- to 30-keV with a detector which consists of a B^{10} slab backed by a NaI(Tl) crystal counting the 480 keV gamma ray from the $B^{10}(n,\alpha)Li^{7*}(\gamma)Li^7$ reaction.

A NaI(Tl) crystal can be used alone to resolve neutron groups down to a few tens of keV in time of flight equipment with reasonable efficiency. The neutrons are captured mostly in the iodine of the crystal and produce high energy gammas which in turn make scintillations in the crystal[3]). These gammas are emitted instantaneously ($<< 10^{-9}$ sec), so the time from production to capture of a neutron can be measured with a precision limited only by the electronics. In order to determine the neutron velocity, a correction must be made for the mean time the neutrons spend in the crystal before capture, which depending on the neutron energy is somewhat longer than the time to traverse half the crystal, due to scattering in it before capture. The efficiency of a NaI(Tl) detector increases with decreasing neutron energy since the neutron capture cross section varies approximately as $1/V$. For neutrons of 30 keV and a 1.75″ D × 2″ long NaI(Tl) cylinder, the probability of making a pulse which corresponds to an electron of energy greater than 4 MeV is about 5%[3]).

2. Apparatus

Preliminary measurements of neutron time of flight with such a detector have been made using an apparatus (figs. 1 and 2) designed for a plastic scintillator at the Saclay 5 MeV Van de Graaff[4,5,6]). The only modification consisted in

† Present address: Naval Research Laboratory, Washington, D.C.

[1]) L. Cranberg and J. S. Levin, Phys. Rev. **109** (1958) 2063.

[2]) W. M. Good, J. H. Neiler and J. H. Gibbons, Phys. Rev. **109** (1958) 926.

[3]) S. M. Shafroth, E. N. Strait and R. T. Carpenter, Nuclear Instruments **3** (1958) 298.

[4]) R. Ballini and L. G. Kuo, J. Phys. Radium **20** (1959) 47A.

[5]) R. Ballini and L. G. Kuo, Rapport intérieur S.R.N.B.E. No. 2, C.E.N., Saclay (1959).

[6]) G. Philippe, Rapport intérieur S.R.N.B.E. No. 3, C.E.N., Saclay (1959).

replacing the usual photomultiplier (RCA 7046) by an RCA 6810 A mounted as shown in fig. 3: short pulses are thus obtained on the anode and pulses lasting a few 10^{-7} sec on the 14th dynode,

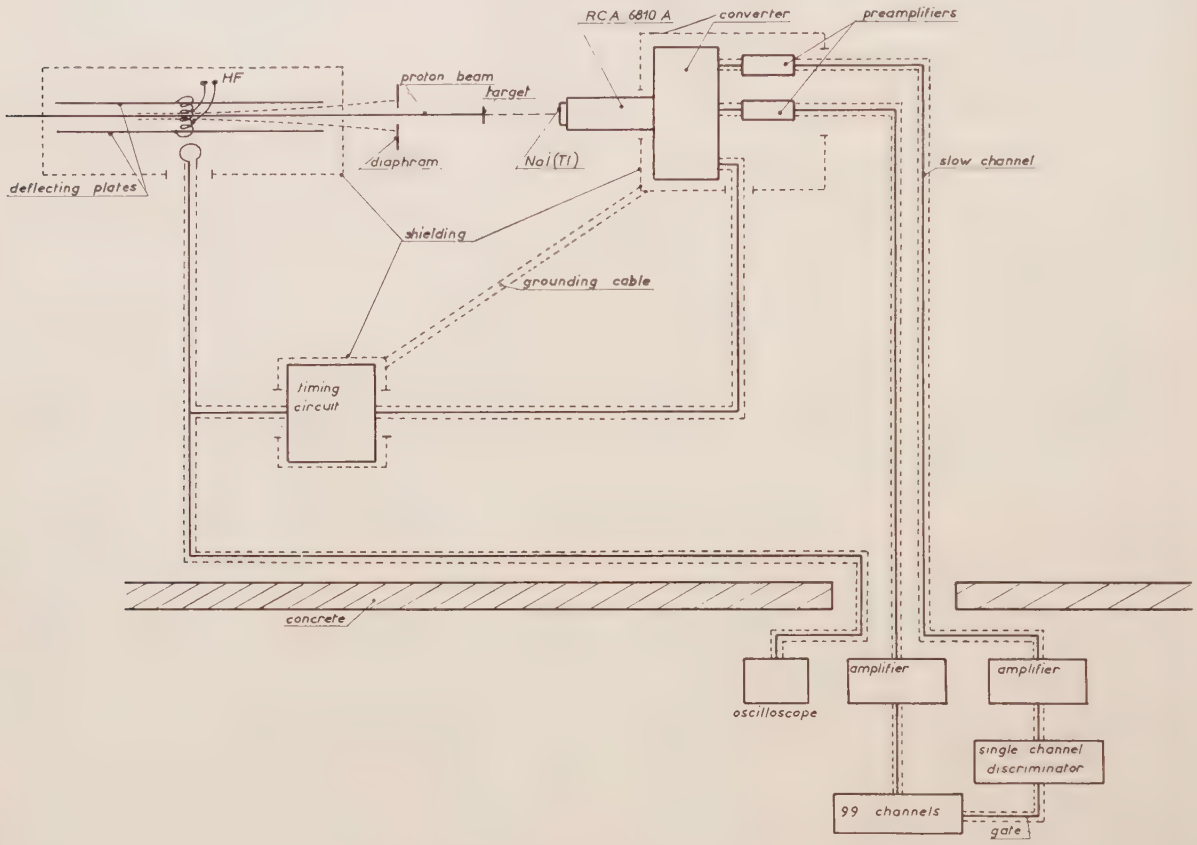

Fig. 1. Block diagram.

as required by the circuitry. A signal is taken from the 10th dynode, amplified and fed into a single channel discriminator, whose output gates the 99 channel analyzer. The pulse height registered by the analyzer then corresponds to the time interval from the 6810 A anode pulse to the following timing signal.

6–7 $\times$ 10^{-9} sec proton bursts of various energies near the $Li^7(p,n)$ threshold (1.881 MeV) were incident every 122 $\times$ 10^{-9} sec on a 20 keV thick LiF target. The peak current was of the order of 10 microamperes.

The proton energy was determined by precisely measuring the 90° deflecting field with a magnetic resonance apparatus, which was calibrated in terms of the threshold frequency for the $Li^7(p,n)$ reaction. It is useful to put the usual formula which gives neutron energy at 0° as a function of proton energy for this reaction in terms of more directly measured quantities, i.e. the velocity of the protons (U) and of the neutrons (V), and their respective threshold values: $U_0 = 1896 \times 10^6$ cm/sec and $V_0 = 237 \times 10^6$ cm/sec.

$$V - V_0 = k\,(U - U_0) \pm K\,(U^2 - U_0^2)^{\frac{1}{2}}\,,$$

with

$$k = m_p/(m_{Be} + m_n) \approx \tfrac{1}{8}\,,$$

$$K = [(m_{Be} + m_n - m_p)\,m_{Be}m_p/m_n]^{\frac{1}{2}}/(m_{Be} + m_n) \approx \tfrac{7}{8}\,.$$

Fig. 4 is a graph of this formula.

3. Results

Fig. 5 shows time spectra obtained with a 1.5″ D $\times$ 0.5″ long NaI(Tl) cylinder at 0° to the proton beam. For these runs the slow channel

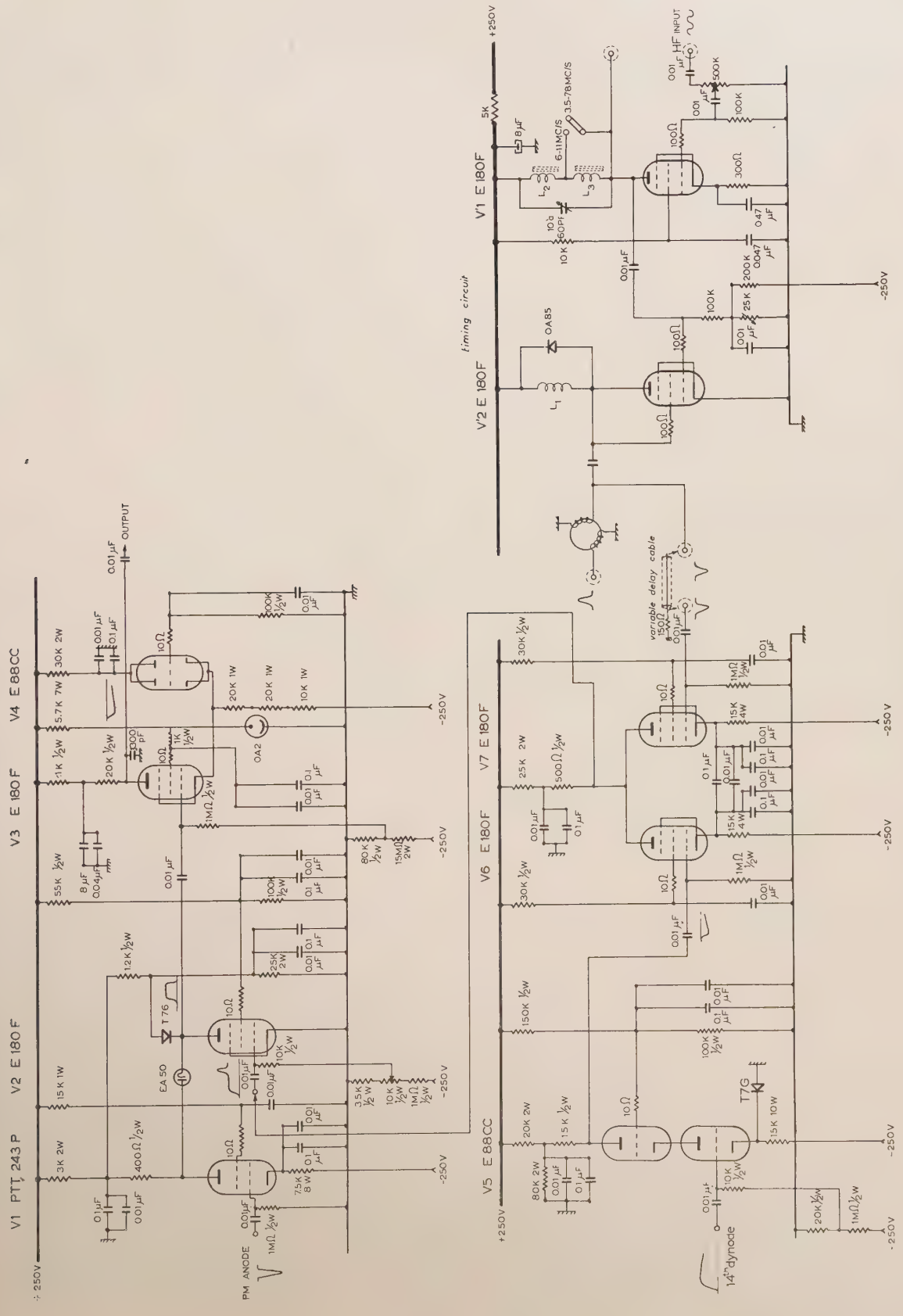

Fig. 2. Time to pulse height converter and timing circuit.

gate opened on all pulses whose electron energy was greater than 4 MeV. The arrows indicate where the peaks should have fallen for an infinitely thin target and for a neutron flight path equal to the distance from the target to the center of the crystal. The prompt peaks are very intense due to the 6–7 MeV gammas arising from the $F^{19}(p,\alpha)O^{16*}(\gamma)O^{16}$ reaction.

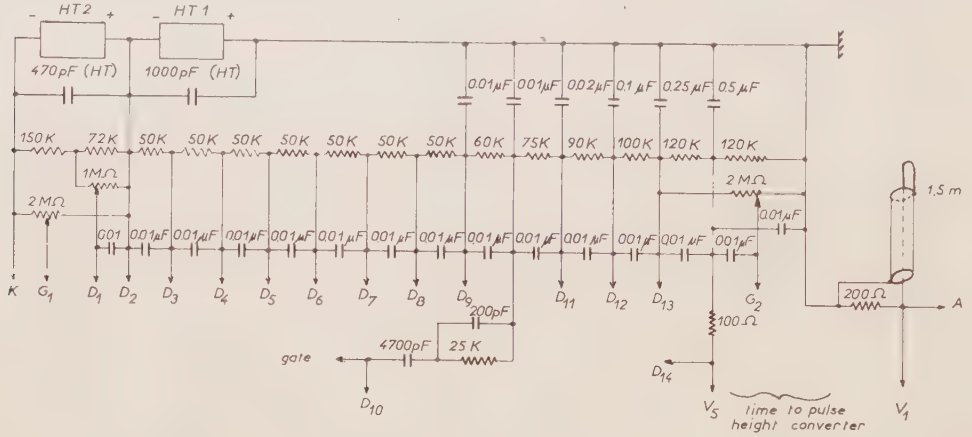

Fig. 3. Circuit diagram used with the RCA 6810 A photomultiplier to detect high energy gammas.

Fig. 6a is the gated time spectrum 9 keV below the (p,n) threshold. Only the two prompt gamma peaks are evident. Figs. 6b and 6c are time spectra 17 keV and 32 keV above the threshold.

In figs. 5b, 6b and 6c the fast group only is

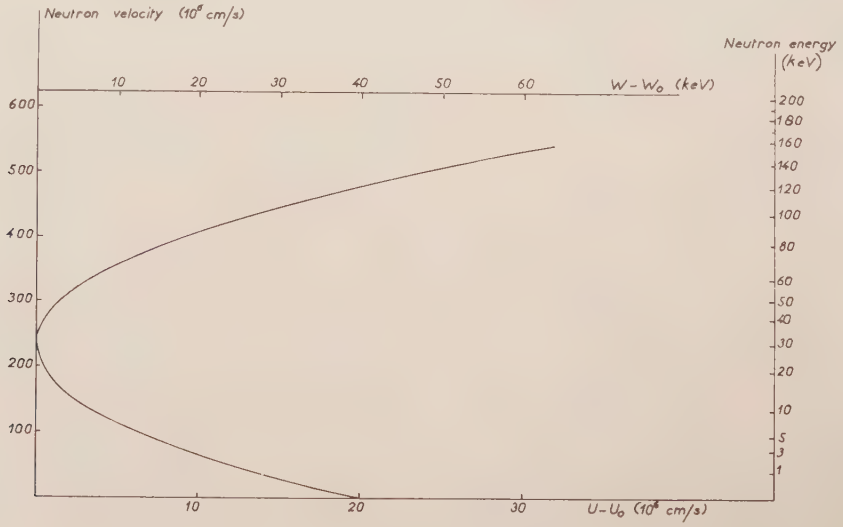

Fig. 4. Neutron velocity near $Li^7(p,n)$ threshold vs proton velocity.

Fig. 6 shows time spectra obtained with a 1.75″ D × 2″ long NaI(Tl) cylinder at 0° to the proton beam. The crystal size was chosen in order to obtain a greater neutron detection efficiency. Furthermore the window of the slow channel was set between about 3.3 and 4 MeV. This greatly reduced the recording of spurious resolved, but it is rather wide and displaced toward longer flight times. The slow group is not resolved. In fig. 5a (proton energy very near the threshold), neutron flight times are registered between the arrows corresponding to the slow and the fast groups. The main features of these curves have a common origin: the neutron

energy at the crystal is spread over a certain range, mainly due to target thickness and to a lesser extent due to the finite solid angle which

4. Discussion

Theoretically, in order to maximize the neutron detection efficiency for a given velocity reso-

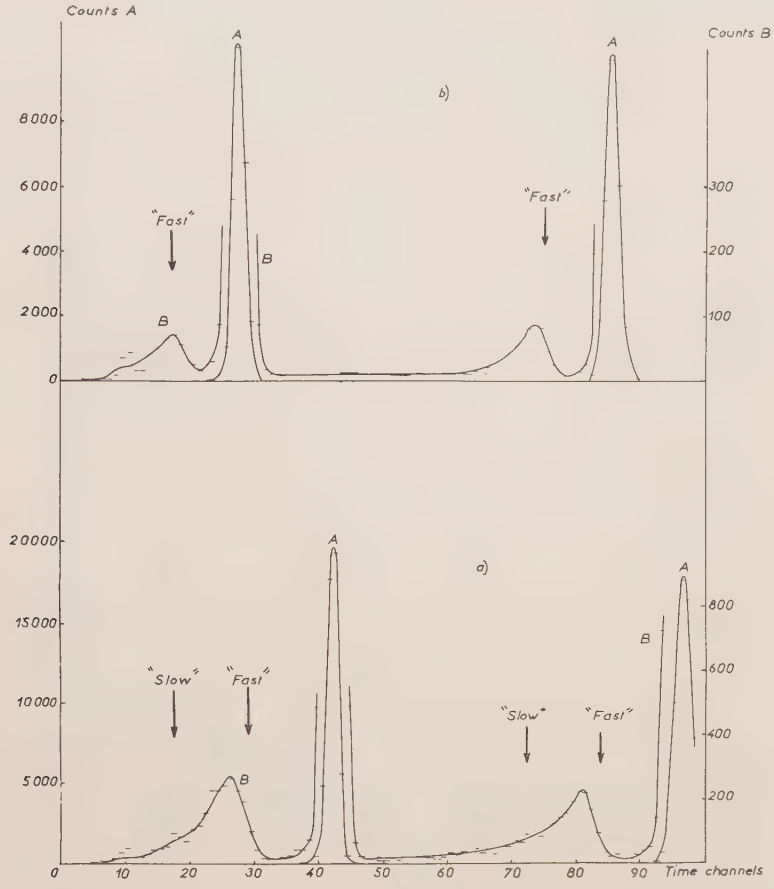

Fig. 5. Time of flight spectra with a 1.5″ D × 0.5″ long NaI(Tl) crystal: (a) 6 keV above $Li^7(p,n)$ threshold. Flight path = 12.7 cm; (b) 23 keV above threshold. Flight path = 8.7 cm.

it subtends[7]). Moreover, the flight times are spread because of the finite depth of the crystal and the fact that its effective length is longer than its physical length. Consequently, the average energy is lower than the maximum indicated by the arrows in the figures, and the peaks are spread out. Clearly a thinner target would yield sharper neutron groups. The fast and slow groups should then be resolved with the thin crystal, however the counting rate would be reduced accordingly. In order partially to compensate for this, a pure lithium target would permit the use of a lower integral bias.

[7]) A. O. Hanson, R. F. Taschek and J. H. Williams, Revs. Mod. Phys. **21** (1949) 635.

lution and a solid angle, one should use a thick crystal of large surface area and a long time base which involves a long interval between beam pulses and permits beam pulses and electronic time definition not much shorter than the time of traversal of the crystal by the neutrons. Practically, an upper limit is imposed: the main limitation is probably that a crystal which is too big scatters most of the neutrons before capture and so spreads the time resolution excessively. A reasonable compromise consists in using a crystal 5 cm deep and 10 cm in diameter, a 50 cm flight path and a beam frequency in accordance with the neutron spectrum.

As a compact neutron detector in the 10 keV

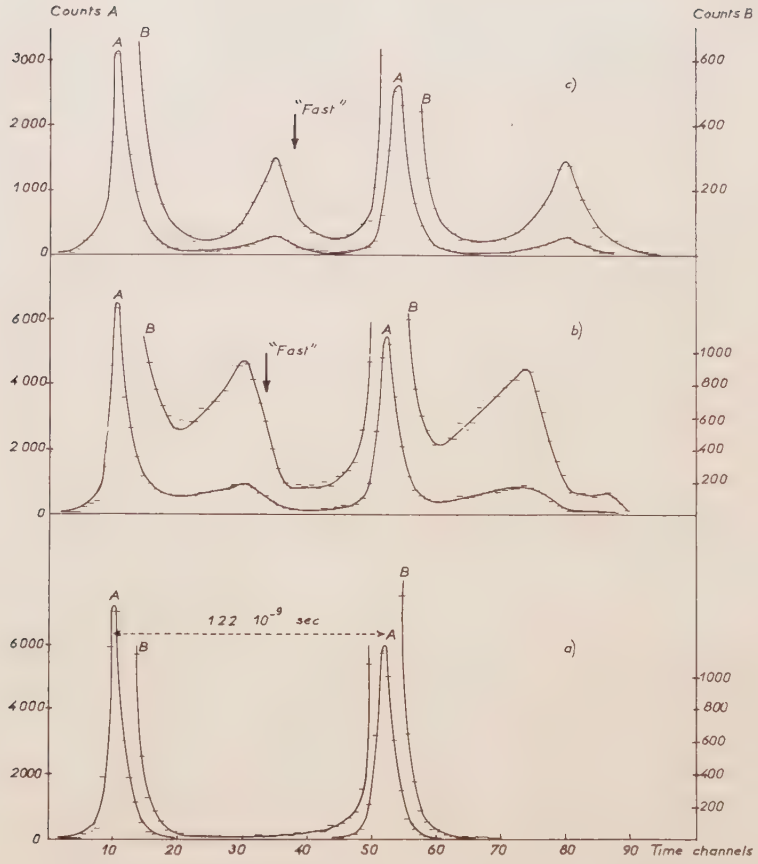

Fig. 6. Time of flight spectra with a 1.75″ D × 2″ long NaI(Tl) crystal. Flight path from the target to the center of the crystal = 20 cm. (a) 9 keV below $Li^7(p,n)$ threshold; (b) 17 keV above threshold; (c) 32 keV above threshold. Integrated proton current on the target in microcoulombs: (a) 200; (b) 200; (c) 75.

range, a LiI or Li^6I crystal[8]) may prove worthwhile in spite of its poor time definition. It may also be advantageous to use an He^3 scintillator[9,10]) as a neutron detector having low sensitivity to gammas.

Such flight time detectors might be used to investigate low energy, low Q (d,n) angular distributions, which in some cases may exhibit excellent stripping curves[11]). In conclusion, these detectors should prove useful in investigating the little studied field of low energy neutron spectra from nuclear reactions.

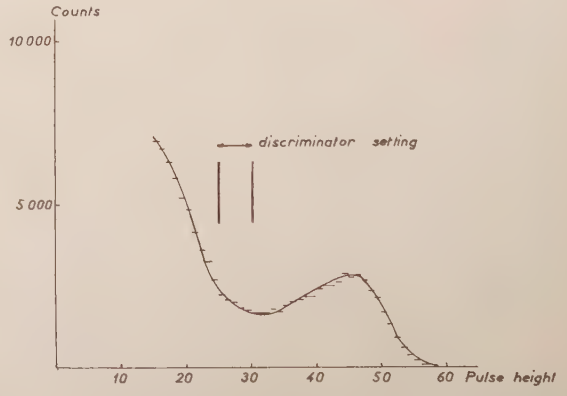

Fig. 7. Tenth dynode pulse height spectrum from LiF + protons, 17 keV above $Li^7(p,n)$ threshold. The crystal is the same as for fig. 6.

[8]) R. B. Murray, Nuclear Instruments **2** (1958) 237.
[9]) J. A. Northrop and J. C. Gursky, Nuclear Instruments **3** (1958) 207.
[10]) L. Koch, Comptes rendus du Colloque International sur l'Electronique Nucléaire, Paris, 1958, p. 151.
[11]) D. H. Wilkinson, Phil. Mag. **3** (1958) 1185.

Note added in proof: J. P. F. Sellschop, Phys. Rev. Letters **3** (1959) 346 has found excellent stripping curves for low Q (d, p) reactions.

NUCLEAR INSTRUMENTS AND METHODS 6 (1960) 337–342; NORTH-HOLLAND PUBLISHING CO.

SOME FACTORS AFFECTING THE GAIN AND RESOLUTION OF PHOTOMULTIPLIER TUBES

R. D. CONNOR and M. K. HUSAIN

Physics Department, University of Manitoba, Winnipeg, Canada

Received 21 September 1959

Changes in the gain and resolution of photomultipliers of the DuMont type are examined with reference to changes in counting rate, axial magnetic fields and temperature. While the magnitudes of these variations are found to vary as between photomultipliers, graphs are given showing typical dependences. The effects of magnetic shielding are presented and the variation of resolution with γ-ray energy in scintillation counters equipped with large NaI crystals is discussed in the light of recent statistical considerations.

1. Introduction

It has been known for some time that sudden changes in the gain of a photomultiplier tube occur when the mean tube current is suddenly increased[1]). In the process of repeating these experiments an additional effect has been observed which apart the intrinsic consequences may have a bearing on the linearity or otherwise of the observed pulse height versus energy curve for a NaI crystal-photomultiplier assembly when recording the photo-peaks of γ-rays of different energies.

This investigation was continued to determine the influence of axial magnetic fields and temperature on the gain and resolution of photomultipliers and the relation between resolution and γ-ray energy has been examined. These effects will be considered under their individual headings below.

2. The Effects of Counting Rate Changes

All the phototubes examined were of DuMont manufacture. In all, four photomultipliers type 6292, two type 6364 and one type 6291 were studied. Tubes 6292 and 6291 were mounted in different combinations with two $1'' \times 1''$ and one $1'' \times 1\frac{1}{2}''$ NaI(Tl) crystals. The larger photomultipliers were optically coupled to appropriately sized crystals. Standard electronic equipment was used and allowed to settle for at least twelve hours prior to the commencement of any experiment. A Zn^{65} source (γ-ray energy 1.114 MeV) was then placed at a distance from the crystal and the position of the γ-ray photopeak was determined every ten minutes using a single channel pulse height analyser. Fig. 1 shows the effect observed for a DuMont 6292 tube with a $1'' \times 1''$ crystal. Over a period of four hours or so the position of the photopeak moved to higher discriminator settings, finally attaining a steady value. The Zn^{65} source was then moved nearer the crystal to give a four-fold increase in the peak counting rate. The sudden shift reported by Bell, Davis and Bernstein in 1955[1]) was at once apparent and thereafter the same slow drift in the peak pulse height was observed. The total shift may be as large as 6% for such an increase in counting

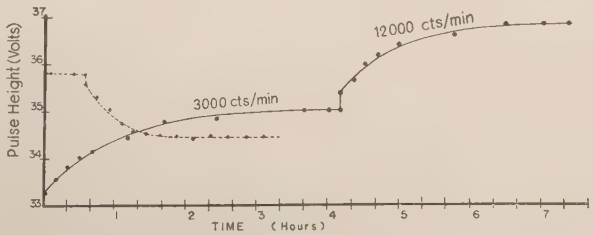

Fig. 1. Variation of photomultiplier gain with time following a change of counting rate.

[1]) P. R. Bell, R. C. Davis and W. Bernstein, Rev. Sci. Instr. 26 (1955) 726.

rate. On withdrawing the source suddenly from the crystal to a more remote point there was a sudden fall in the voltage reading corresponding to the peak followed by a similar long term fall to a stable level.

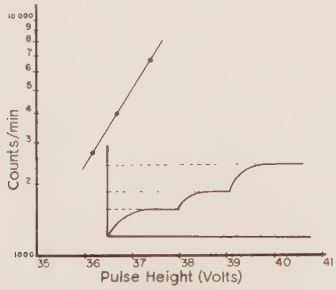

Fig. 2. Variation of gain with logarithm of the counting rate.

For a given γ-ray the final position of the peak pulse height varies linearly with the logarithm of the counting rate for a particular photomultiplier assembly. A typical set of observations is given in fig. 2.

Concurrently with the shifts in the position of the photopeak changes in the resolution have been noted. In every instance as the photopeak moves to higher discriminator settings, the resolution improves and the improvement always exceeds that to be expected had the photopeak been simply translated to higher discriminator values with preservation of its shape. It is clear therefore that the statistical spread in pulse height is reduced while the gain increases with time. Fig. 3 shows corresponding values of the resolution

$$\left(\text{ie, } \frac{\text{full width at half height} \times 100}{\text{peak value}}\right)$$

and peak position plotted against time.

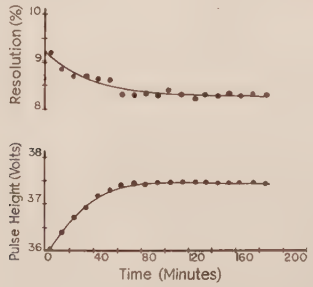

Fig. 3. Simultaneous variation of gain and resolution with time following a change of counting rate.

Tests were made to ensure that these gain and resolution changes did not have a trivial origin in the electronic equipment. A given photomultiplier showed similar effects regardless of the crystal used or the associated circuitry while no variation in output pulse height could be detected when pulses from a pulse generator were injected into the cathode follower circuit of the photomultiplier.

The magnitudes of these effects vary very much as between photomultipliers, a further indication that the ancillary equipment was not responsible. For example, one of the two 6364's tested showed practically no sudden or slow shift while all the other tubes gave a variation corresponding to that shown in fig. 1 to a greater or lesser degree.

It is not easy to understand fully the nature or the reasons for these effects. Space charges can be ruled out for these would be expected to cause a reduction in gain with increase of tube current and even the highest counting rates appearing in these experiments are well within the handling capacity of the tube and its associated electronic circuitry. Any counts lost at the photopeak would serve only to broaden it, not to make it narrower as is observed. Pulse pile up, one on the tail of the other, would not be expected to improve the resolution even if the counting rates had been great enough to make this effect likely. The effect cannot be associated with electrode conditioning effects, for then, once having conditioned the dynodes to a certain bombardment, a reduction in tube current by decreasing the counting rate would not cause a drop in gain.

It may be that this effect can be traced to the dynodes themselves where under stronger bombardment the effective work function is reduced, perhaps by local heating. It has been stated, however[2]), that current density and temperature does not change the secondary emission ratio of the dynode surfaces directly, and there is no report that local dynode heating could increase its emissive properties. Under different ex-

[2]) L. Cathey, I.R.E. Trans. Nuclear Sci. V55, No. 3 (1958) 109.

perimental conditions a somewhat similar slow variation in gain has been observed elsewhere[3]) and it is probable that the two effects are related.

Whatever the origin, this effect, unless guarded against, may cause apparent non-linearity in the energy response of scintillation counters and may well be (at least in part) the cause of the widely differing opinions as to the linearity or otherwise of the voltage pulse from a photomultiplier as a function of γ-ray energy[4]).

3. The Effect of Axial Magnetic Fields

To examine the effect of axial magnetic fields on DuMont 6292 photomultipliers a small non-magnetic cathode follower unit was constructed together with a solenoid 60 cm long and 7 cm inside diameter into which the multiplier and its cathode follower could be inserted. The winding was such that a current of 5 amperes was expected to produce a central field of 100 oersteds. Tests showed that over the volume occupied by the photomultiplier the field was uniform to within 2%, that the field was linear with current and that one ampere produced a central field of 20.3 oersteds.

Prior to making a set of observations, the contents of the solenoid were demagnetized with a decreasing alternating current in the usual manner. This avoided possible errors due to residual magnetization in the metal parts of the photo-tube.

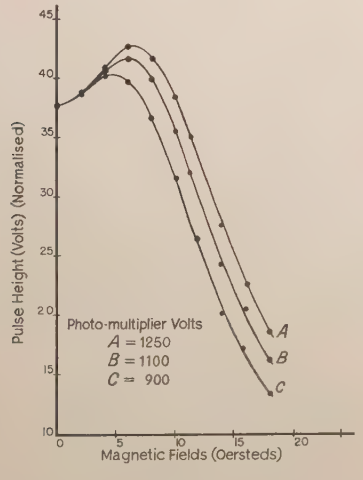

Fig. 4. Variation of gain with axial magnetic field.

The variation in gain was found to be independent of the direction of the field with respect to the photomultiplier tube. Fig. 4 shows this variation for an unscreened photo-tube to which is applied three different H.T. voltages. The

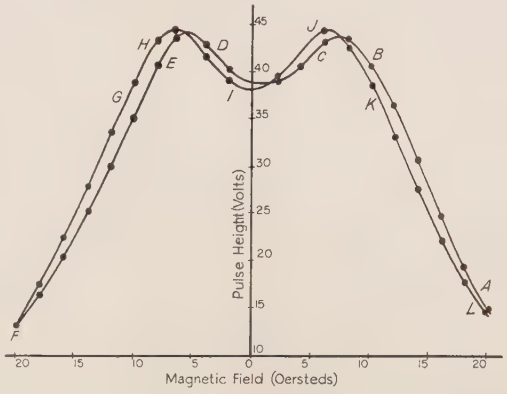

Fig. 5
Hysteresis effects in DuMont photomultiplier type 6292.

amplifier gain was adjusted to bring the photo-peak to 37.5 volts in each case when the magnetic field was zero. It would appear that moderately weak fields of the order of few oersteds, introducing a spiraling effect in the electron trajectories produce a focussing action and hence a rise in gain of the photomultiplier. This does not, however, last long for further increase in the field causes a rapid deterioration of the tube's performance, the electrons being deflected to increasing extents away from their normal paths between successive dynodes. It was interesting to see if there was anything resembling a hysteresis effect in photomultipliers of this type. The tube was subjected initially to a field of 20 oersted (point A in fig. 5) which was reduced in steps to zero then reversed and increased to about the same value in the opposite direction (point F). The cycle of operation was then reversed until the field was back at its original magnitude and direction (point L). The letters on the graph in fig. 5 denote the path of the cycle and the small

[3]) R. L. Caldwell and S. E. Turner, Nucleonics **12**, No. 12 (1954) 47.

[4]) W. E. Mott and R. B. Sutton, Handbuch der Physik **45** (1958) 86.

asymmetry, showing that the scintillation counter tube (DuMont-6292) is slightly magnetic, is apparent.

Because photomultipliers have numerous applications in situations where magnetic fields

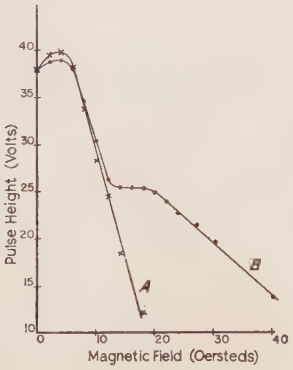

Fig. 6. Variation of gain with axial magnetic field for type 6292 tube (A) unshielded and (B) shielded with mu-metal can which does not extend beyond photocathode.

are present, it was thought important to examine in detail the effectiveness of several methods of shielding. In fig. 6 the performance of a DuMont-6292 photo-tube shielded with a mu-metal can is compared with that of the same tube unshielded. The can extended from the photo-cathode to a little below the top of the base, and it is seen to

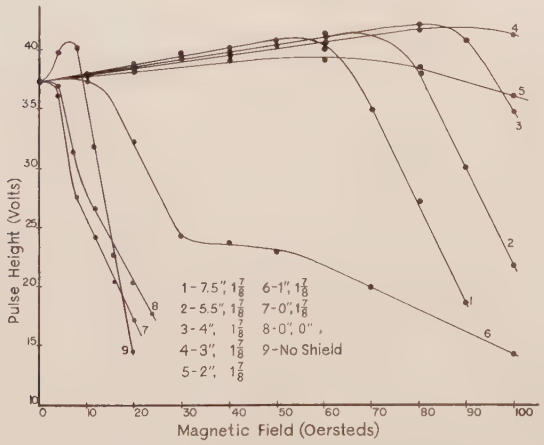

Fig. 7. Variation of gain with axial magnetic field for tube type 6292 shielded with various lengths of mild steel pipe.

be relatively ineffective as a shield for axial magnetic fields. A number of additional tests were made using different lengths of mild steel pipe all cut from the same piece, and all having inside and outside diameters of 2.25 ins. and 2.50 ins. respectively. In fig. 7 each curve is described by two lengths measured in inches. The first is the length by which the steel cylinder extends beyond the photo-cathode and the second is the length it extends below the junction of the glass envelope and the base. It will be noticed that as the length of the pipe extending beyond the photo-cathode is reduced from 7.5 inches the effectiveness of the steel pipe as a magnetic shield increases and then decreases, the optimum being obtained with this steel pipe extending approximately 2.0 inches beyond the photo-cathode and 1.9 inches below the junction of the glass envelope and the base. A little consideration will show that an optimum length of the shield is to be expected, for the induced magnetism will create a field within the steel cylinder in opposition to that of the solenoid. The actual degree of shielding will depend on the exactness of the cancellation of the two opposing fields, most particularly in the volume between the photo-cathode and the first dynode and this will be dependent on the value of the permeability of the steel, the relative positions of the ends of the steel cylinder with respect to the photomultiplier tube and the length and diameter of the cylinder itself.

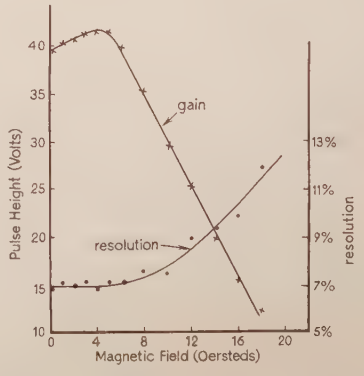

Fig. 8. Simultaneous variation of gain and resolution with magnetic field.

One recommended procedure for effective shielding has been to extend the shield beyond the photo-cathode for a distance equal to the radius of the tube. From this study it would

seem that a distance equal to the diameter would be more appropriate in view of the very rapid change observed between curves 5 and 6 of fig. 7.

The change in resolution of an unscreened photomultiplier with axial magnetic field is shown in fig. 8. It can be observed that the resolution has deteriorated along with the shift in gain of the photomultiplier as should be expected.

4. The Effect of Temperature Changes

Whereas there is no general agreement as to the effect of temperature on photomultipliers, the work of Van Sciver (1955–1956) has shown that for the normal type of NaI crystal used in scintillation work (10^{-3} mole fraction Tl), the light emission intensity rises as the temperature is reduced from normal room temperature, reaching a maximum at about — 130° C, and thereafter decreasing as the temperature is further lowered. Several investigators reported the variation of multiplier gain with temperature around room temperature, but the results are quite conflicting. Seliger and Zeigler (1956) reported an increase in the response of 0.2% per degree centigrade for two DuMont-6292's, while a third tube of the same type gave results somewhat lower than that. Kinard (1957) found a decrease in sensitivity of from about 0.1 to 0.5% per degree centigrade for the same type of photomultiplier (DuMont-6292). According to him the gain changes are associated with the dynode structure rather than with the cathode.

The overall variation of a counting assembly is clearly due to the crystal and the photomultiplier together. In the present work the variation of gain with temperature is found to be non-linear between 0° C to 35° C. For small variations around normal room temperature (20° C), the change in gain is found approximately linear with temperature, and is about — 0.3% per degree centigrade for a 1″ × 1″ NaI(Tl) crystal and DuMont-6292 photo-multiplier. For a DuMont-6364 type of tube and a 5″ × 4″ NaI(Tl) crystal the corresponding value was found to be about — 2.0% per degree centigrade. Such temperature effects are not negligible, and for work of the highest precision it is most desirable to operate scintillation counters at a controlled temperature.

No appreciable change in resolution was observed in the range of temperature between 0° C to 35° C.

5. The Relation between Resolution and γ-ray Energy

A theoretical treatment of the statistical processes involved in scintillation counting[5]) has shown the relation to be expected is of the form $\eta^2 = \alpha + \beta/E$ where η is the resolution as defined above, E is the γ-ray energy and α and β are constants for a given assembly. Using $1\frac{1}{2}'' \times 1''$ NaI crystals, deviations from this relation have been found by Bernstein[6]), Kelley[7]) and Bisi and Zappa[8]) in the energy range $\gtrsim 400$ keV. At higher γ-ray energies the resolution is better than that given by this

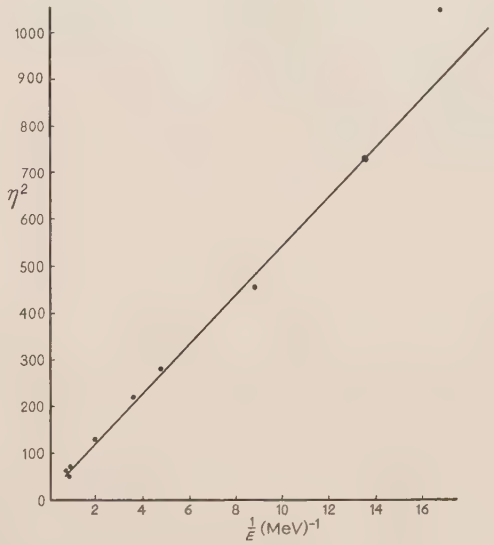

Fig. 9. Graph showing the variation in the square of the resolution as a function of the reciprocal of the γ-ray energy for a 5″ × 4″ NaI crystal coupled to DuMont photo-multiplier type 6364.

[5]) E. Breitenberger, Prog. Nuclear Physics **4** (1955) 56.
[6]) W. Bernstein, Nucleonics **14**, No. 4 (1956) 46.
[7]) G. G. Kelly, P. R. Bell, R. C. Davis and N. H. Lazar, Nucleonics **14**, No. 4 (1956) 53; I.R.E. Trans Nuclear Sci. N S 3, No. 4 (1956) 57.
[8]) A. Bisi and L. Zappa, Nuclear Instruments **3** (1958) 17.

relation. From statistical reasoning, these latter authors have shown that the width of a peak corresponding to the total absorption of a γ-ray in a series of interactions in the crystal is narrower than that obtained were the γ-ray to be absorbed in a single photoelectric process. Multiple processes, such as the production of a Compton electron with subsequent absorption of the scattered quantum in a photoelectric process are more likely to occur with γ-rays of higher energy.

On the other hand, the chance of multiple processes occurring in large crystals is greater than in small crystals as is evidenced by the relative reduction in the size of the Compton distribution.

Other things being equal, therefore, it might be expected that these deviations would occur for γ-rays of even lower energy and be much more marked. To test this, the resolution of a $5'' \times 4''$ crystal coupled to a DuMont 6364 photomultiplier was examined as a function of γ-ray energy from 60 to 1330 keV. The graph of $\eta^2 - 1/E$ is shown in fig. 9 and it will be seen to be linear. A search of the literature revealed corresponding data for an $8'' \times 5''$ crystal[9]) for the energy range 87–2620 keV which when graphed as above again yielded a straight line.

It therefore appears that the effect observed with small crystals does not appear with large ones. It is possible that other effects inherent in large crystals destroy the improvement in resolution to be expected from the greater probability of multiple processes. Such an effect might be the variable internal absorption of the scintillations and the varying efficiency of light collection from scintillations occurring in different parts of the crystal, but it is perhaps unexpected that the loss of resolution occasioned by such effects should so nearly compensate for the improvement anticipated theoretically. It would be interesting to examine this effect with a much larger range of crystals of intermediate size in an attempt to elucidate the observed behaviour.

Acknowledgements

The support of the National Research Council of Canada for this work is gratefully acknowledged, and one of us (M. K. H.) wishes to thank the Governments of Canada and Pakistan for financial assistance under the Colombo Plan.

[9]) H. W. Koch and R. S. Foote, Nucleonics **12**, No. 3 (1954) 51; Rev. Sci. Instr. **25** (1954) 740.

NUCLEAR INSTRUMENTS AND METHODS 6 (1960) 343–353; NORTH-HOLLAND PUBLISHING CO.

AN INVESTIGATION OF PROPERTIES OF THIN LITHIUM FILMS BY USE OF THE $Li^7(p,n)Be^7$ REACTION†

J. E. MONAHAN and F. P. MOORING

Argonne National Laboratory, Lemont, Illinois

Received 21 November 1959

The (p,n) reaction in thin films of lithium and lithium fluoride evaporated on tantalum backings is used to obtain a quantitative measure of possible irregularities in the thickness of such films. Evidence is presented that metallic lithium films are not only nonuniform in thickness but also that this apparent nonuniformity becomes more pronounced as these films are bombarded with protons. On the other hand, lithium fluoride films seem to be of uniform thickness but the effect of proton straggling produces an apparent nonuniformity which can be analyzed to give the energy spectrum of protons emerging from the films. Consequently this type of measurement can be used to obtain the stopping power and straggling distribution of protons in targets which give rise to a (p,n) or (p,γ) reaction. A simple method of analyzing conventional "rise-curve" measurements is suggested. It gives a more nearly accurate calibration of neutron energies and a more complete description of the neutron energy spectrum.

1. Introduction

In neutron physics at medium energies, reactions induced by charged particles incident on thin films are a primary source of nearly monoenergetic neutrons[1]). Nonuniformities in these films can lead to errors in the estimation of the mean energy and in the energy distribution of the resulting neutron flux. Such errors are a cause of misinterpretation of the results of many neutron experiments.

For energies above a few kilovolts a commonly used neutron source is the (p,n) reaction in thin lithium targets. The threshold energy for this reaction is one of the most extensively used energy calibration points in nuclear physics. The results of an investigation of some of the properties of thin lithium films evaporated onto a tantalum backing will be discussed in this paper.

Our first indication that lithium films can be sufficiently nonuniform to cause a serious distortion in the energy spectrum of the neutron flux was obtained from an analysis of measured neutron self-indication cross sections[2]). The results of these measurements could be understood only by assuming that the energy spectrum of the incident neutron flux was extremely skewed. Further studies[3]) indicated that the metallic lithium films which were being used as neutron sources were not only nonuniform but also that the apparent nonuniformity increased with continued proton bombardment. Electron-microscopic studies[4]) of the properties of films containing lithium evaporated onto various substrates confirmed these conclusions and also suggested techniques which might lead to more nearly uniform and stable neutron sources. Recent reports from Harwell[5]) and Duke University[6]) indicate similar difficulties in the use of metallic lithium as a neutron source.

During a more thorough investigation of this

† Work performed under the auspices of the U.S. Atomic Energy Commission.

[1]) Hanson, Taschek and Williams, Revs. Mod. Phys. **21** (1949) 635.

[2]) Langsdorf, Monahan and Mooring, Phys. Rev. **98** (1955) 1148A.

[3]) F. P. Mooring, Program of the Medium Energy Neutron Conference, Argonne National Laboratory (June 3, 1955) p. 2.

[4]) Weber, Bryant, Ai-Chun Fung and Rhoads, The Investigation of Thin Lithium Layers Produced by Evaporation in Vacuum Upon a Tantalum Substrate or Other Acceptable Base Material (St. Louis University, July, 1958).

[5]) W. D. Allen (private communication).

[6]) Bowman, Weston, Bilpuch and Newson, Bull. Am. Phys. Soc., Ser. II, **4** (1959) 285.

problem, a technique was developed which permits a simple and rapid determination of the "thickness profile" of any thin film which under charged-particle bombardment is a measurable source of neutrons or gamma-rays. This method is described in the succeeding sections.

2. Theory

First consider the case of a target of uniform thickness τ. (All distances within the target are measured in terms of the "number of scattering centers per unit area" normal to the direction of the incident beam.) From such a target the time rate of yield of neutrons per unit solid angle in the direction $\Omega(\theta,\phi)$ relative to the direction of the incident proton beam[7]) is denoted by $Y(E_p,\tau;\Omega)$, where

$$Y(E_p,\tau;\Omega) = \int_0^\tau dx \int_{E_t}^{E_p} dE\, \phi(E_p;E,x)\,\sigma(\Omega;E)\,. \qquad (1)$$

Here E_p is the energy of the incident beam, $\phi(E_p;E,x)$ is the proton current per unit energy that has energy E at depth x within the target, $\sigma(\Omega;E)$ is the differential cross section for the (p,n) reaction in the target, and E_t is the threshold energy for this reaction.

If the statistical fluctuations in energy loss as the protons penetrate the target are neglected, the proton current reduces to a delta-fonction,

$$\phi(E_p;E,x) = \phi_0\,\delta(E_p - E - kx)\,, \qquad (2)$$

where the "space rate" of energy loss, k, is assumed to be independent of E, and ϕ_0 is the incident proton current. In this case eq. (1) reduces to the equivalent expressions

$$Y_I(E_p,\tau;\Omega) = \phi_0 \int_0^\tau dx\,\sigma(\Omega;E_p - kx) =$$

$$= k^{-1}\phi_0 \int_{E_p-k\tau}^{E_p} dE\,\sigma(\Omega;E)\,. \qquad (3)$$

The subscript "I" denotes that eq. (3) represents the yield from an "idealized" target which is perfectly uniform in thickness and gives rise to no straggling effects.

That this ideal yield is actually a measurable quantity is the basis of the present investigation. From eq. (1) the yield from an infinitely thick target is

$$Y(E_p,\infty;\Omega) = k^{-1}\phi_0 \int_{E_t}^{E_p} dE\,\sigma(\Omega;E)\,, \qquad (1a)$$

provided the stopping power k is essentially constant over the energy range of interest. This is an extremely good approximation for those endothermic reactions for which the range of incident energies which is of interest is small compared with the threshold value. By an elementary transformation of variables, eq. (3) can be written in the form

$$Y_I(E_p,\tau;\Omega) = Y(E_p,\infty;\Omega) - Y(E_p - k\tau,\infty;\Omega)\,, \qquad (4)$$

i.e., the yield at incident energy E_p from an idealized target of thickness τ is the difference in yields from an infinitely thick target[8]) measured at incident energies E_p and $E_p - k\tau$. Equation (4) makes possible the generation of $Y_I(E_p,\tau;\Omega)$ for any target thickness τ once the yield from an infinitely thick target has been measured as a function of the incident proton energy.

The apparent nonuniformity of a real target may be deduced from the deviation of the measured neutron yield from this ideal yield. In order to justify this interpretation and also to develop the formalism used to obtain a measure of this nonuniformity, it is necessary to investigate the expected yield from thin nonuniform targets and to correct the result for the effect of straggling. The essential simplicity of these arguments is somewhat better preserved if these effects are considered separately.

First consider a nonuniform target but neglect the effect of straggling. Obviously the physical target can be represented as a superposition of uniformly thick targets of varying area normal to the proton beam; and, since straggling effects are neglected, the yield Y_p from the physical target is just the weighted "sum" of the yields from this set of idealized targets. It

[7]) While the emphasis is on (p,n) reactions, it is obvious that these considerations apply to any charged-induced reaction giving rise either to neutrons or gamma-rays.

[8]) According to eq. (3), any thickness τ greater than $(E_p - E_t)/k$ is essentially infinitely thick for protons of energy E_p.

will prove convenient to represent this weighted "sum" as a Stieltjes integral of the ideal yield with respect to the distribution function $T(\tau)$ of the target thickness, i.e.,

$$Y_p = \int_0^{\tau_M} dT(\tau)\, Y_I(E_p,\tau;\Omega)\,, \qquad (5)$$

where τ_M is the maximum thickness of the target and $1 - T(\tau)$ is the ratio of the effective area of the target measured at depth τ within the target to the maximum effective area of the target. From its definition the distribution function $T(\tau)$ is a nondecreasing function of τ ranging from zero at $\tau = 0$ to unity at $\tau = \tau_M$.

Next consider the effects of straggling on the measured yield from a perfectly uniform target. In this case the neutron yield is given by eq. (1), where the proton current density $\phi(E_p; E,x)$ includes the fluctuations in energy loss as the protons penetrate the target material. This can be written in a slightly more convenient form by noting that, by eq. (3),

$$\frac{d}{d\tau} Y_I(E_p,\tau;\Omega) = \phi_0 \sigma(\Omega; E_p - k\tau)\,.$$

If $\sigma(\Omega; E)$ in eq. (1) is replaced as indicated by the above equality and the result is integrated by parts, the expression for the yield from a uniform target when straggling is taken into account is found to be

$$Y(E_p,\tau;\Omega) = S(\eta;\tau)\, Y_I(E_p,\eta;\Omega) - \\ - \int_0^{\eta} dy \frac{\partial S(y;\tau)}{\partial y} Y_I(E_p,y;\Omega)\,, \qquad (6)$$

where $k\eta$ is the energy loss which reduces the energy of a proton with incident energy E_p to the threshold energy, i.e.,

$$k\eta \equiv E_p - E_t\,, \qquad (7)$$

and

$$S(y;\tau) = k\phi_0^{-1} \int_0^{\tau} dx\, \phi(E_p; E_p - ky,x)\,. \qquad (8)$$

The distribution function $S(y;\tau)$ is the fraction of proton current that has energy $E_p - ky$ within the target. For a fixed thickness τ, $S(y;\tau)$ is a nonincreasing function of y ranging in value from unity at $y = 0$ to zero for values of y sufficiently greater than τ.

Let μ denote a measure of the width of the energy distribution of the proton current, and assume that this distribution vanishes for values of the energy loss greater than this width, i.e.,

$$\phi(E_p; E_p - ky,x) \approx 0 \qquad |x - y| > \mu\,.$$

Then for target thicknesses τ greater than or equal to $\eta + \mu$ all of the protons are degraded to an energy below threshold within the target and there is no contribution from the second term in eq. (6). In this case eq. (6) reduces to

$$Y(E_p,\tau;\Omega) = Y_I(E_p,\tau;\Omega) \qquad \tau \geq \eta + \mu\,. \qquad (6a)$$

This last expression is simply a restatement of the already observed fact that straggling has no effect on the neutron yield at incident energies E_p for which the target is infinitely thick. On the other hand, for values of E_p such that $\tau < \eta + \mu$ eq. (6) can be written in the approximate form

$$Y(E_p,\tau;\Omega) \approx \alpha Y_I(E_p,\tau + \mu;\Omega) + \\ + (1 - \alpha)\, Y_I(E_p,\tau - \mu;\Omega) \qquad \tau < \eta + \mu\,, \qquad (6b)$$

where α is the value of $S(y,\tau)$ when y is in the interval between $\tau - \mu$ and $\tau + \mu$, so that $0 \leqslant \alpha \leqslant 1$. Note that eq. (6b) can be written as an integral of the type of eq. (5) by formally defining a target distribution function having the values[9])

$$T(x) = \begin{cases} 0, & x < \tau - \mu\,. \\ 1 - \alpha, & \tau - \mu \leqslant x < \tau + \mu\,. \\ 1, & \tau + \mu \leqslant x\,. \end{cases}$$

[9]) The approximations used to obtain these results consisted in neglecting the details of the proton distribution function for $|x - y| < \mu$ and approximating the contribution of the second term of eq. (6) from the region $\eta - \mu < \tau < \eta + \mu$ by a single-step function. The generalization to higher order step functions is obvious and will be used in section 4. However, no further insight into the physical meaning of these expressions is gained by the formal exhibition of these higher order approximations. Actually, for the present purposes, all that is necessary is the demonstration that a distribution function $F(\tau)$ of the form

$$\int_0^{\tau} dT(x)\, dx$$

exists, so that the yield can be written in the form of eq. (10). That this is so can be seen from an examination of eq. (9).

Thus it is not possible, on the basis of yield measurements alone, to distinguish the effects of straggling from those of nonuniformity in the target.

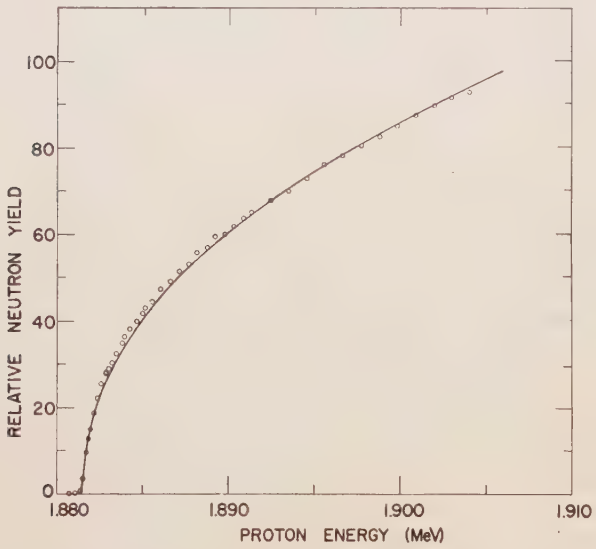

Fig. 1. A comparison of the calculated (solid curve) and measured neutron yield at 0° from an "infinitely thick" lithium target. The calculated curve was normalized to the measured curve at a proton energy of 1.893 MeV in order to evaluate the product of proton flux and mean efficiency of the neutron detector which occurs as a parameter in the calculation. One unit in the neutron yield represents 1000 counts.

With these preliminaries it is now possible to discuss the neutron yield $\mathscr{Y}(E_p,\tau_M;\Omega)$ from a nonuniform target of maximum thickness τ_M when the effect of straggling is included. Formally this yield is given by the expression

$$\mathscr{Y}(E_p,\tau_M;\Omega) = \int_0^{\tau_M} dT(\xi)\, Y(E_p,\xi;\Omega) \qquad (9)$$

where $T(\xi)$ is the target distribution function introduced in eq. (5) and $Y(E_p,\xi;\Omega)$, as defined by eq. (1) or (6), is the yield from a uniform target of thickness ξ when the effect of straggling is included. In view of the approximations introduced above, eqs. (6a) and (6b), it is possible to rewrite eq. (9) in the form

$$\mathscr{Y}(E_p,\tau_M;\Omega) = \int_0^{\tau_M} dF(\xi)\, Y_I(E_p,\xi;\Omega), \qquad (10)$$

where

$$F(\xi) \approx \begin{cases} T(\xi) & \xi \geq \eta + \mu \\ \alpha T(\xi - \mu) + (1-\alpha)\, T(\xi + \mu) & \xi < \eta + \mu \end{cases}. \qquad (11)$$

As is evident from the definition, the function $F(\xi)$ combines the effects of target nonuniformity and straggling and it is this distribution function which is measured in these experiments. Since $1 - F(\xi)$ is the ratio of the "apparent" effective area measured at a depth ξ within the target to the maximum effective area of the target, the function $F(\xi)$ will be called the apparent target distribution function. The properties of $F(\xi)$ are very similar to those of $T(\xi)$; e.g., $F(\xi)$ is a nondecreasing function of its argument and ranges from zero at $\xi = 0$ to unity at $\xi = \tau_M + \mu$.

The method used in obtaining the distribution $1 - F(\xi)$ from the measured values of $\mathscr{Y}(E_p,\tau_M;\Omega)$ and $Y_I(E_p,\tau;\Omega)$ will be demonstrated in section 4.

In order to verify that the thick targets used in these experiments were essentially infinitely thick for proton energies less than $E_t + k\tau$, i.e. for $\tau \geq \eta + \mu$, the theoretical yield averaged over the solid angle $\Delta\Omega$ subtended by the neutron counters,

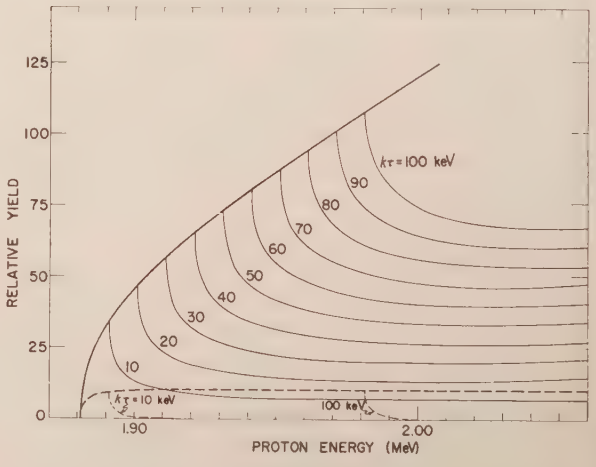

Fig. 2. The calculated neutron yield at 0° from uniform lithium targets of various thicknesses $k\tau$. The dotted curve is the contribution from the lower energy (back angle) group of neutrons. The solid curves represent the total yield.

$$\int_{\Delta\Omega} d\Omega\, Y(E_p,\infty;\Omega)/\Delta\Omega\,,$$

was evaluated as a function of E_p by making a theoretical fit to the measured $Li^7(p,n)Be^7$

cross section[10–11]). These results are compared with the corresponding measured quantity in fig. 1. The agreement is interpreted as an indication not only that the above mentioned condition for an "infinitely thick" target is satisfied but also as a measure of the validity of the approximation used in obtaining eq. (6a).

Several ideal thin-target yields were computed from the theoretical fit to the $Li^7(p,n)Be^7$ cross section. The results are shown in fig. 2. The solid curves are, for each thickness, the calculated total yield of neutrons at 0°; the dashed curves are the yield of the lower energy ("back angle") neutron group. The envelope is found to be identical with the theoretical infinite-target yield. The results obtained by calculating each curve individually agree, within the accuracy of the calculation, with those obtained by use of eq. (4).

Since there is considerable interest in the $Li^7(p,n)Be^7$ reaction, it is perhaps worthwhile to describe briefly our attempt to "fit" the total cross section measurements of Newson *et al.* and Macklin and Gibbons[10]) together with the angular distribution measured by Taschek and Hemmendinger[11]). It is generally accepted that the main contributions to this reaction in the vicinity of the threshold energy are a spin-3 even-parity state of Be^8, 19.2 MeV above the ground state, together with an S-wave background due to a state (or states) of spin-2 and odd parity. In this case the differential cross section can be written in the form

$$4\pi\sigma(E_p;\Omega) = [\sigma(E_p;3^+) + \sigma(E_p;2^-)]\,P_0(\cos\theta) +$$

$$+ (14/\sqrt{35})\,[\sigma(E_p;3^+)\,\sigma(E_p;2^-)]^{\frac{1}{2}}\cos\psi\,P_1(\cos\theta)$$

$$+ (12/25)\,\sigma(E_p;3^+)\,P_2(\cos\theta)\,,$$

where $\sigma(E_p;J\pi)$ is the total (integrated over angles) (p,n) cross section due to the spin-J, parity-π state of Be^8 and ψ is the phase of the interference between the S- and P-wave contributions. For an interaction radius of 3 fermis, an excellent fit to the measured total cross section and an adequate fit[12]) for the measured angular distribution is obtained with the following parameters. For the S-wave background the components of the R-matrix are $R_{nn} = R_{pp} = -R_{np} = 25.6$; and for the spin-3 state at a center-of-mass resonance energy of 1.96 MeV, $\gamma_n = 1.37\ \text{MeV}^{\frac{1}{2}}$, $\gamma_p = 0.62\ \text{MeV}^{\frac{1}{2}}$. The sign and magnitude of the R-matrix are consistent with Adair's interpretation[13]) that the S-wave background is due to contributions from far-off levels at high energies. On the other hand, the large difference between the neutron and proton reduced-width amplitudes is not consistent with the interpretation that the 19.2 MeV state of Be^8 and the 2.3-MeV state of Li^8 are members of an isotopic-spin-1 multiplet. However, Adair's results are predicated on a value for the interaction radius considerably (about 30%) larger than that used here.

3. Measurements

The yield of neutrons from targets containing lithium was observed for a range of incident proton energies extending from the threshold energy for the $Li^7(p,n)Be^7$ reaction to approximately 30 keV above threshold. Neutrons were detected simultaneously by two conventional long counters[14]), one placed at 0° and the other at 30° with respect to the direction of the incident proton beam. Both counters were placed at a distance of 50 in. from the neutron source. No corrections were made for in-scattering or other backgrounds.

[10]) Newson, Williamson, Jones, Gibbons and Marshak, Phys. Rev. **108** (1957) 1294; R. L. Macklin and M. H. Gibbons, Phys. Rev. **109** (1958) 105.

[11]) R. Taschek and N. Hemmendinger, Phys. Rev. **74** (1948) 373.

[12]) The calculated coefficient of the P_1-term for the differential cross section duplicated the positions of the maxima and minima of the measured coefficient as a function of proton energy. However, the amplitude of this oscillation exceeded the measured value by as much as a factor of two. This is not as satisfactory agreement as Adair obtained but it is quite adequate for the present purpose since the neutron yield for energies just above threshold depends only slightly on the details of the angular distribution.

[13]) Robert K. Adair, Phys. Rev. **96** (1954) 709.

[14]) A. O. Hanson and J. L. McKibben, Phys. Rev. **72** (1947) 673.

Two kinds of targets were used[15]). The first type was a film of lithium fluoride evaporated onto a backing of 0.010-in. tantalum. The procedure developed by Weber *et al.*[4]) was used with slight modifications to prepare the subtrates (tantalum discs) for evaporation. The tantalum discs were mechanically polished to a mirror finish and then electro-polished. Next they were chemically cleaned by washing them with aqua regia, distilled water, concentrated potassium hydroxide, distilled water, carbon tetrachloride, and ethyl alcohol, in that order, and then air dried. The tantalum plates were next outgassed by electron bombardment in a vacuum of about 5×10^{-5} mm of Hg. The outgassing was continued for several minutes after it was found that an additional increase in electron current would no longer produce a measurable rise in pressure.

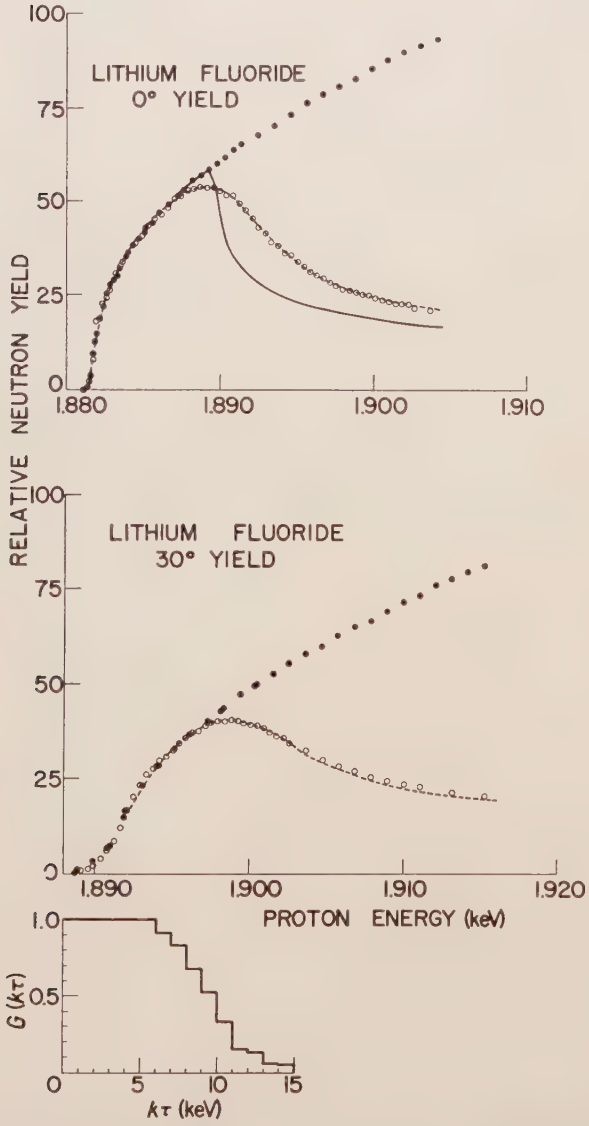

Fig. 3. The result of an investigation of thin lithium fluoride films evaporated onto tantalum backings. In the top graph of the solid curve, which was calculated from a curve drawn through the closed circles, is the neutron yield for an ideally uniform target. In both of the top two graphs the closed circles represent the measured yield from an "infinitely thick" target and the open circles represent the measured yield from a thin target. The dashed curves are the expected neutron yield from a target whose apparent thickness distribution is plotted in the bottom graph. One unit in the neutron yield represents 1000 counts.

Reagent-grade lithium fluoride was evaporated onto the tantalum backings. A shutter shielded the substrates from the evaporation source while it was being preheated. After evaporation the targets were transferred in air to the target chamber. Several of the lithium fluoride targets were removed from the target chamber after use, carried in air to a dessicator where they were stored under vacuum, and several days later used in repeat runs. No detectable difference between the original and the repeated yield curve was observed for any of these targets.

The second type of target was a film of metallic lithium evaporated onto a thin tantalum cup[16]). The procedure usually followed here at Argonne was used in the preparation of these targets. The lithium to be evaporated was a small cylinder of the metal about $\frac{1}{8}$ in. in diameter and $\frac{3}{8}$ in. long. It was first scraped to remove the oxide layer and then washed with petroleum ether, acetone and methyl alcohol. The cup was first cleaned with crocus cloth and facial tissues to remove traces of old targets; and then washed with the same sequence of solvents. The lithium metal was evaporated from an oven in the target chamber. The thickness of

[15]) Weber *et al.* (ref. [4])) suggests that a thin ($\approx$ 200 Å) coating of carbon evaporated over suitably prepared metallic lithium films may result in more nearly stable targets with a greater degree of uniformity. Attempts to use this technique to prepare lithium targets for the present experiment were not successful.

[16]) Manufactured by Fansteel Metallurgical Corp., Chicago, Illinois.

the film was monitored by observing the neutron yield in the forward direction during evaporation. Even for immediately successive runs with the same target, yield curves from targets of the second type differed by an amount considerably outside of any experimental or statistical uncertainty (cf. fig. 7).

The Argonne wobble-target assembly was used throughout the experiments in order to minimize the effects of local heating by the incident proton beam and, as much as possible, to eliminate sources of oil vapor near the targets. Proton currents were kept below 5 μA.

Fig. 3 shows typical results observed with both long counters for the lithium fluoride targets; and fig. 4 shows similar results obtained with the lithium metal targets. The open circles on each graph represent the yields from thin targets; the closed circles, yields from infinitely thick targets. (A target is considered to be infinitely thick if, for the entire range of incident protons energies used, a proton is degraded in energy to a value below the threshold for the (p,n) reaction for lithium before emerging from the thinnest portion of the target.)[17]).

4. Discussion of Results

As indicated by eq. (1a), the neutron yield from an infinitely thick target at bombarding energy E_p is inversely proportional to the atomic stopping power of the target material; thus for energies below threshold for the F^{19}(p,n) reaction we have, in the notation of eq. (4),

Table 1

The neutron yield from lithium and lithium fluoride for a range of energies of the incident proton beam.

E_p (MeV)	Y(Li) (Counts)	Y(LiF) (Counts)	$\frac{Y(\text{Li})}{Y(\text{LiF})}$
1.890	200 000	60 900	3.284
1.891	209 500	63 800	3.283
1.892	219 000	66 600	3.288
1.893	227 500	69 400	3.278
1.894	236 000	72 000	3.277
1.895	244 000	74 600	3.270
1.896	252 000	76 900	3.276
1.897	259 500	79 200	3.276
1.898	267 000	81 400	3.280
1.899	274 000	83 600	3.277
1.900	282 500	85 800	3.292
1.904	305 800	91 400	3.250
			Average 3.279

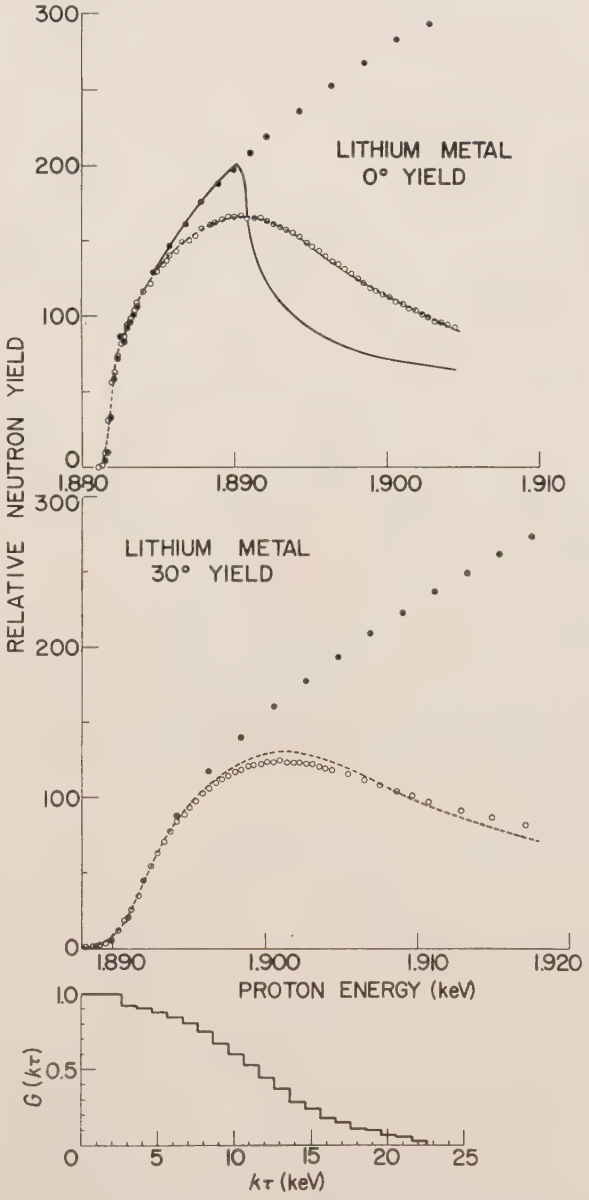

Fig. 4. The result of an investigation of thin lithium films evaporated onto tantalum backings. The meaning of these graphs is precisely the same as for those in fig. 3. One unit in the neutron yield represents 1000 counts.

$$\frac{Y_{\text{Li}}(E_p, \infty; \Omega)}{Y_{\text{LiF}}(E_p, \infty; \Omega)} = \frac{k_{\text{LiF}}}{k_{\text{Li}}}. \tag{12}$$

Hence the ratio of neutron yields at E_p from infinitely thick targets of compounds containing

lithium is independent of bombarding energy. Table 1 shows the yields at 0° read off smooth curves drawn through the experimental points for infinitely thick targets of both lithium and lithium fluoride for a range of incident proton energies. The fourth column of this table gives the ratio of the yield from the lithium target to

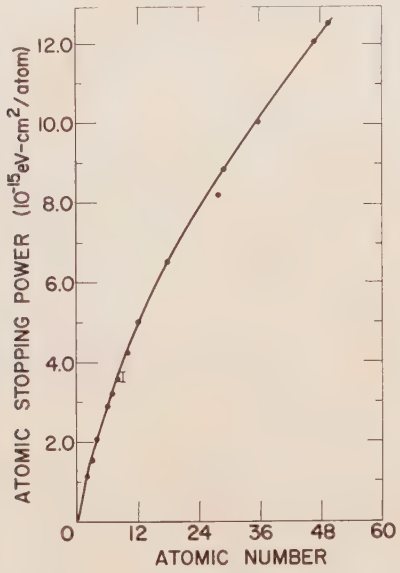

Fig. 5. The atomic stopping power calculated from empirical formulae for 2-MeV protons for various elements. The error bar denotes the value measured for fluorine.

that from the lithium fluoride targets as well as the average value of the ratio. The constancy of the ratio is a second indication that both targets are infinitely thick over the range of proton energies for which the ratio was calculated.

Fig. 5 shows the stopping power obtained at $E_p = 2$ MeV by using empirical formulas[18]) for various elements, plotted as a function of the atomic number of the element (for those elements for which such formulas were known). The value for lithium falls slightly below a smooth curve drawn through the points. On the assumption that for lithium fluoride the stopping powers of lithium and fluorine add linearly, eq. (12) can be used to calculate a value for fluorine. Both the value for lithium obtained from the empirical formula and that read off the smooth curve were used to obtain values for fluorine. A vertical line in fig. 5 represents the two extremes of this calculation. If the lithium metal target had oxidized extensively during the course of the experiment, the agreement obtained could not have been expected. In fact exact agreement between the calculated value for fluorine and the curve can be obtained if one assumes that from 3.0 to 5.8 atom percent of lithium combined with oxygen to form Li_2O. In any event it seems unlikely that "thickening" of thin lithium targets is caused by chemical combination of lithium with other elements.

To obtain information concerning the apparent uniformity of the thin targets, the data were treated in the following manner. Smooth curves were drawn through the experimental points for both the thin and the infinitely thick target. Values were read off the curves at small but equal energy increments starting at the threshold energy for the reaction. Eq. (4) was used to calculate the expected yield for an ideal target of that thickness $k\tau$ which corresponds to the maximum in the observed thin target yields. The results of these calculations at 0° are shown as solid lines in figs. 3 and 4. It is immediately evident by comparing the ideal yields with the measured yields that the thin targets used in the present experiment were "apparently" nonuniform. However, the lithium fluoride target is much more nearly uniform than the lithium metal target.

In order to obtain the apparent target distribution function defined in Section 2, it is convenient to integrate eq. (10) by parts. The result is

$$\mathscr{Y}(E_p,\tau_m;\,\Omega) = Y_I(E_p,x;\,\Omega) - \\ - \int_0^{\tau_M} F(x)\,\frac{d}{dx}\,[Y_I(E_p,x;\,\Omega)]\,dx\,.$$

In the limit for which $F(x)$ is constant over energy intervals $k_{j-1} \leqslant kx < k\tau_j$, the expression for $\mathscr{Y}$ reduces to

[17]) An attempt to use a crystal of lithium fluoride $\frac{1}{8}$ in. thick as an infinitely thick target was prevented by the charging of the crystal by the proton beam.

[18]) Ward Whaling, The Energy Loss of Charged Particles in Matter, Handbuch der Physik, Vol. 34 (Springer-Verlag, Berlin, 1958) p. 193.

$$\mathscr{Y}(E_p,\tau_m;\,\Omega) = \sum_{j=1}^{M} [1 - F(\tau_{j-1})]\,[Y_I(E_p,\tau_j;\,\Omega) - Y_I(E_p,\tau_{j-1};\,\Omega)]\,. \quad (13a)$$

Defining the quantity $G_j = 1 - F(\tau_{j-1})$ leads to the following expression for the neutron yield:

$$\mathscr{Y}(E_p,\tau_M;\,\Omega) = \sum_{j=1}^{M} G_j Y_I(E_p - k\tau_{j-1}\,,\,\tau_j - \tau_{j-1};\,\Omega)\,. \quad (13b)$$

In eq. (13b) the quantity $Y_I(E_p - k\tau_{j-1};\,\tau_j - \tau_{j-1};\,\Omega)$, defined by eq. (3), represents the yield at a proton bombarding energy

$$(E_p - k\tau_{j-1})$$

from an ideal target of thickness

$$(\tau_j - \tau_{j-1})$$

in the direction Ω. From the properties of $F(\tau)$ it follows that G_j is a monotonically decreasing function of the index j and that $G_1 = 1$ and $G_M = 0$.

For a range of proton energies

$$E_t \leqslant E_p < E_t + k\tau_1$$

only the first term in the sum of eq. (13b) is finite. Thus from the definitions of G_1 and Y_I, eq. (13b) reduces to

$$\mathscr{Y}(E_p,\tau_M;\,\Omega) = Y_I(E_p,\tau_1;\,\Omega) \qquad E_t \leqslant E_p < E_t + k_\tau\,.$$

The value of τ_1 is obtained from the smallest upper bound of the region for which this equality is satisfied. (Both $\mathscr{Y}$ and Y_I are experimental numbers.) Subtracting $Y_I(E_p,\tau_1;\,\Omega)$ from the measured yield, one obtains

$$\Delta_1\mathscr{Y}(E_p,\tau_M;\,\Omega) \equiv \mathscr{Y}(E_p,\tau_M;\,\Omega) - Y_I(E_p,\tau_1;\,\Omega) = \sum_{j=2}^{M} G_j Y_I(E_p - k\tau_{j-1},\,\tau_j - \tau_{j-1};\,\Omega)\,.$$

For a new range of energies

$$E_t + k\tau_1 \leqslant E_p < E_t + k\tau_2\,,$$

only the $j = 2$ term in this sum is finite so that G_2 can be obtained from the values of $\Delta_1\mathscr{Y}$ and Y_I in the lower part of the range and the value of τ_2 is obtained in the same manner as for τ_1 above. Once the $j = 2$ term has been evaluated, the second difference

$$\Delta_2\mathscr{Y}(E_p,\tau_M;\,\Omega) \equiv \Delta_1\mathscr{Y} - G_2 Y_1(E_p - k\tau_1,\tau_2 - \tau_1;\,\Omega)$$

is formed and compared with the $j = 3$ term of the sum in eq. (13b). Continuing in this manner, one can obtain the entire set of G_j and the corresponding τ_j. The upper limit M is obtained from the condition

$$\Delta_M\mathscr{Y} \approx 0 \quad \text{for} \quad E_p \geqslant E_t + k\tau_M\,.$$

The yield at 0° was used to obtain the quantities G_j for both the thin lithium and lithium fluoride targets. A plot of G_j vs $k\tau_j$ is shown in figs. 3 and 4. The function G_j was then used to predict the measured yield at both 0° and 30° for both types of thin target. These results are shown as the dashed curves in figs. 3 and 4. The fit for the lithium target at 30° can be brought into better agreement without spoiling the fit at 0° by readjusting the energy intervals defined by the τ_j especially for the lower j-values.

A comparison of figs. 3 and 4 shows that the irregularities in thickness are much more pronounced for the metallic lithium than for the lithium fluoride films. In fact, it is possible to explain the measured distribution G_j for lithium fluoride on the assumption that this target was prefectly uniform in thickness. For any physically reasonable distribution of proton energies, we have

$$\left(\frac{\partial\phi}{\partial y}\right)_x \approx -\frac{\mathrm{d}\phi}{\mathrm{d}\,x}\,.$$

With this approximation, we obtain from eq. (8)

$$-\frac{\partial S(y;\,\tau)}{k\partial y} = \frac{\phi(E_p;\,E_p - ky,\tau)}{\phi_0}\,.$$

For a target which is physically uniform, $G_j = S(y_{j-1};\,\tau)$ so that

$$\left(\frac{\partial S(y;\,\tau)}{k\ \partial y}\right)_{y_j} \approx \frac{G_{j+1} - G_j}{k(y_j - y_{j-1})} \approx -\frac{\phi(E_p;\,E_p - ky_j,\tau)}{\phi_0}\,.$$

Thus the distribution G_j of fig. 3 can be interpreted as a measure of the normalized energy spectrum of the proton beam which emerges from the back side of the target. The histogram in fig. 6 shows the result obtained for this energy spectrum by use of the measured values of G_j for the thin lithium fluoride target. The smooth curve represents the results obtained by

using Symon's[19]) curve to calculate the theoretical straggling distribution for a 2-MeV proton beam after it passes through a 5.5×10^{-5} g/cm^2 layer of lithium fluoride. The agreement suggests that within the accuracy of the experiment the apparent nonuniformity of the lithium fluoride target can be attributed entirely to straggling.

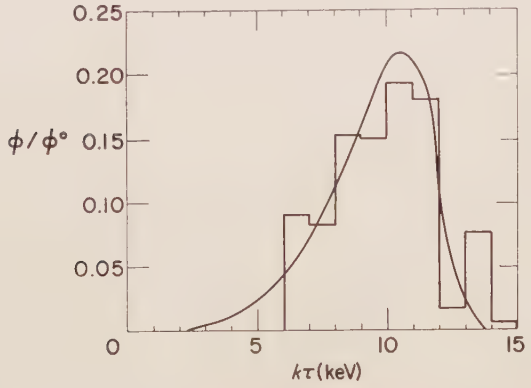

Fig. 6. The distribution of energy loss of protons emerging from a lithium fluoride film. The histogram is the measured distribution based on the "thickness distribution" shown in fig. 3. The smooth curve shows Symon's solution of the diffusion equation for this case.

It should be pointed out that a direct measurement of the energy distribution function for the emergent protons from such thin targets would be extremely difficult. A charged-particle spectrometer with extremely high resolution would be required, and the distribution function would have to be inferred by observing protons scattered at back angles from targets evaporated onto very thin backings. Such an extrapolation seems much less direct than the method described above.

Fig. 7 shows the result of an attempt to repeat the yield curve for the thin lithium metal target. The runs were taken one immediately following the other. Lithium metal targets not only tend to be physically nonuniform, but they seem to change their structure under proton bombardment. Possible causes of the changes are evaporation of lithium from the tantalum cup, chemical combination with impurities, and increased nonuniformity as a result of migration of lithium on the substrate. To minimize the effect of heating by the proton beam the wobble target was used, the tantalum cup was cooled by a blast of air, and the value of the proton

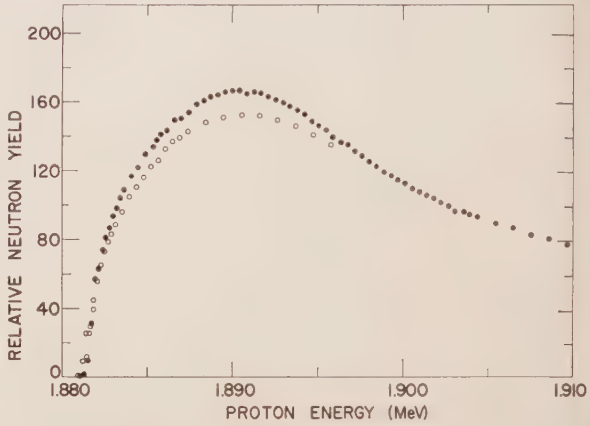

Fig. 7. The neutron yield from the same thin metallic lithium target measured in two immediately successive runs. One unit in the neutron yield represents 100 counts.

current was kept low. Previous experience under similar conditions[3]) indicates that evaporation of lithium from the target is not an important mechanism for producing the observed changes. It has been observed that though the curve for a rerun differs near threshold, it returns to agreement with the original run at those portions of the curve for which the yield is constant with energy. Hence the integrated amount of lithium struck by the incident proton beam remains constant. This indicates a negligible amount of lithium is evaporated from the target. The measurements of stopping power seem to rule out chemical combination as an important factor in producing the changes. For these reasons it is believed that the apparent structural change in thin lithium targets is caused by migration of lithium atoms on the target backing, which does not change the average number of atoms/cm^2 but results in greater nonuniformity.

5. Conclusions

One aim of this work was to develop a method by which the mean energy as well as the energy

[19]) K. R. Symon, Harvard University, Thesis (1948). The results of this thesis pertinent to this work are contained in Bruno Rossi: High-Energy-Particles (Prentice-Hall, Inc., New York, 1952), p. 29 ff.

spectrum of a neutron beam from a thin lithium source could be determined more accurately but no more laboriously than by the conventional "rise-curve" method. In fact, by normalizing a measured 0° threshold curve for infinite thickness to the curve of fig. 1 for values of the proton energy just above threshold, the minimum thickness of the measured target can be estimated quite accurately by inspection. Performing the subtraction process described in section 4 yields a measure of the nonuniformity of the target. Needless to say, the experimental information necessary to this procedure is identical with that required by previous methods. For very thin lithium targets it may be necessary to take into account the energy spectrum of the incident proton beam before this normalization can be carried out.

In view of the straggling effect, it is obviously impossible to obtain a target which is perfectly uniform as measured from the neutron yield. It is equally obvious that the lithium films are grossly nonuniform in physical thickness in comparison with the lithium fluoride films since for equivalent neutron yields the straggling in lithium is certainly less than in lithium fluoride. (See, however, footnote [15].)

The choice between metallic lithium and lithium compounds as a neutron source depends, of course, on the requirements of a particular experiment. The lithium fluoride films can be used as source of more nearly monoenergetic neutron beams and have a greater degree of stability than metallic lithium (see ref. [4]); but these qualities are bought at a sacrifice of approximately 60% in neutron yield.

During the course of this work the neutron yield at 120° from the (p,n) reaction in lithium was calculated. The result is shown in fig. 8. As mentioned previously, the $Li^7(p,n)Be^7$ threshold is one of the principal energy calibration points for cross-section measurements. It might be pointed out that a more accurately reproducible threshold is the "back-angle threshold"[20]) for this reaction. This latter threshold does not suffer the distortions caused by the cone of neutrons opening up inside the solid angle subtended by the detector. Furthermore, the back-angle threshold is not dependent on angle over the range of angle for which it is defined, whereas the conventional forward threshold is defined only at zero degrees.

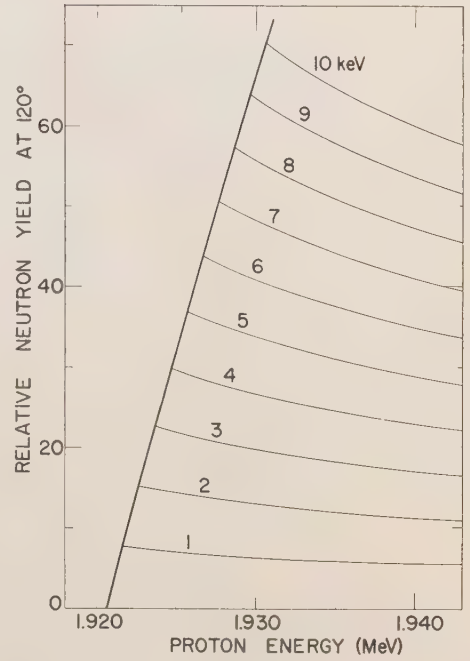

Fig. 8. The calculated neutron yield from various thicknesses of a lithium target at 120°. One unit in the neutron yield represents 1000 counts.

Acknowledgements

The authors would like to thank Mr. Merle Burgy for many helpful discussions and suggestions concerning the problem of straggling. Also the help given them during the course of the experiment by Mr. Edwin Saller and the calculations by Mr. Morris Firebaugh is appreciated. We also wish to thank Dr. F. E. Throw for his comments concerning the original manuscript.

[20]) J. Monahan, Kinematics of Neutron-Producing Reactions. Section I. B. in Fast Neutron Physics, edited by Marion and Fowler (Interscience Publishers, Inc., New York 1, N. Y.) in press.

NUCLEAR INSTRUMENTS AND METHODS 6 (1960) 354–356; NORTH-HOLLAND PUBLISHING CO.

SYSTEME DE SOUSTRACTION A TUBE CATHODIQUE MEMOIRE

A. BOUCHERIE

Centre d'Etudes Nucléaires de Saclay, Gif-sûr-Yvette, (S & O), France

Received 15 November 1959

This paper describes a method whereby a digital substracting system by the means of a memory cathode-ray tube is obtained. This system can be associated with a pulse height analyzer which uses the principle of storing pulses along vertical lines on the screen of a memory cathode-ray tube and analyzing them by horizontal scanning. In this case, one has a it leads to a simple way of direct convection the integral spectrum given by the scanning into a differential spectrum.

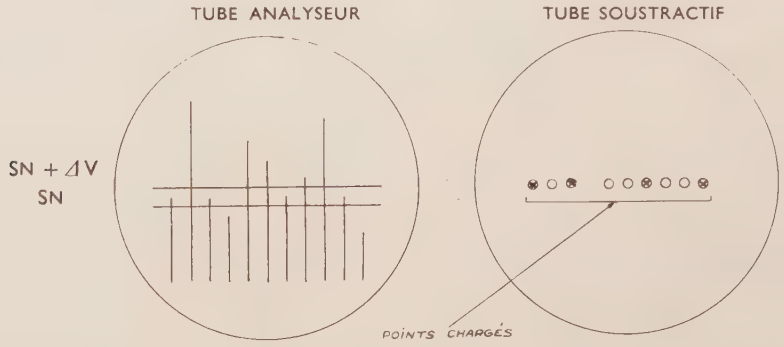

Figure 1

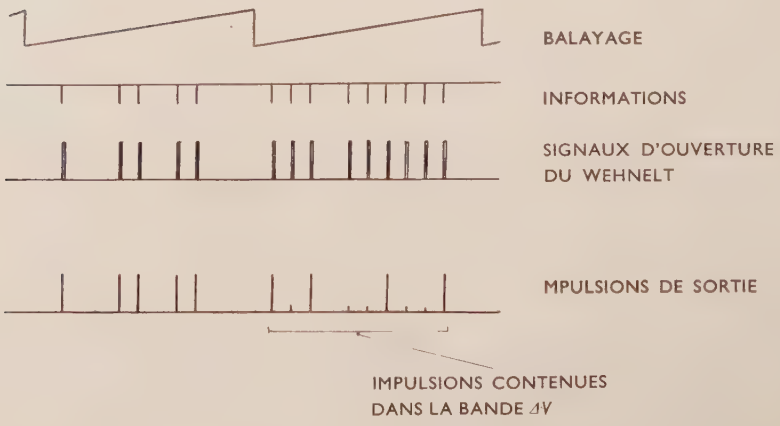

Figure 2

1. Introduction

L'intérêt d'un système de soustraction est justifié dans le cas particulier de la sélection d'amplitude du type Reaves[1]). La soustraction envisagée permet alors de transformer le spectre intégral en spectre différentiel. Rappelons brièvement le principe utilisé par Reaves: les impulsions à analyser sont réparties sous forme de segments chargés sur la face d'un tube cathodique mémoire; la longueur d'un segment est proportionnelle à l'amplitude correspondante.

Les résultats de l'analyse sont obtenus par un balayage horizontal croisant perpendiculaire-

[1]) John Reaves, N.B.S. report No. 4498, p. 20.

ment les traces chargées. Le niveau du balayage de lecture caractérise le seuil. Toutes les informations obtenues à un niveau donné représentent le nombre d'impulsions analysées, d'amplitude supérieure ou égale au niveau considéré, conduisant ainsi à un spectre intégral.

2. Principe

La soustraction peut être avantageusement effectuée à l'aide d'un deuxième tube mémoire, balayé virtuellement suivant une trace unique en synchronisme avec le premier sur lequel l'analyse s'effectue de haut en bas (fig. 1). Le résultat des lectures est transformé en signaux

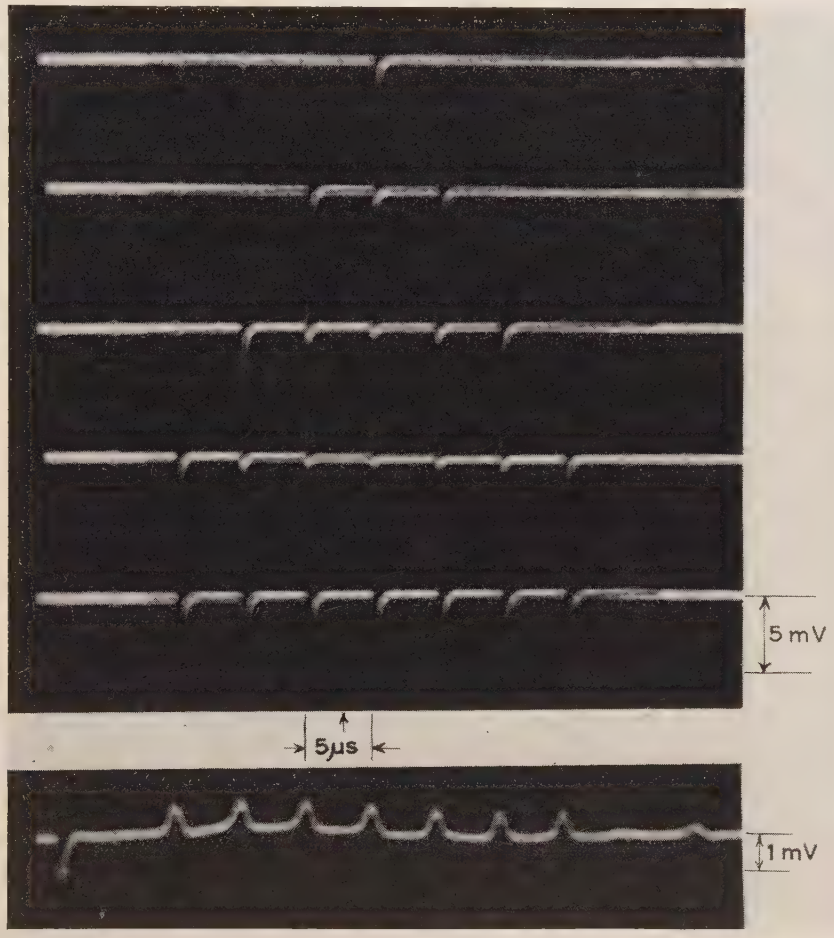

Figure 3

Considérons deux lectures consécutives correspondant respectivement aux niveaux S_n et $S_n + \Delta V$, ΔV représentant la largeur de bande.

Le système soustractif effectuera alors la différence entre les nombres d'impulsions correspondant à ces deux lectures consécutives, cette différence représentant le nombre d'impulsions relatives à la bande $(S_n, S_n + \Delta V)$.

rectangulaires d'ouverture de faisceau du tube soustractif (fig. 2).

Si les signaux sont suffisamment courts devant la vitesse du balayage, ils contribueront à inscrire des points disposés sur la même ligne (fig. 1).

Le principe repose essentiellement sur le fait qu'à chaque inscription d'un nouveau point, un signal est recueilli à la sortie du tube tandis que

si le point considéré a déjà été chargé lors d'une première inscription, aucun signal ne sera recueilli au cours des inscriptions suivantes.

Le système a été essayé en simulant quatre lectures consécutives correspondant respectivement à un nombre d'impulsions impair s'échelonnant de un à sept. Les signaux correspondant sont représentés sur la figure 3.

Les conditions de mesure étaient les suivantes:

– tube mémoire: R.C.A. 6571

– haute tension: 1000 V

– polarisation de repos du Wehnelt: — 20 V

– caractéristiques des signaux d'ouverture du faisceau: + 20 V, 0.2 μs

– caractéristiques du balayage: attaque en symétrique $\pm$ 50 V, 75 μs.

Le signal de sortie recueilli aux bornes d'une résistance de 10 kΩ était le suivant:

– point non préalablement chargé: 5 mV

– point préalablement chargé: < 1 mV

soit un rapport

$$\frac{\text{signal utile}}{\text{résidu}} > 5 .$$

Il est nécessaire d'effacer systématiquement tous les points chargés lors d'un dernier balayage (analyse terminée). Le Wehnelt est alors ouvert par un signal positif rectangulaire pendant toute la durée du balayage. Les signaux de lecture recueillis doivent représenter la somme de tous les signaux d'inscription obtenus précédemment; d'ou un moyen de contrôle simple du bon fonctionnement du système.

NUCLEAR INSTRUMENTS AND METHODS 6 (1960) 357–360; NORTH-HOLLAND PUBLISHING CO.

A NUCLEAR MAGNETIC RESONANCE SPECTROMETER

V. J. KOWALEWSKI† and R. A. HOFFMAN

Institute of Physics, University of Uppsala, Uppsala

Received 29 November 1959

A bridge and pre-amplifier system for observation of nuclear magnetic resonance at various frequencies is described.

1. Introduction

The purpose of the present note is to describe a bridge and pre-amplifier arrangement for the observation of nuclear magnetic resonance (NMR) at various frequencies. Features are incorporated which permit the temperature of the (spinning) sample to be varied within wide ranges. Since only few such devices have been described to date[1]), it may be worth while to give some details of the construction.

In this institute we have at our disposal a Varian Associates model V 4300-B high resolution NMR spectrometer operating at 40 Mc/s. including a 12″ electromagnet model V 4012-HR, and we have tried to make use of this equipment in our spectrometer. Since we find it desirable to work at other frequencies, we have, however, attached a different rf-unit and a different resonance head.

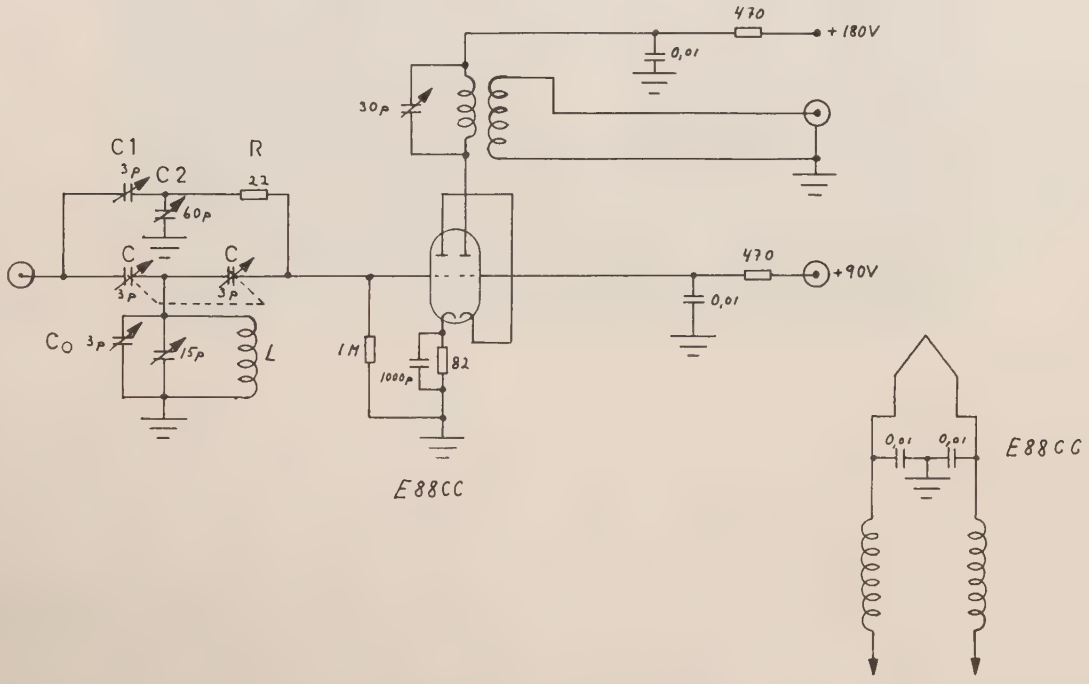

Fig. 1. Rf-bridge and pre-amplifier schematic.

† Permanent address: Facultad de Ciencias Exactas, Buenos Aires, Argentina.

[1]) J. A. Pople, W. G. Schneider and H. J. Bernstein, High-resolution nuclear magnetic resonance (McGraw-Hill, New York, 1959) p. 71.

2. Description of the Apparatus

Temperature variation is more easily attained with a single coil spectrometer, so our resonance head is of the bridge-type. The bridge is the double-T arrangement of Grivet *et al.*[2])which has several distinguishing features such as ease of adjustment, low input and low output impedances[3]), Also it has only one coil, the sample coil, with one end grounded.

The bridge can be used at other frequencies simply by changing the coil and rebalancing.

The temperature control is obtained by immersing the sample coil assembly in a silvered Dewar (inner diameter 27 mm) through which a pre-heated or pre-cooled air stream is blown. The heating of the air stream is effected in a 0.7 meter long glass tube in which a 5 meter long spiral (100 ohm) of Kanthal A-1 0.3 mm

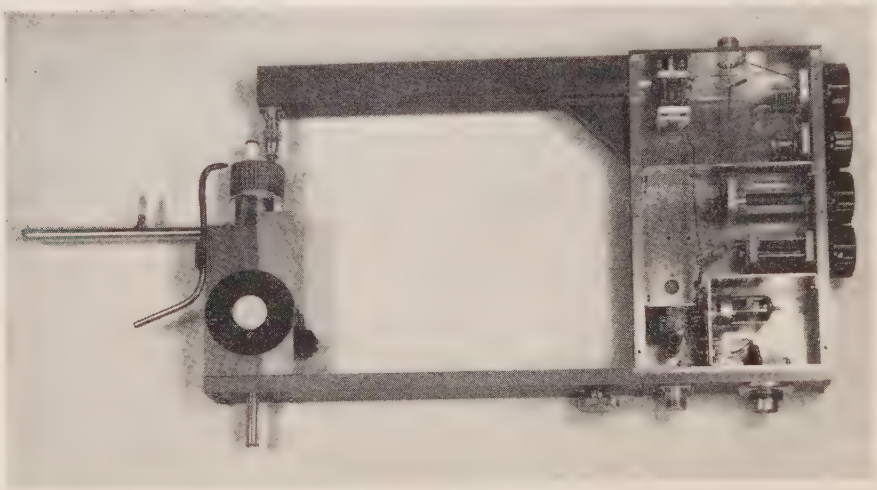

Fig. 2. The bridge and pre-amplifier arrangement shown uncovered. To the left the Dewar and modulation coils can be seen. The controls on the right are from top to bottom C_0, C_0, C_1 and C_2. The twin condenser C is in the upper left of the bridge.

In our bridge all condensers were made variable. Those condensers which have no grounded end are either seldom used (such as the twin condensers $C = 3$ pF which are only re-set when the frequency of operation is changed) or has an insulating shaft ($C_1 = 3$ pF). The two halves of the bridge are well separated in space and by a metal shield. At 15 Mc/s, where the bridge has been most used, the sample coil (L) consists of 15 turns of 0.28 mm copper wire wound on a 7 mm (outer diameter) glass tube. The length of the coil is 4.6 mm. The inner diameter of the supporting glass tube is slightly more than 5 mm allowing standard 5 mm sample tubes to be inserted and rotated.

[2]) P. Grivet, M. Soutif and M. Buyle, C. R. Acad. Sci. (Paris) **229** (1949) 113.

[3]) P. Grivet, M. Soutif and R. Gabillard, Physica **17** (1951) 420.

resistance wire is suspended on tungsten electrodes. Because of the temperature requirements the only plastic used in the Dewar is teflon which can withstand temperatures up to the softening point of the soldering.

The silvercoating of the Dewar also provides partial shielding of the resonance coil against disturbing signals. The Dewar is supported by a wooden block outside of which a pair of coils of 23 turns each 0.85 mm enamelled copper wire are wound. These coils provide the modulation field necessary for oscilloscope presentation. The modulation frequency was originally 50 c/s, but it was found that a slower sweep greatly improves the signal/noise ratio, so we have later used the sweep unit of the Varian Spectrometer. A small resistor was coupled in series with the coils to make the sweep generator load equal to the design value (20 ohm). The total width of the

Dewar and modulation coil assembly is 43 mm, slightly less than the magnet air gap (1.75″).

The sample may be rotated by means of an air-driven teflon turbine. This sample spinning introduces some vibrations, and it was soon realized that one of the main problems was to get rid of microphonics.

Thus although electric requirements would favour an un-supported, air-insulated coaxial lead between the main part of the bridge and the sample coil, we now use a rigid teflon insulated coaxial system. Also the coaxial tube and the glass tube inside the Dewar have elastic supports of teflon.

The bridge and the preamplifier are built in a rigid aluminium shielding box (probe). The supporting bottom plate, which is screwed directly onto the magnet probe holder is made of 12 mm duralumin and other walls of 6 mm and 4 mm aluminium plate. With this arrangement no spinning noise was observable and the bridge is fairly insensitive to vibrations.

The pre-amplifier is built in with a separating shield. It is of low noise design with a grounded cathode, grounded grid sequence (cascode)[4], using the double triode E 88 CC. The power supply has efficient filtering using double π filters. The high tension (+ 180 V) and the grid bias of the second stage (+ 90 V) are stabilized with two voltage-regulating valves (OB-3).

[4]) G. E. Valley and H. Wallman, Vacuum tube amplifiers, Radiation Laboratory Series Vol. 18 (McGraw Hill, New York, 1948) p. 615.

3. Performance

This set-up has been tested in conjunction with a free-running Marconi type TF 801/B1 signal generator and an Airmec type C 864 receiver followed by a Sanborn recorder. The audio amplifier part of the receiver was disposed of and the output taken from the second detector to satisfy the need for direct coupling when using slow seep speed.

The proton resonance signal from a mixture of water and acetic acid having a shift of 6.0 ppm between the resonance peaks has been recorded at 15 Mc/s. The line width at half-amplitude is around 5 c/s for both components and the signal/noise ratio better than 50:1.

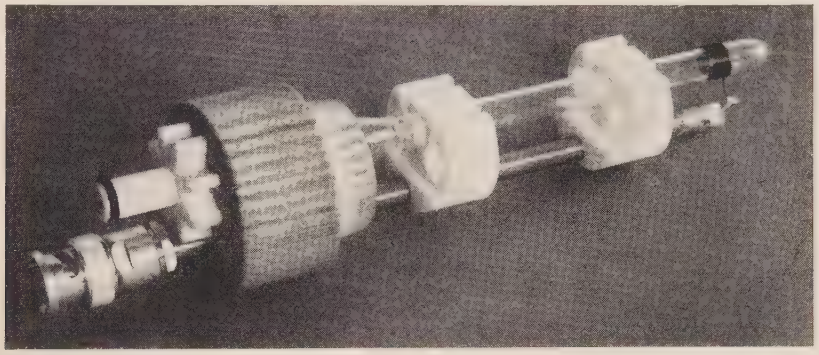

Fig. 3. The sample coil insert. To the left the teflon turbine and coaxial connector to the bridge chassis can be seen.

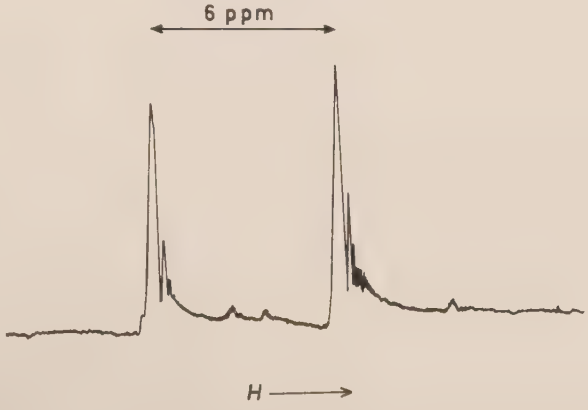

Fig. 4. The proton magnetic resonance signal from a mixture of acetic acid and water at 15.00 Mc/s. The sweep is 1.25 ppm/sec.

The resolution is effectively limited by the short-time stability of the signal generator, which does not permit sweep speeds slower than

0.5 ppm/sec. A crystal controlled oscillator would remove this limitation and this would probably improve the signal/noise ratio too,

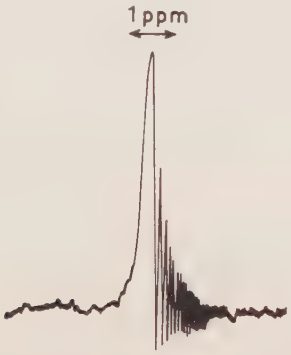

Fig. 5. The phosphorus (P^{31}) nuclear magnetic resonance signal from white phosphorus dissolved in carbon disulfide The resonance frequency is 16.22 Mc/s. The sweep speed is 1 ppm/sec.

since a reduction in line-width means increased amplitude.

We have also recorded the signal from a concentrated solution of white phosphorus in carbon disulfide. The apparent line width of the P^{31} signal is 10–15 c/s at 16.22 Mc/s and the signal/noise ratio is better than 20:1. The optimum rf input voltage to the bridge is around 5 mV in both cases, but the phosphorus signal is more easily saturated.

Acknowledgements

The authors wish to express their thanks to professor Kai Siegbahn for all facilities put at our disposal and for his interest in our work. A grant to one of us (V.J.K.) from the Consejo Nacional de Investigaciones Cientificas y Tecnicas (Argentina) is gratefully acknowledged. We are indebted to Mr. W. Parker for correcting the English.

This work has been sponsored by the Swedish Technical Research Council.

NUCLEAR INSTRUMENTS AND METHODS **6** (1960) 361; NORTH-HOLLAND PUBLISHING CO.

LETTER TO THE EDITOR

A PROPOSAL TO DECREASE THE DEADTIME OF THE HUTCHINSON-SCARROT TYPE PULSE HEIGHT ANALYSER

W. S. C. WILLIAMS

Department of Natural Philosophy, The University, Glasgow

Received 30 November 1959

The object of this note is to propose a modification to the Hutchinson-Scarrot type pulse height analyser, which reduces the dead time by a factor equal to the number of channels. This is done by inserting a temporary store between input and the normal circulating binary store.

Consider a 100-channel analyser in which the main store occupies 1000 microsec and is circulating without a gap between the last and first channels. A channel marking oscillator running at 100 kc/s marks in a separate circuit the time of the beginning of each channels binary number by a pulse 20 nanosec long. The temporary store is also circulating without a gap and has a capacity of only one count per channel; it occupies a time $\frac{100}{101} \times 10$ microsec and is controlled by an oscillator running at 101 kc/s. The presence of a count in the mth channel of the temporary store is indicated by a 20 nanosec pulse at a distance $\frac{m}{10.1}$ microsec from the beginning of this store's cycle. Pulses are put into the temporary store by the usual height to time conversion. However, this process takes only $\frac{1}{101}$ of the time normally required in an analyser with a 1000 microsec main store and the average dead time for access to the temporary store is just less than 5 microsec.

The length of the temporary store is such that vernier coincidences will occur between the channel marker pulses and count pulses in the temporary store. Let us suppose there is a count pulse in the mth channel of the temporary store and we consider the instant at which the channel 1 marker coincides with the position of a count in channel 1 of the temporary store. Then 10 $(m - 1)$ microsec later the mth channel pulse in the temporary store is in time coincidence with the mth channel marker and such a coincidence is at the right time position to cause the operation of add-one to the mth channel binary number in the main store. The coincidence is also used to erase the count in the mth channel of the temporary store. In this way counts in the temporary store are continuously transferred to the main store.

Although the average time for a count to reach the main store is still 500 microsec the temporary store is free to accept pulses in all other unoccupied channels during the time of transfer from the temporary to the main store. Thus the dead time is 500 microsec in each channel, an improvement by a factor equal to the number of channels. The disadvantage is that two dead time corrections must be made. The first is a 500 microsec dead time correction to the counting rate in each channel separately. The second is an overall correction for the temporary store dead time of 4.95 microsec.

There are some practical difficulties: for example, it may be necessary to sacrifice the last channel of the temporary store to accommodate the flyback time of the comparison sawtooth waveform. The 100th channel can be restored by adjusting the parameters of the instrument. The numbers used in this note are meant to serve as an example and there is no difficulty in arranging other time scales.

Since this idea was formulated, I have learnt of a similar scheme suggested by Dr. G. Scarrot at the Edinburgh Nuclear Physics Conference in September, 1959. I am indebted to Dr. Scarrot for information about his method.

AUTHOR INDEX

ANDREWS, HOWARD L., Accelerators in biology and medicine 96

ARTANDI, CHARLES and ALBERT A. STONEHILL, Rigid vinyl film dosimeter 279

BALLINI, R. and S. M. SHAFROTH, Detection of low energy neutrons with a NaI(Tl) crystal and time of flight 331

BASHANDY, EKBAL, Energy dependent instrumental time delays in millimicrosecond delayed coincidence experiments 289

BASSEL R. H. and R. S. BENDER, The Oak Ridge relativistic isochronous cyclotron. Addendum: Some recent results of orbit studies 234

BENDER, R. S., *see* BASSEL

BENDER, R. S., *see* COHEN

BERKO, S., *see* STETSON

BIRKHOFF, R. D., *see* RITCHIE

BLOSSER, H. G., *see* COHEN

BOUCHERIE, A., Système de soustraction à tube cathodique mémoire 354

BROMLEY, D. A., *see* LITHERLAND

BRÜCKMANN, HANNO, Ein Modulator für das Synchrozyklotron Bonn mit ferroelektrischer Keramik 169

BURGE, EDWARD J., Statistical errors in particle polarization measurements (Letter to the Editor) 101

BÜHRING, WOLFGANG und JOACHIM HEINTZE, Eine Aufdampfapparatur für radioaktive Substanzen 286

CAMPANILE, V. A., *see* WAGNER

CERNIGOI, C., I. GABRIELLI and G. IERNETTI, Behaviour of photomultipliers against high-frequency modulated light 193

CHEKA, J. S., *see* RITCHIE

COHEN, B. L., H. G. BLOSSER, E. D. HUDSON, R. S. LORD and R. S. BENDER, The Oak Ridge relativistic isochronous cyclotron. Part II. Magnetic field design for the isochronous cyclotron . . . 105

CONNOR, R. D., The action of fast spherical ionization chambers 301

CONNOR, R. D. and M. K. HUSAIN, Some factors affecting the gain and resolution of photomultiplier tubes 337

DATTILO, J. A. and J. VAN BLADEL, Fields in gap-excited circular ducts 283

DELATTRE, P., Deux piles atomiques considérées comme instruments de physique 83

ELLS, C. E., Irradiation of metals at controlled elevated temperatures in the M.I.T. cyclotron 276

FISCHMAN ARBEL, ARIEH, Precision Schmitt Trigger (Erratum) 104

GABRIELLI, I., *see* CERNIGOI

GARG, JAGADISH B., A fast neutron time-of-flight spectrometer 72

GARG, J. B., A fast coincidence unit of variable resolving time 187

GOOD, W. M., Millimicrosecond pulsing – Its application and technique 323

GORDON, M. M. and T. A. WELTON, The Oak Ridge relativistic isochronous cyclotron. Part III. Analysis of ion orbits in the isochronous cyclotron 221

GRIVET, PIERRE et ALBERT SEPTIER, Les lentilles quadrupolaires magnétiques (I) 126

GRIVET, PIERRE et ALBERT SEPTIER, Les lentilles quadrupolaires magnétiques (II) 243

GUINN, V. P., *see* WAGNER

GUTMANN, P. F. et D. T. JOVANOVIČ, Attaque des tubes compteurs EZ-10 par transistors 206

HASSLER, W., *see* LOTZ

HEINTZE, JOACHIM, *see* BÜHRING

HOFFMAN, R. A., *see* KOWALEWSKI

HOUGH, PAUL V. C., Performance of a nuclear emulsion scanner 33

HOWARD, F. T., *see* LIVINGSTON

HUDSON, E. D., *see* COHEN

HUSAIN, M. K., *see* CONNOR

HUSAIN, S. ABID and A. A. JAFFE, The proportional counter as a charged particle spectrometer 50

HUSTER, E. und W. RAUSCH, Nachtrag zu unserem Beitrag: Zur Herstellung sehr dünner elektrisch leitender Präparatenunterlagen für absolute β-Zählung (Nuclear Instruments **3** (1958) 213–217) (Letter to the Editor) 217

IERNETTI, G., *see* CERNIGOI

JAFFE, A. A., *see* HUSAIN ABID S.

JENNINGS, R. E. and P. I. P. KALMUS, A gas Čerenkov detector for the accurate determination of electron beam energy 209

JOHANSSON, B., A new solution of the finite rise time problem by means of a distributed amplifier with automatic gain control 201

JOVANOVIČ, D. T., *see* GUTMANN

KALMUS, P. I. P., *see* JENNINGS

KING, W. G., *see* VINCENT

KOLTAY, E., Elektronenoptische Konstruction von inhomogenen Beschleunigungsröhren 45

KOWALEWSKI, V. J. and R. A. HOFFMAN, A nuclear magnetic resonance spectrometer 357

KUMAGAI, HIROO, On a design of wide range magnet for cyclotron 213

KUROYANAGI, T., *see* MORINAGA

Layson, W. M., J. Malos and D. D. Millar, Angular selectivity of a Geiger telescope arrangement for cosmic ray air showers 179
Litherland, A. E. and D. A. Bromley, A two-dimensional pulse-height analyser 176
Livingston, R. S. and F. T. Howard, The Oak Ridge relativistic isochronous cyclotron Part I 1
Lord, R. S., *see* Cohen
Lotz, W., A. Sittkus und W. Hassler, Untersuchungen an einer Anordnung zur Messung der Nukleonenkomponente der kosmischen Strahlung 296

Malos, J., *see* Layson
Meunier, R., et J. Teiger, Circuit de coïncidence rapide à trois diodes (Nuclear Instruments **5** (1959) 148) (Erratum) 220
Millar, D. D., *see* Layson
Monahan, J. E. and F. P. Mooring, An investigation of properties of thin lithium films by use of the $Li^7(p,n)Be^7$ reaction 343
Mooring, F. P., *see* Monahan
Mórinaga, H. and T. Kuroyanagi, Internal target for a betatron 66

Orient, O. J., On the mechanism of multiple discharges in self-quenching Geiger counters . . . 309

Parker, W., *see* Sevier Jr.
Pryor, A. W., The input stage of a transistor pulse amplifier. 164

Rausch, W., *see* Huster
Ritchie, R. H., J. S. Cheka and R. D. Birkhoff, The spherical condenser as a high transmission particle spectrometer. I. Point source 157

Septier, Albert, *see* Grivet
Sevier Jr., K. and W. Parker, Aluminium oxide films for nuclear spectroscopy 218
Shafroth, S. M., *see* Ballini
Sittkus, A., *see* Lotz
Stetson, R. F. and S. Berko, A directional scintillation counter for neutrons 94
Stonehill, Albert, *see* Artandi
Szabó, P., On the effect of total reflection on the optimum dimensions of collimators for neutron crystal spectrometers and diffractometers . . . 183

Teiger, J., *see* Meunier
Trageser, D. A., Engineering methods for electron-beam processing 26

Van Bladel, J., *see* Dattilo
Vincent, C. H. and W. G. King, A pulse to direct current voltage comparator 57

Wagner, C. D., V. A. Campanile and V. P. Guinn, Techniques of chemical research with the electron Van de Graaff 238
Welton, T. A., *see* Gordon
Williams, W. S. C., A proposal to decrease the dead-time of the Hutchinson-Scarrot type pulse height analyser (Letter to the Editor) 361

BOOK REVIEWS

Ajzenberg-Selove, F., and T. Lauritsen, Energy levels of light nuclei VI (T. R. Gerholm) . . . 103
Brown, Sanborn C., Basic data of plasma physics (Lars Block) 104
Flügge, S., (Editor), Encyclopedia of Physics, Vol. 38-2 (E. Sokolowski) 103
Flügge, S., (Editor), Encyclopedia of Physics, Vol. 44 (K. G. Malmfors) 103

SUBJECT INDEX

Accelerators and Reactors

The Oak Ridge relativistic isochronous cyclotron. Part I. R. S. Livingston and F. T. Howard . . . 1
Engineering methods for electron-beam processing, D. A. Trageser . . . 26
Elektronenoptische Konstruktion von inhomogenen Beschleunigungsröhren, E. Koltay . . . 45
Internal target for a betatron, H. Morinaga and T. Kuroyanagi . . . 66
Deux piles atomiques considérées comme instruments de physique, P. Delattre . . . 83
Accelerators in biology and medicine, Howard L. Andrews . . . 96
The Oak Ridge relativistic isochronous cyclotron. Part II. Magnetic field design for the isochronous cyclotron, B. L. Cohen, H. G. Blosser, E. D. Hudson, R. S. Lord and R. S. Bender . . . 105
Les lentilles quadrupolaires magnétiques (I), Pierre Grivet et Albert Septier . . . 126
On a design of wide range magnet for cyclotron, Hiroo Kumagai . . . 213
The Oak Ridge relativistic isochronous cyclotron. Part III. Analysis of ion orbits in the isochronous cyclotron, M. M. Gordon and T. A. Welton . . . 221
The Oak Ridge relativistic isochronous cyclotron. Addendum: Some recent results of orbit studies, R. H. Bassel and R. S. Bender . . . 234
Techniques of chemical research with the electron Van de Graaff, C. D. Wagner, V. A. Campanile and V. P. Guinn 238
Les lentilles quadrupolaires magnétiques (II), Pierre Grivet et Albert Septier . . . 243
Irradiation of metals at controlled elevated temperatures in the M.I.T. cyclotron, C. E. Ellis . . . 276
Fields in gap-excited circular ducts, J. A. Dattilo and J. van Bladel . . . 283

Detectors

Performance of a nuclear emulsion scanner, Paul V. C. Hough . . . 33
The proportional counter as a charged particle spectrometer, S. Abid Husain and A. A. Jaffe . . . 50
A directional scintillation counter for neutrons, R. F. Stetson and S. Berko . . . 94
A gas Čerenkov detector for the accurate determination of electron beam energy, R. E. Jennings and P. I. P. Kalmus 209
Rigid vinyl film dosimeter, Charles Artandi and Albert A. Stonehill . . . 279
The action of fast spherical ionization chambers, R. D. Connor . . . 301
On the mechanism of multiple discharges in self-quenching Geiger counters, O. J. Orient . . . 309
Detection of low energy neutrons with a NaI(Tl) crystal and time of flight, R. Ballini and S. M. Shafroth . . . 331

Errata

Arieh Fischmann Arbel, Nuclear Instruments **5** (1959) 56 . . . 104
R. Meunier et. J. Teiger, Circuit de coïncidence rapide à trois diodes (Nuclear Instruments **5** (1959) p. 148) . . . 220

Instruments and Methods for Nuclear Spectroscopy

A fast neutron time-of-flight spectrometer, Jagadish B. Garg . . . 72
The spherical condenser as a high transmission particle spectrometer. I. Point source, R. H. Ritchie, J. S. Cheka and R. D. Birkhoff . . . 157
A two-dimensional pulse-height analyser, A. E. Litherland and D. A. Bromley . . . 176
On the effect of total reflection on the optimum dimensions of collimators for neutron crystal spectrometers and diffractometers, P. Szabó . . . 183
Aluminium oxide films for nuclear spectroscopy, K. Sevier Jr. and W. Parker . . . 218
Eine Aufdampfapparatur für radioaktive Substanzen, Wolfgang Bühring und Joachim Heintze . . . 286
An investigation of properties of thin lithium films by use of the $Li^7(p,n)Be^7$ reaction, J. E. Monahan and F. P. Mooring . . . 343
A nuclear magnetic resonance spectrometer, V. J. Kowalewski and R. A. Hoffman . . . 357

Instruments and Methods for High Energy Physics

Angular selectivity of a Geiger telescope arrangement for cosmic ray air showers, W. M. Layson, J. Malos and D. D. Millar 179
Untersuchungen an einer Anordnung zur Messung der Nukleonenkomponente der kosmischen Strahlung, W. Lotz, A. Sittkus und W. Hassler 296

Letters to the Editor

Statistical errors in particle polarization measurements, Edward J. Burge 101
Nachtrag zu unserem Beitrag: Zur Herstellung sehr dünner elektrisch leitender Präparatunterlagen für absolute β-Zählung (Nuclear Instruments **3** (1958) 213–217), E. Huster und W. Rausch 217
A proposal to decrease the deadtime of the Hutchinson-Scarrot type pulse height analyser, W. S. C. Williams 361

News Items

Foire Internationale de Liège (Belgique), Journée internationale d'information sur l'Energie Nucléaire (P. Fourmarier, 9 June 1960) 220
The Fifth International Instruments & Measurements Conference, Stockholm, Sweden, September 13–15, 1960. . . 288
The National Electronics Conference, Chicago, Illinois, October 10–12, 1960 288

Nuclear Electronics

A pulse to direct current voltage comparator, C. H. Vincent and W. G. King. 57
The input stage of a transistor pulse amplifier, A. W. Pryor 164
Ein Modulator für das Synchrozyklotron Bonn mit ferroelektrischer Keramik, Hanno Brückmann 169
A fast coincidence unit of variable resolving time, J. B. Garg 187
Behaviour of photomultipliers against high-frequency modulated light, C. Cernigoi, I. Gabrielli and G. Iernetti 193
A new solution of the finite rise time problem by means of a distributed amplifier with automatic gain control, B. Johansson 201
Attaque des tubes compteurs EZ-10 par transistors, P. F. Gutmann et D. T. Jovanovič 206
Energy dependent instrumental time delays in millimicrosecond delayed coincidence experiments, Ekbal Bashandy 289
Millimicrosecond pulsing – Its application and technique, W. M. Good 323
Some factors affecting the gain and resolution of photomultiplier tubes, R. D. Connor and M. K. Husain 337
Système de soustraction à tube cathodique mémoire, A. Boucherie 354